THE DEVELOPMENT OF SELECTIVE INHIBITORS FOR ER α-MANNOSIDASE I BY COMBINATORIAL MODIFICATION OF KIFUNENSINE AND DEOXYMANNOJIRIMYCIN

by

JESSICA CARDOT

(Under the Direction of Geert-Jan Boons)

ABSTRACT

Selective inhibitors of endoplasmic reticulum α-mannosidase I (ER Man I) have the potential to be used for treatment of a number of genetic diseases. Although potent inhibitors for this enzyme have been described, in general these compounds display poor selectivity and often inhibit Golgi α-mannosidase I. To address this difficulty, we have synthesized and combinatorial modified kifunensine, which is a potent GH47 α-mannosidase I inhibitor, and 1-deoxymannojirimycin, a weak α-mannosidase I inhibitor. Kifunensine was modified by a hydrazone moiety, which could easily be extended by reaction with a range of aldehydes. The library of hydrazone-linked analogues was screened for inhibition of human ER Man I and mouse Golgi Man I. It was found that a pyridine functionalized kifunensine analog selectively inhibited ER Man I. Based on this finding, a second generation of analogues was prepared in which a functionalized pyridine scaffold was coupled to kifunensine through the hydrazone moiety. 1-Deoxymannojirimycin was modified by a hydrazine moiety, which could easily be extended by reaction with a range of aldehydes. The library of hydrazone-linked DMJ analogues was screened for inhibition of human ER Man I and mouse Golgi Man I.

INDEX WORDS: Mannosidase Inhibitors, Kifunensine, Deoxymannojirimycin

THE DEVELOPMENT OF SELECTIVE INHIBITORS FOR ER α-MANNOSIDASE I BY COMBINATORIAL MODIFICATION OF KIFUNENSINE AND DEOXYMANNOJIRIMYCIN

by

JESSICA CARDOT

BS Chemistry, Nazareth College of Rochester, 2006

A Dissertation Submitted to the Graduate Faculty of The University of Georgia in Partial Fulfillment of the Requirements for the Degree

DOCTOR OF CHEMISTRY

ATHENS, GEORGIA

2011

THE DEVELOPMENT OF SELECTIVE INHIBITORS FOR ER α-MANNOSIDASE I BY COMBINATORIAL MODIFICATION OF KIFUNENSINE AND DEOXYMANNOJIRIMYCIN

by

JESSICA CARDOT

Major Professor: Geert-Jan Boons

Committee: Kelley Moremen
Robert phillips

Electronic Version Approved:

Maureen Grasso
Dean of the Graduate School
The University of Georgia
December 2011

DEDICATION

I would like to dedicate this dissertation to my parents, Andy and Jan Cardot, and my brother Andy Cardot for all of their love and support.

TABLE OF CONTENTS

ABBREVIATIONS

Ac…….. ……Acetyl

Ac_2O…….Acetic Anhydride

C……Celsius

DCM ……Dichloromethane

DMAP…… N,*N*-dimethylaminopyridine

DMF……..N,*N*-dimethylformamide

DMJ ……...1-Deoxymannojirimycin

DMP……..Dess Martin Periodinane

EDC…… 1-ethyl-3-(3-dimethylaminopropyl) carbodiimide hydrochloride)

ERAD……. Endoplasmic Reticulum Associated Degradation

ER Man I…… Endoplasmic Reticulum α-mannosidase I

Et_2O ……Diethyl ether

EtOH…….Ethanol

HCl……Hydrochloric acid

HOBt……..*N*-Hydroxybenzotriazole

KIF…….Kifunensine

Me……...Methyl

MeOH…….Methanol

NMR…….Nuclear magnetic resonance

NaN_3 …….. Sodium azide

$NaNO_2$ ……. Sodium Nitrite

NaOMe ……...Sodium methoxide

OST……..Oligosaccharyltransferase

Ph……Phenyl

Piv……Pivoyal

Piv-Cl……Trimethyl acetyl chloride

TBAF……..Tetrabutylammonium Fluoride

TFA ……...Trifluoroacetic acid

THF……..Tetrahydrofuran

LIST OF TABLES

Page

LIST OF FIGURES

Page

CHAPTER 1

INTRODUCTION AND LITERATURE REVIEW

Introduction and Literature Review

N-linked Glycoproteins

The most common covalent modification in eukaryotic cells is *N*-linked glycosylation.[1] The majority of proteins synthesized in the ER are in fact *N*-linked glycoproteins which are responsible for a diverse set of cellular functions. Glycoproteins serve as ligands for many recognition processes such as modulation of immune response, enhanced solubility, facilitation of protein orientation, protein rigidity, regulation of protein turnover, protein stabilization against proteolysis, as well as to mediate interactions with pathogens. Not only is *N*-linked glycosylation the most prevalent covalent modification but no other modification is so widely utilized for a variety of purposes.[1,2]

Biosynthetic Pathway of *N*-glycans

Although the *N*-glycans expressed on the cell service contain complex oligosaccharide motifs, they all stem from a basic core structure, $Glc_3Man_9GlcNAc_2$ (Figure 1).[3]

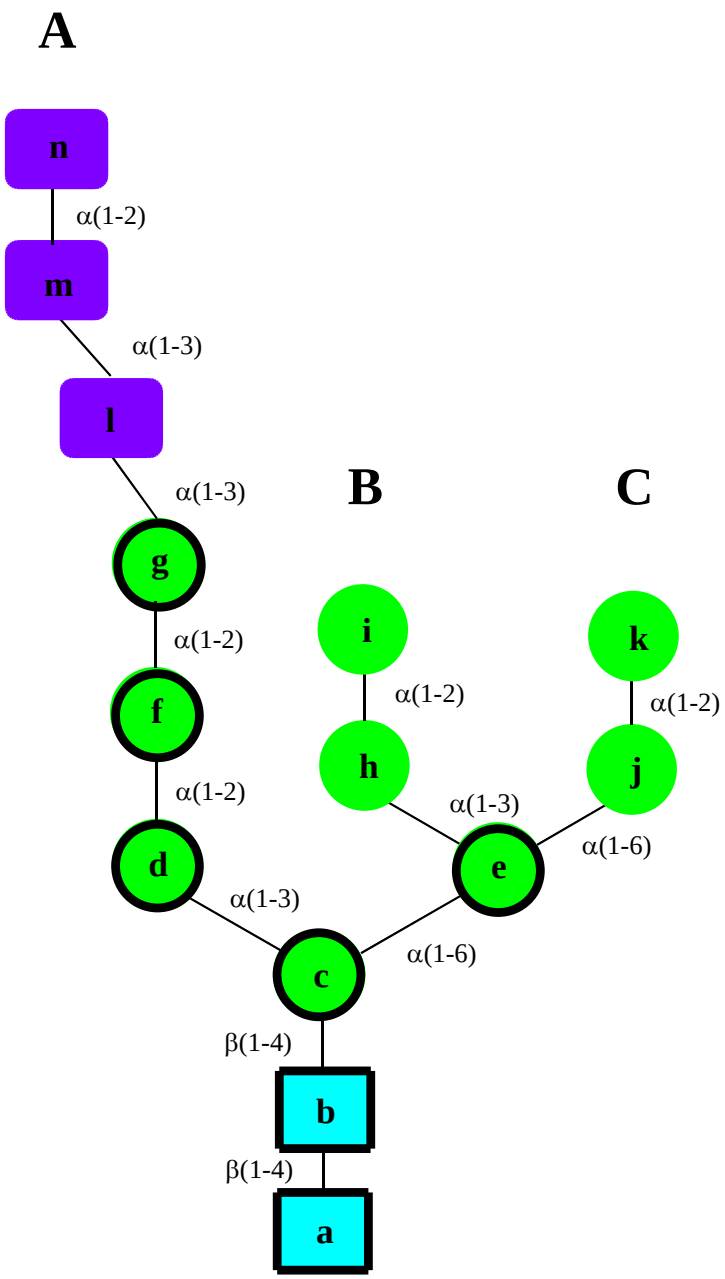

Figure 1: Core oligosaccharide structure containing three glucose residues (purple), nine mannose residues (green) and two *N*-acetyl-glucosamine residues (teal), $Glc_3Man_9GlcNAc_2$. The monosaccharide subunits highlighted in bold circles (a-g) are glycosylated to the glycan on the cytosolic surface, where as the rest are added lumenally. Residues d,f,g,l are responsible for interactions with the calnexin/calreticulin cycle. Where as mannose residue i is cleaved by ER Man I, which is believed to be a key enzyme ERAD.

The biosynthetic pathway of *N*-glycans is shared between the ER and Golgi apparatus. The core oligosaccharide and the polypeptide are synthesized in the ER and cytosol at which point an *N*-glycosylation reaction occurs between the $Glc_3Man_9GlcNAc_2$ and the side chain of an Asn residue of the polypeptide facilitated by an oligosaccharide transferase (OST) enzyme. The newly formed glycoprotein will undergo numerous trimming steps to allow for the proper folding and oligomerization to the native form. Once the native form is achieved the glycoprotein is translocated to the Golgi compartment at which point it is subjected to numerous trimming and elongation steps to form the complex glycans found on mature glycoproteins. The modifications to the glycan in the ER result in limited diversification because the alterations are shared by all glycoproteins. However, these modifications in the ER appear to correspond to glycoprotein folding, quality control, sorting, degradation, and secretion. The various configurations of the *N*-linked glycan in the ER are not merely just intermediates in a biosynthetic pathway but each have a specific function that determines the fate of the individual glycoproteins. These biosynthetic intermediates play a vital role in three main phases of the glycoproteins existence. Phase 1 occurs solely in the ER where truncated versions of the core oligosaccharide are necessary for proper protein folding and quality control. The second phase occurs in the ER, Golgi and *trans*-Golgi network and determines the intracellular transport and targeting. The final phase is solely in the Golgi and takes place after extensive modifications of the Glycan portion giving rise to a tremendous amount of diversification. The change from structural uniformity in the ER to structural complexity in the Golgi corresponds to the marked change in glycoprotein

function. Phase 1 or glycoprotein biosynthesis in the ER will be discussed in detail as it pertains to the current dissertation work.

Biosynthesis of *N*-glycans in the ER

In the ER during the early stages of the secretory pathway, the *N*-glycans have a common role in promoting protein folding, quality control and certain sorting events. The core glycan is produced in the ER membrane by monosaccharyl-transferases and is added to the protein as $Glc_3Man_9GlcNAc_2$ in the lumen of the ER (Figure 2). [12]

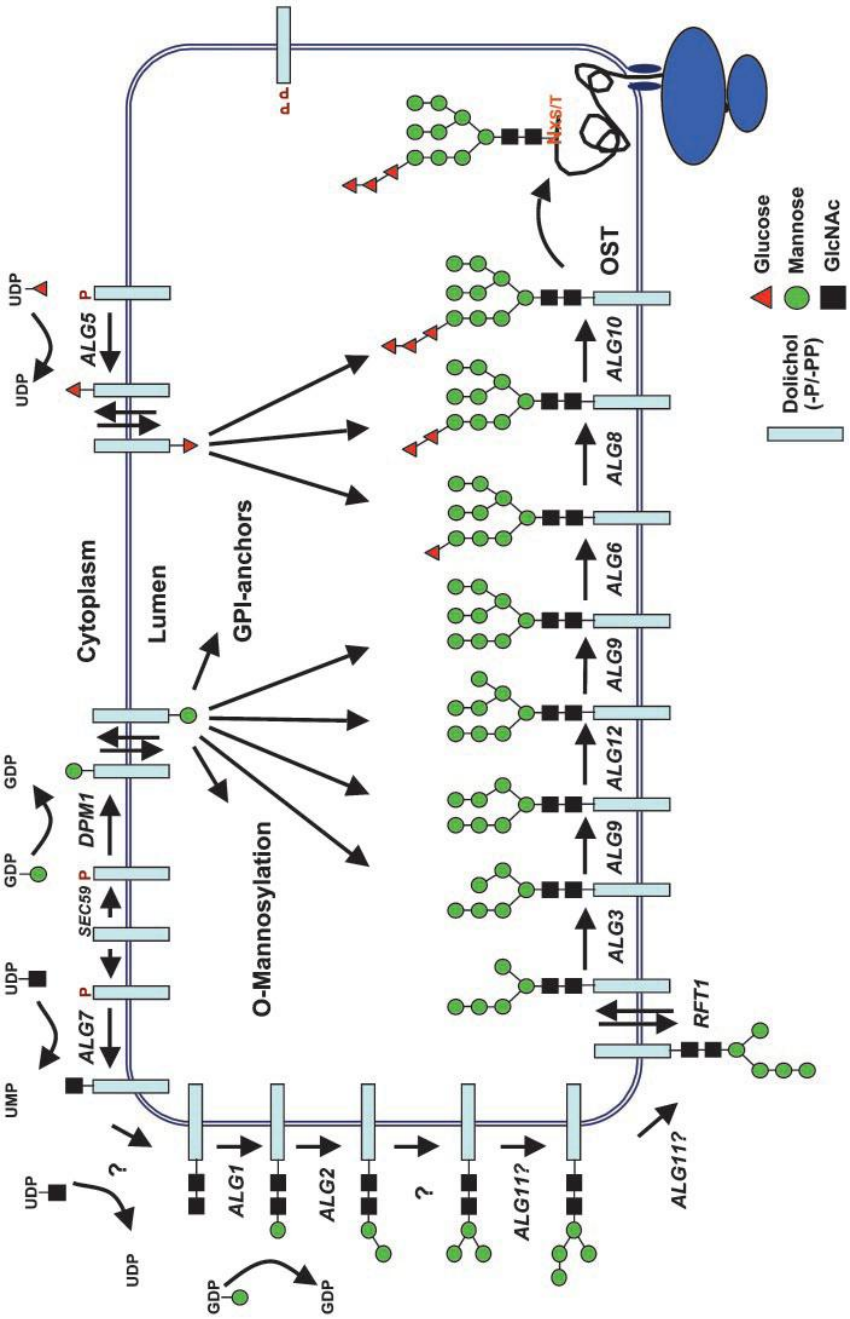

Figure 2: Biosynthetic scheme for *N*-glycans in the ER. The two GlcNAc residues followed by the first five mannose residues are added on the cytosolic service by monosacchoryl transferases. The dolichylpyrophosphate linked $Man_5GlcNAc_2$ is flipped to the luminal side where the remaining four mannose residues and three glucose residues are added. Once the $Glc_3Man_9GlcNAc_2$ structure is synthesized the oligosaccharide is transferred from the lipid carrier to the growing polypeptide by OST enzyme.[13]

The monosaccharides are first attached to a lipid carrier by monosaccharyl-transferases in the cytosol.[1,11] Once the heptasaccharide is synthesized, the sugar unit is rotated to the lumenal side catalyzed by an ATP-independent bi-directional flippase.[12] The glycosylase enzymes in both the lumenal and cytosol compartments of the ER are highly specific for individual sugar moieties; thus allowing for the linear synthesis of the branched oligosaccharide.[16] The final step in the core oligosaccharide synthesis is the addition of the terminal α-1,2-glucose residue which is essential for sufficient recognition by the OST enzyme that transfers the $Glc_3Man_9GlcNAc_2$ from the lipid carrier to the Asn side chain of the glycosylation sequon As*N*-X-Ser/Thr forming an *N*-glycosidic bond.[17,18] For many years it was widely accepted that this sequon was necessary because of the relatively chemically inert nature of the Asn side chain nitrogen.[19] The polypeptide would form a loop which allows for the side chain hydroxyls of Ser/Thr to interact with the amide side chain of Asn thereby increasing the nucleophilic nature of nitrogen. The need for this loop explained why the X amino acid could not be a proline residue do to the rigid cyclic side chain.[21,22] Once the $Glc_3Man_9GlcNAc_2$ is added to the polypeptide, protein folding can commence. However, recent studies preformed by Locher and co-workers[47] brought new insights to the OST mode of action. The catalytic subunit, STT3, of the OST enzyme has homologues in bacteria and archea. Locher and coworkers obtained an x-ray crystal structure of a bacterial OST in complex with an acceptor protein (Figure 3).[47]

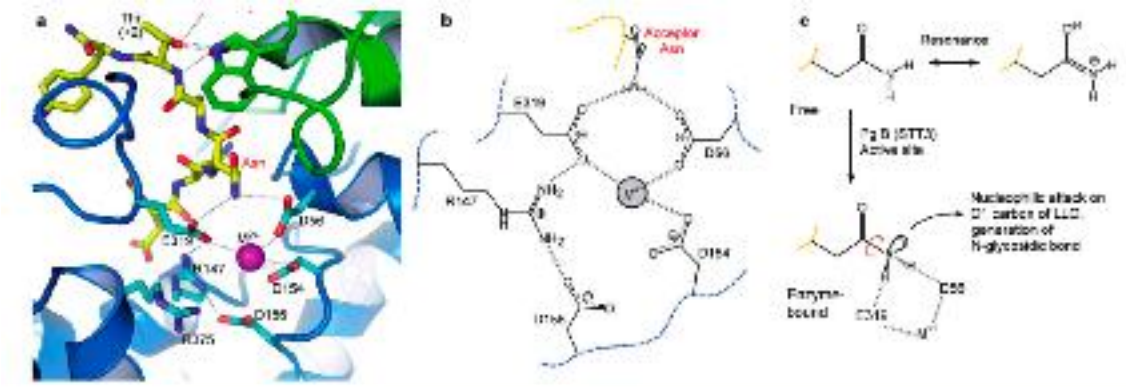

Figure 3. **Catalytic site and amide nitrogen activation**. **a**, Transmembrane and periplasmic domains of PglB are coloured blue and green, respectively. Selected side chains are in ball and stick representation, with carbon atoms coloured cyan and green for transmembrane and periplasmic domain residues, respectively, and yellow for receptor peptide. Grey dashed lines indicate hydrogen bonds or intereactions with divalent cation M^{2+}. **b**, Chemical structure of the catalytic site, indicating interactions as in **a**. Blue and yellow dashed lines indicate transmembrane domain and peptide backbones, respectively. **c**, Presumed mechanism of amide nitrogen activation. Yellow dashed lines indicate peptide backbone. The amido group of free acceptor Asn features electron delocalization, indicated by resonance. When bound to PglB, the amido group may form hydrogen bonds with the catalytically essential D56 and E319, requiring rotation around the C-N bond (red arrow). [47]

As previously discussed in this section, previous explanations for the amide activation included direct involvement of the Ser/Thr residues; however, this new X-ray structure illustrates that the Thr residue is firmly bound to the side chains of the STT3 protein and not involved with the amide motif (figure 3a).[47] Locher and coworkers propose that the Asn residue forms hydrogen bonds with STT3 and through the rotation required for these interactions the double bond character of the amide residue is abolished, thus increasing the nucleophilicity of the nitrogen (figure 3b-c).[47] These findings offer new insights to the catalytic mechanism of the OST enzyme.

N-Glycans Direct and Indirect Roles in Glycoprotein Folding

The large, polar carbohydrate moiety directly affects the properties of the polypeptide chain and can profoundly change the conformation.[19] The polar saccharide unit is likely to affect local protein structure by orienting the polypeptide segment towards the surface of the protein domains. The sugar unit also limits the conformational space available for protein folding resulting in a more rigid structure. Furthermore, interactions between the acetamido group of the first GlcNAc residues and the polypeptide encourage β-turns. These interactions are believed to help stabilize and promote local structure in a peptide, as well as potentially effecting global folding. In comparisons studies of native glycoproteins verse the no*N*-glycosylated counter parts it was demonstrated that the presence of the glycan helps to increase stability, solubility, and resistance to proteases.[20-22] However, it is important to note that although the glycan aids in the initial protein folding the glycans are not usually important for maintaining the overall folded protein structure. It has been shown that when *N*-glycosylation is inhibited the most common effect is aggregation of misfolded proteins that never reach a functional state. The importance of the glycan on protein folding is highly dependent on the protein and the physiological context. Some proteins are completely dependent on glycosylation, others are semi-dependent where as others display no dependence at all. In some cases, each individual glycosylation site has been shown to be insignificant individually, but if all glycosylation sites are knocked out then the protein function is compromised. These findings again indicate that glycans play not only a role in local protein folding but also can have global effects.

Glycoproteins also bind to lectins in the ER which indirectly affect protein folding. It is thought that the glycans act as sorting signals that can be modified by the cell to reveal the folding status of a protein; thus giving glycans an indirect role in protein folding as well. The use of glycans as a sorting and quality control mechanism was postulated due to four main observations. The first being that *N*-linked glycans retain a glucose residue on the A branch of the glycan in misfolded glycoproteins, which undergoes de- and re-glucosidation.[43] The second, ER glucosyltransferase is selective for misfolded glycoproteins.[14] The third observation was that newly synthesized glycoproteins bind selectively to resident ER protein Calnexin.[45] The final observation was that the binding of the glycoprotein to Calnexin is blocked by ER glucosidase inhibitors.[46] These findings have lead to the widely accepted model of the Calnexin/Calreticulin Cycle.

Calnexin/Calreticulin Cycle

Binding to the Calnexin/Calreticulin cycle is one of the most important indirect effects that the *N*-glycans have on protein folding (Figure 4).[46]

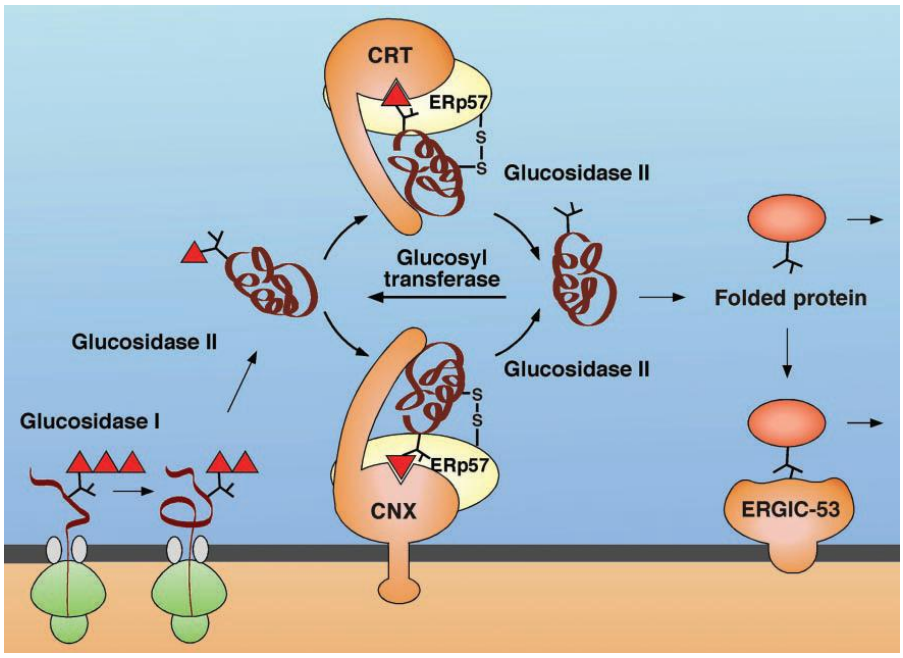

Figure 4: The Calnexin/Calreticulin cycle. Once the oligosaccharide is transferred to the polypeptide, the outermost glucose residues (n and m from figure 1) are rapidly removed. The mono-glucosidated structure is recognized by calnexin or calreticulin and the *N*-glycan binds to one of the lectins. Once bond, the glycoprotein is exposed to ERp57, an ER cofactor, that promotes protein folding through disulfide bond formation. Once the glycoprotein has folded, the final glucose residue is cleaved and the glycoprotein is released from the lectin. If the Glycoprotein is not folded then the *N*-glycan is re-gucosylated and sent through the calnexin/calreticulin cycle again. [46]

The *N*-glycan acts as a signaling system for binding to the lectins in the ER acting as a pre-requisite for entry into the cycle. Once the $Glc_3Man_9GlcNAc_2$ is covalently attached to the protein the outer most glucose residue is rapidly removed by ER-Glucosidase I, with subsequent removal of the second glucose residue by ER-Glucosidase II. The monoglucosylated core glycan then acts as a binding ligand to Calnexin or Calreticulin lectin. Calnexin, being a membrane bound lectin, and Calreticulin, being a soluble lectin, both are homologous ER lections that transiently bind to nearly all newly synthesized glycoproteins. These two lectins serve as molecular gate keepers preventing

aggregation as well as export of incompletely folded proteins from the ER. Both lectins are highly asymmetric and contain a long, curved hydrophilic peptide arm. This arm is thought to interact with co-chaperones or form a region to protect the bound substrate against premature degradation; however, it is not believed to form the glycoprotein binding site.[23-27] The Calnexin/Calreticulin cycle not only protects glycoprotein from premature degradation, but also exposes the substrates to ERp57, an ER cofactor that is a thiol-disulfide oxidoreductase. This cofactor aids in proper disulfide formation during the ongoing folding process in the ER. ERp57 temporarily creates disulfide bonds between the cysteine residues of the Calnexin/Calreticulin bound glycoprotein and itself resulting in key intermediates in oxidation and isomerization events that lead to the formation of correctly paired disulfide bonds between cysteine residues within the glycoprotein. Although the interaction with the Calnexin/Calreticulin cycle tends to slow down the rate of the folding process there tends to be an increase in folding efficiency. The release of the glycoprotein form the cycle is obtained once ER-Glucosidase II removes the final glucose residue. If the glycoprotein has reached its native conformation then it is exported to the Golgi apparatus, however, if the glycoprotein is still misfolded then it is recognized by ER-Glucosyltransferase (ER-GT) enzyme. The ER-GT serves as a folding sensor for the glycoprotein because only incompletely folded glycoproteins are re-glucosylated.; at which point the glycoprotein can rebind to the Calnexin/Calreticulin cycle and continue the folding process. The glycoprotein can be de-glucosylated and re-glucosylated until it is properly folded, oligomerized, or degraded. If the glycoprotein fails to fold upon numerous turns through

this cycle then they are sequestered in the ER eventually degraded. This degradation process is known as ER-associated degradation (ERAD).

ER-Associated Degradation (ERAD)

The process known as ERAD is a biological process full of checks and balances. Misfolded and unassembled glycoproteins should be targeted for disposal, but folding intermediates should not. How does the ER distinguish between aberrant glycoproteins and glycoproteins that just have not completed the folding process? A widely accepted mechanism is that ERAD functions on a time scale. Newly synthesized proteins are given a lag period, usually 30-90 minutes, to allow them ample time to fold. Although the timer mechanism is widely accepted it does not explain how glycoproteins whose final destination is the ER are not degraded after the lag period. To explain this aspect, it is proposed that the timer mechanism works in conjunction with a folding sensor. It has been shown that the ERAD process is delayed by the trimming of the mannose residues on the core glycan structure. The most important mannosidase in the ER is ER-α-mannosidase I (ER Man I) which is responsible for selectively removing the terminal mannose residue (i) of the B branch of the core glycan.[35] It has been shown that if the ER Man I is genetically mutated or inhibited by a mannosidase inhibitor, then glycoprotein degradation is significantly slower.[37] On the other hand, if ER Man I is over expressed then the degradation process is increased.[38] ER Man I is a slow acting enzyme and is likely to act as the timer protecting newly synthesized glycoproteins from early degradation. Once the mannose is trimmed from the B branch by ER Man I, it is thought that ER degradatio*N*-enhancing α-mannosidase-like protein (EDEM) competes with the Calnexin/Calreticulin cycle for substrates.[44] Therefore, impairing ER Man I could give

the glycoprotein more time to reach the native conformation before being recognized be ERAD and sent to the cytosol for disposal.

Diseases Associated with ERAD

Diseases associated with ERAD are usually caused by the ERAD machinery being overwhelmed by misfolded glycoproteins causing a buildup of aberrant proteins in the cellular matrix. The molecular basis for several human diseases such as cystic fibrosis, familial hypercholesterolemia, a heritable form of pulmonary emphysema and many others can be associated with the ERAD process (Table 1).

Table 1: A selection of diseases associated with ERAD

ERAD Substrate	**Associated Disease**
a_1-protease inhibitor	Emphysema liver disease
Aquapori*N*-2	Nephrogenic diabetes insipidus
β-hexosaminidase	Tay-Sachs disease
CD4	AIDS
Collagen	Osteogenesis Imperfecta
Connexin	Charcot-Marie-tooth disease
DF508 CFTR	Cystic fibrosis
Fibrinogen Familial	hypofibrinogenemia
HMG-CoA reductase	Heart disease

Some heritable forms of pulmonary emphysema are caused by impaired secretion of misfolded genetic variants of human α_1-antitrypsin (AAT) from the liver hepatocytes. Human AAT helps protect lung elastin fibers from elastolytic destruction. This monomeric glycoprotein is part of the serine proteinase inhibitor superfamily and defective intracellular transport of misfolded glycoproteins diminishes the levels of this

inhibitor in the system. Lower levels of AAT result in the elastolytic destruction of lung elastin. It has been observed that multiple rounds of binding to the Calnexin cycle are required for proper folding of the newly synthesized AAT glycoproteins into functional conformations. Sifers *et. al*. investigated the role of intracellular ER mannosidases in the quality control machinery of the cell by looking at the intracellular degradation of misfolded AAT. It was determined that modification of the glycoprotein by ER Man I mediates the proteosomal degradation of terminally misfolded AAT. Their findings provided insight that ER Man I activity plays a significant role in glycoprotein folding and quality control.

Inverting and Retaining Enzymes

There are two major mechanisms in which almost all glycosidic bonds can be hydrolyzed by an enzyme: inverting and retaining. Both mechanisms require two residues, a proton donor and a nucleophile/base (Figure 5). The proton donor is positioned above the sugar residue and within hydrogen bonding distance of the anomeric

oxygen for both mechanisms.

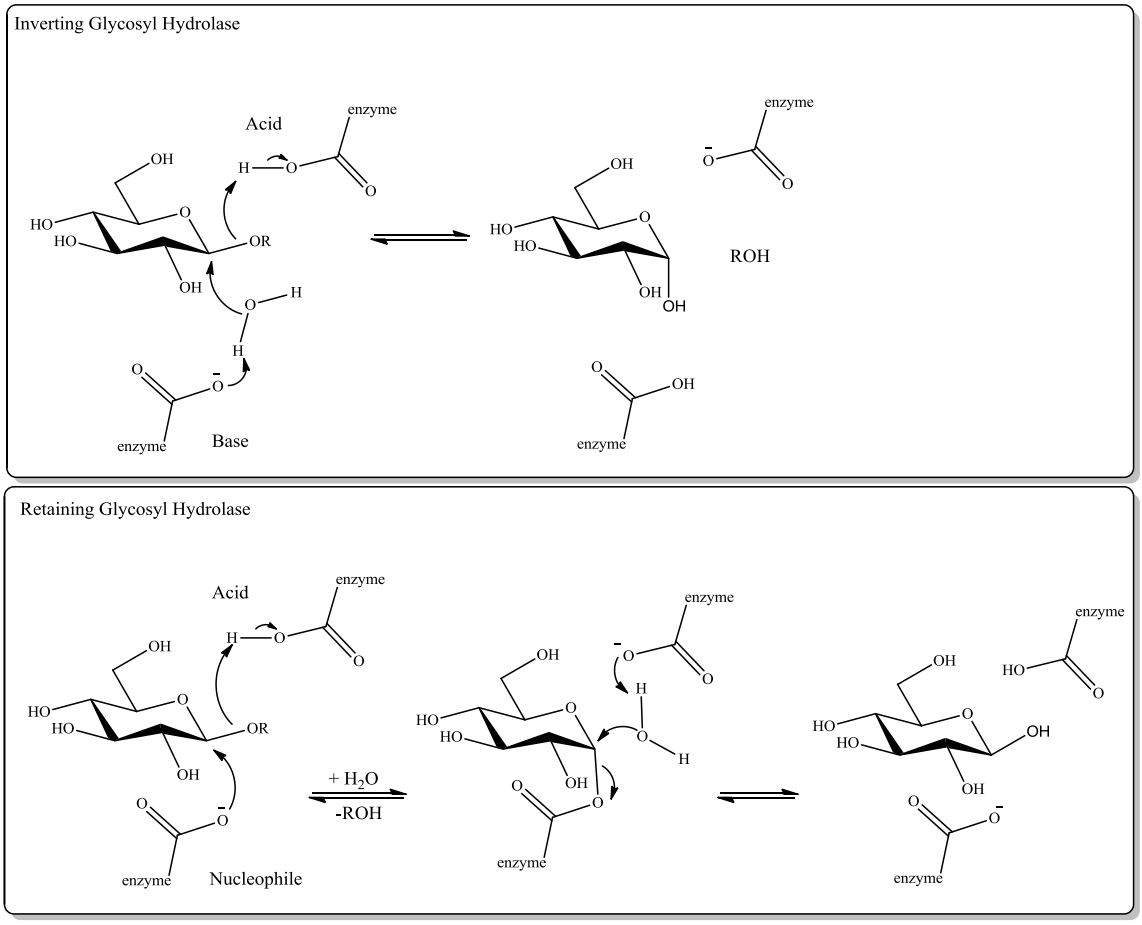

Figure 5: General inverting and retaining enzyme mechanisms for most glycosidase enzymes.

The difference in the mechanisms occurs on the base/nucleophile side. In an inverting mechanism, the enzyme residue acts as a base and will deprotonate a water molecule which subsequently attacks the anomeric center displacing the ligand. The distance between the enzyme residue and the sugar molecule must be large enough to accommodate a water molecule. On the other hand, the enzyme is much closer to the sugar molecule in the retaining mechanism due to the enzyme acting directly as the nucleophile. Once the ligand is displaced a water molecule can attack the anomeric

center, releasing the enzyme and resulting in a sugar residue with the original anomeric configuration.

The catalytic mechanism and classification of these enzymes is dependent on sequence similarities, and preferred substrates. However, inverting and retaining enzymes can be further classified into CAZy glycosyl hydrolase (GH) families based on product stereochemistry, bond specificity, and inhibitor structure. Therefore, α-mannosidases within the same CAZy GH family will have remarkably similar catalytic binding domains and substrate specificity.

Glycosyl Hydrolase Family 47 (GH 47)

Although nearly all glycosidase enzymes have the two common inverting or retaining mechanisms previously discussed, GH47 mannosidases have a distinct catalytic mechanism setting them apart from other glycosidases. The GH47 family contains three subfamilies: ER Man I, Golgi Man IA-IC (α-1,2-mannosidases), and EDEM1-3 (ER stress induced proteins). ER Man I is believed to play a vital role in *N*-glycan biosynthesis and degradation.

To help determine the catalytic mechanism of GH47 enzymes Dr Moremen and coworkers evaluated the conformational changes of the glycan during hydrolysis and the various residues involved in the process.[49] Figure 6 demonstrates the unusual $^{1}C_{4}$ conformation that the inhibitor substrate (dMNJ) adopts in the catalytic site.[49,50]

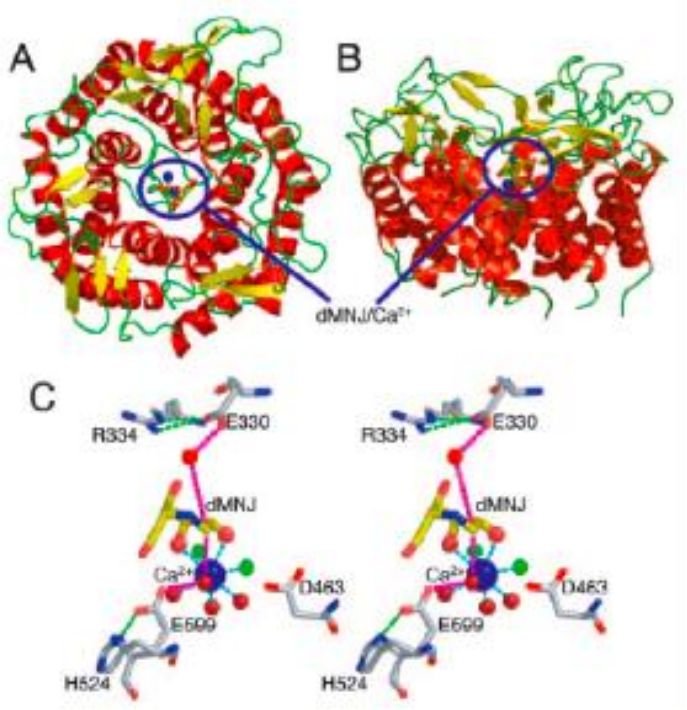

Figure 6: Model for the structure and catalytic residues for ER Man I used in mutagenesis studies described in this paper. The structure of the co-complex between human ER Man I and dMNJ (PDB 1FO2(20)) was used to select potential residues involved in catalysis. The end (A) and side (B) views of the human ER Man I *ribbon diagram* display the $(\alpha\alpha)_7$ barrel structure with the inhibitor (dMNJ;*stick representation*) bound in the core of the barrel directly coordinated to the protei*N*-bound Ca^{2+} ion (*blue space fill*) as highlighted by the *blue circle*. The residues examined in this study are shown in the stereo diagram (C), where the *stick representation* of dMNJ is shown in yellow, the Ca^{2+} ion is shown in *blue space fill,* and the relevant residues described throughout are shown as *white stick diagrams.* The *small red space fill structures* connected through *cyan dotted lines* to the Ca^{2+} ion are water molecules that coordinate Ca^{2+} ion. The *small green space fill structures* connected through *cyan dotted lines* to the Ca^{2+} ion represent the carbonyl oxygen and O-γ- of Thr^{688}, the only protein residue directly coordinated to the Ca^{2+} ion. Proposed acid, base and nucleophile trajectories as described throughout are illustrated with *magenta dotted lines.* Hydrogen bonds between Glu^{330} and Arg^{334} as well as Glu^{599} and His^{524} are shown as *green dotted lines.*[49]

Moremen and co-workers describe a unique inverting hydrolytic mechanism in which a novel $^{3}H_{4}$ sugar conformation is proposed for the exploded transition state.[49]

Although the GH47 enzymes have been implicated in nascent glycoprotein disposal, their roles and actual involvement is under investigation. Therefore, the development of a selective inhibitor that could distinguish between the various GH47 enzymes would not only be a target for drug development but would also aid in the understanding of the degradation pathway.

Mannosidase Inhibitors

Polyhydroxylated iminosugars are widely known as strong glycosidase inhibitors and have demonstrated promising results as therapeutic agents. Although iminosugars are strong glycosidase inhibitors there have been limited successful mannosidase inhibitors developed (Figure 7). The lack of safe and efficacious glycosidase inhibitors is largely dictated by the promiscuity and lack of selectivity towards glycosidase families inherent of these iminosugars. There are many potent inhibitors in the literature and modification of these known substrates with motifs to increase selectivity is a promising avenue for drug development.

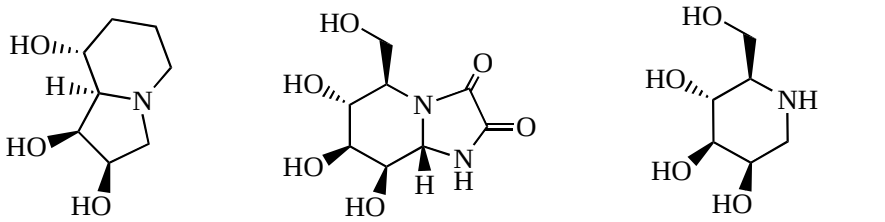

Figure 7: Known α-mannosidase inhibitors

Numerous α-mannosidase inhibitors have been discovered from natural sources as well as manually synthesized. 1-Deoxymannojirimycin was isolated from legume *Lonchocarpus sericeus*. Originally thought to selectively inhibit Golgi mannosidase enzymes, however recent studies have determined that DMJ does in fact inhibit both the ER and Golgi mannosidases; however, the potency of DMJ is limited. The poor inhibition can be attributed to the flexibility of the substrate leading to an entropically unfavorable interaction due to the large amount of energy required to obtain the $^{1}C_{4}$ conformation needed in the binding pocket.

Swainsonine, an indolizidine alkaloid, was the first reported glycoprotein processing mannosidase inhibitor and was found to be a potent Golgi α-mannosidase II (GMII) inhibitor. GMII is a GH 38 family enzyme and is a key enzyme in the Golgi processing pathway responsible for the trimming of two mannose residues. Kuntz and co-workers published co-crystal structures of DMJ and swainsonine bound in the catalytic site of GMII (figure 8) .[50]

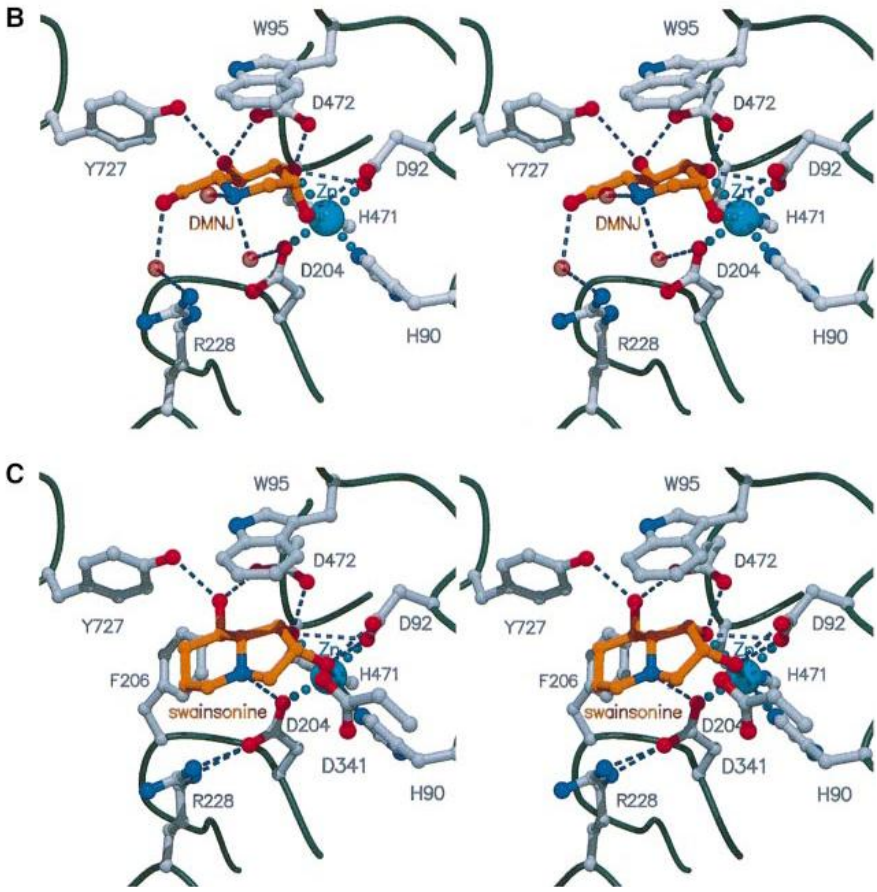

Figure 8: **Stereo views of the active site of dGMII with bound DMJ (B) and swainsonine (C) molecules.** The active site zinc ion is shown in turquoise, the bound inhibitor molecules are rendered in gold and water molecules are represented as transparent red spheres. Interatomic distances <3.2 angstom are shown as blue dashed lines. [50]

Through analysis of the co-crystal structures, one can see why swainsonine is a potent GH38 inibitor with an IC_{50} of 20 nM, and DMJ is a weak inhibitor with an IC_{50} of 400 μM.[50] The naturally occurring transition state for the mannose residue is a scewed boat conformation and the mannosyl residue undergoes standard retaining mechanism hydrolysis in which Asp204 is thought to act as the nucleophile. Although both inhibitor structures bind to the catalytic site in a similar manner a look at the specific binding forms gives insight into the drastic change in inhibitory properties. During substrate

binding to the enzyme, binding of the C2 and C3 hydroxyls of swainsonine to the Zn ion flattens the 5-membered ring of swainsonine. Flattening of this ring causes the molecule to orient in such a way that the bridge head nitrogen, which mimics C1 in the natural substrate, is brought significantly closer to the nucleophilic Asp204. On the other hand, a look at DMJ in the binding site illustrates that the endocyclic nitrogen is oriented farther away from the nucleophilic amino acid residue Asp204 caused by the O2 and O3 hydroxyls coordinating with the Zn ion. These differences in orientation could lead to the significant difference in potency between swainsonine and DMJ.

Although swainsonine was shown to reduce tumor growth and metastasis with limited side effects in preliminary clinical trials for treatment of late-stage cancer, swainsonine was later found to inhibit lysosomal mannosidases when tested *in vivo*; thus resulting in the animals developing lysosomal storage disease symptoms.

Kifunensine was discovered in actinomycete *Kitasatosporia kifunense* 9482, and is an alkaloid corresponding to the cyclic oxamide derivative of 1-amino mannojirimycin. Kifunensine has been reported to inhibit both the ER and Golgi mannosidase enzymes in nanomolar concentrations; thus making it one of the most potent and effective glycoprotein processing inhibitors to date for GH47 enzymes. The bicyclic nature of KIF naturally locks the substrate in the $^{1}C_{4}$ conformation making the substrate an entropically favorable inhibitor that mimics the transition state of the naturally occurring mannosyl residue. However, this compound is not selective and will inhibit both the ER and Golgi enzymes.

Through modification of Kifunensine there is a potential to synthesize new potent and selective inhibitors. The two most common methods for iminosugars modification

are alkylation of the amine group and functionalization of the hydroxyls. Previous studies have shown that amide alkylations of Kifunensine were unable to increase selectivity while maintaining potency. A co-crystal structure of Kifunensine bound in the catalytic site of ER Man I has been published and gives insight as to why *N*-alkylation was not favorable. Upon examination of the co-crystal structure (Figure 9) it is evident that the amine group is positioned along the wall of the catalytic domain, thus leaving very little room for modifications.

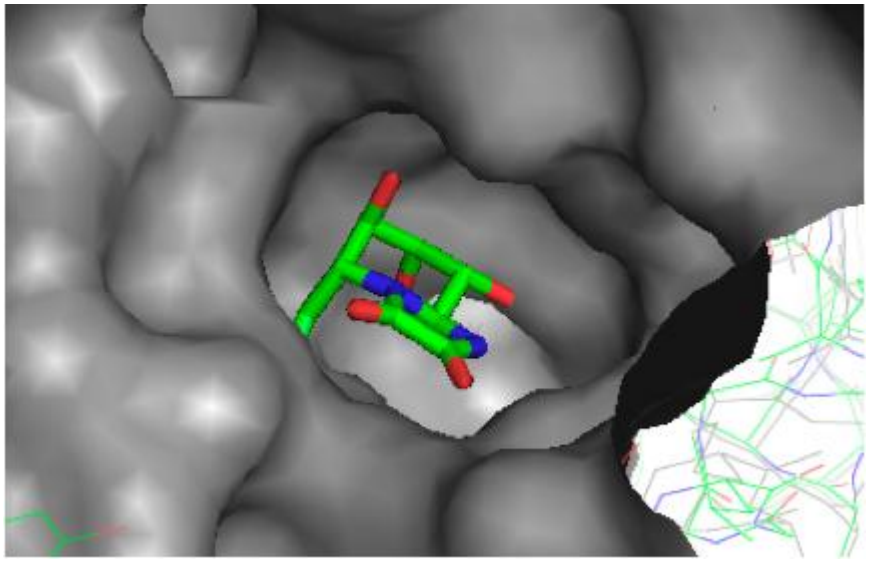

Figure 9: Co-crystal structure of Kifunensine in the binding pocket of ER Man I (adopted from a co-crystal structure obtained from Dr Kelley Moremens lab.)

However, a closer look at the co-crystal structure of KIF in the binding pocket of ER α-Man I indicates that the Carbonyl moieties may be a good handle for modification due to the orientation extending outside the binding pocket.

REFERENCES

1. Kornfeld R, Kornfeld S. Assembly of asparagine-linked oligosaccharides, *Annu. Rev. Biochem*, **1985**,*54*, 631-64.

2. Trombetta ES. Biological roles of oligosaccharides: all of the theories are correct *Glycobiology*, **1993**, *3*, 97-130.

3. Apweiler R, Hermjakob H, Sharon N. On the frequency of protein glycosylation, as deduced from analysis of the SWISS-PROT database, *Biochim. Biophys. Acta,* **1999**, *1473*, 4-8.

4. Wormald MR, Petrescu AJ, Pao YL, Glithero A, Elliot T, Dwek RA. Conformational Studies of Oligosaccharides and Glycopeptides: Complementarity of NMR, X-ray Crystallography, and Molecular Modelling, *Chem. Rev,* **2002,** *102,* 371-86.

5. Petrescu AJ, Milac A-L, Petrescu SM, Dwek RA, Wormald MR. Statistical analysis of the protein environment of *N*-glycosylation sites: implications for occupancy, structure, and folding, *Glycobiology*, **2004**,*14*,103-14.

6. Rudd PM, Wormald MR, Stanfield RL, Huang M, Mattsson N, et. Al. Roles for glycosylation of cell surface receptors involved in cellular immune recognition, *J. Mol. Biol.*, **1999**, *293*, 351-66.

7. Lowe JB, Marth JD. A Genetic Approach to Mammalian Glycan Function, *Annu. Rev. Biochem.*, **2003**, *72*, 643-91.

8. Weis WI, Drickamer K. Structural Basis of Lecti*N*-Carbohydrate Recognition, *Annu. Rev. Biochem.* **1996**, *65*, 441-73.

9. Lis H, Sharon N. Lectins: Carbohydrate-Specific Proteins That Mediate Cellular Recognition**,** *Chem. Rev.* **1998**, *98*, 637-74.

10. Burda P, Aebi M. The dolichol pathway of *N*-linked glycosylation, *Biochim Biophys. Acta.*, **1999**,*1426*, 239-57.

11. Hirschberg CB, Snider MD. Topography of glycosylation in the rough endoplasmic reticulum and Golgi apparatus, *Annu. Rev. Biochem,* **1987,** *56*, 63-87.

12. Helenius J, Ng DTW, Marolda CL, Walter P, Valvano MA, Aebi M. Translocation of lipid-linked oligosaccharides across the ER membrane requires Rft1 protein, *Nature*, **2002**,*415*, 447-50.

13. Balasubramanian K, Schroit AJ. Aminophospholipid asymmetry: A matter of life and death, *Annu. Rev. Physiol.*, **2003**, *65*,701-34.

14. Helenius J, Aebi M. Transmembrane movement of dolichol linked carbohydrates during *N*-glycoprotein biosynthesis in the endoplasmic reticulum, *Semin. Cell Dev. Biol,*. **2002**,*13*,71-78.

15. Burda P, Jakob CA, Beinhauer J, Hegemann JH, Aebi M. Ordered assembly of the asymmetrically branched lipid-linked oligosaccharide in the endoplasmic reticulum is ensured by the substrate specificity of the individual glycosyltransferases, *Glycobiology,* **1999**, *9*, 617-25.

16. Burda P, Aebi M. The ALG10 locus of Saccharomyces cerevisiae encodes the alpha-1,2 glucosyltransferase of the endoplasmic reticulum: the terminal glucose of the lipid-linked oligosaccharide is required for efficient *N*-linked glycosylation, *Glycobiology,* **1998**, *8*, 455-62.

17. Spiro RG. Glucose residues as key determinants in the biosynthesis and quality control of glycoprote, *J. Biol. Chem.,* **2000**, *275*, 35657-60.

18. Nilsson IM, von Heijne G. Determination of the distance between the oligosaccharyltransferase active site and the endoplasmic reticulum membrane, *J. Biol. Chem.*, **1993**, *268*, 5798-801.

19. Helenius A. How *N*-linked oligosaccharides affect glycoprotein folding in the endoplasmic reticulum, *Mol. Biol. Cell*, **1994,** *5*, 253-65.

20. Imberty A, Perez S. Stereochemistry of the *N*-Glycosylation Sites in Glycoproteins, *Protein Eng.*, **1995**, *8*, 699-709.

21. Wormald MR, Dwek RA. *Struct. Fold. Des.*, **1999,** *7*, R155-60.

22. Kundra R, Kornfeld S. Asparagine-linked oligosaccharides protect Lamp-1 and Lamp-2 from intracellular proteolysis, *J. Biol. Chem.*, **1999**, *274*, 31039-46.

23. Ellgaard L, Molinari M, Helenius A. Setting the standards: quality control in the secretory path- way, *Science,* **1999**, *286*, 1882-88.

24. Parodi A. Protein glucosylation and its role in protein folding, *Annu. Rev. Biochem.,* **2000,** *69*, 9-93.

25. Schrag JD, Bergeron JJ, Li Y, Borisova S, Hahn M, et al. The Structure of calnexin, an ER chaperone involved in quality control of protein folding, *Mol. Cell*, **2001**, *8*, 633-44.

26. Chevet E, Cameron PH, Pelletier MF, Thomas DY, Bergeron JJ. The endoplasmic reticulum: integration of protein folding, quality control, signaling and degradation, *Curr. Opin. Struct. Biol,*. **2001,** *11*, 120-24.

27. Ellgaard L, Helenius A. Quality control in the endoplasmic reticulum, *Nat. Rev. Mol. Cell Biol.*, **2003,** *4*, 181-91.

28. Tsai B, Ye Y, Rapoport TA. Retro-translocation of proteins from the endoplasmic reticulutn into the cytosol, *Nat. Rev. Mol. Cell Biol*, **2002**, *3*, 246-55.

29. Kostova Z, Wolf DH. For whom the bell tolls: protein quality control of the endoplasmic reticulum and the ubiquitin–proteasome connection, *EMBO J.*, **2003**, *22*, 2309-17.

30. McCracken AA. Evolving questions and paradigm shifts in endoplasmic-reticulum-associated degradation (ERAD), *BioEssays,* **2003**, *25*, 868-77.

31. Yoshida Y. A novel role for *N*-glycans in the ERAD system, *J. Biochem.* **2003,** *134*, 183-90.

32. Lippincott-Schwartz J, Bonifacino JS, Yuan LC, Klausner RD. Degradation from the endoplasmic reticulum: disposing of newly synthesized proteins, *Cell*, **1988**, *54*, 209-20.

33. Molinari M, Calanca V, Galli C, Lucca P, Paganetti P. Role of EDEM in the release of misfolded glycoproteins from the calnexin cycle, *Science,* **2003**, *299,* 1397-400.

34. Mancini R, Aebi M, Helenius A. Multiple endoplasmic reticulum-associated pathways degrade mutant yeast carboxypeptidase Y in mammalian cells, *J. Biol. Chem.*, **2003**, *278*, 46895-905.

35. Jakob CA, Burda P, Roth J, Aebi M. Degradation of misfolded endoplasmic reticulum glycoproteins in *Saccharomyces cerevisiae* is determined by a specific oligosaccharide structure, *J. Cell Biol.*, **1998**, *142*, 1223-33.

36. Herscovics A. Structure and function of Class I alpha 1,2-mannosidases involved in glycoprotein synthesis and endoplasmic reticulum quality control, *Biochimie,* **2001**, *83*, 757-62.

37. Liu Y, Choudhury P, Cabral CM, Sifers RN. Oligosaccharide Modification in the Early Secretory Pathway Directs the Selection of a Misfolded Glycoprotein for Degradation by the Proteasome, *J. Biol. Chem.*, **1999**, *274*, 5861-67.

38. Wu Y, Swulius MT, Moremen KW, Sifers RN. Elucidation of the molecular logic by which misfolded α1-antitrypsin is preferentially selected for degradation, *Proc. Natl. Acad. Sci. USA*, **2003,** *100*, 8229-34.

39. Jakob CA, Bodmer D, Spirig U, Battig P, Marcil A, et al. Htm1p, a mannosidase-like protein, is involved in glycoprotein degradation in yeast, *EMBO Rep.* **2001**, *2*, 423-30.

40. Nakatsukasa K, Nishikawa S, Hosokawa N, Nagata K, Endo T. Mnl1p, an α-Mannosidase-like Protein in Yeast *Saccharomyces cerevisiae*, Is Required for Endoplasmic Reticulum-associated Degradation of Glycoproteins, *J. Biol. Chem.*, **2001**, *276*, 8635-38.

41. Hosokawa N, Wada I, Hasegawa K, Yorihuzi T, Tremblay LO, et al. Mnl1p, an alpha -mannosidase-like protein in yeast Saccharomyces cerevisiae, is required for endoplasmic reticulum-associated degradation of glycoproteins**,** *EMBO Rep.* **2001**, *2*, 415-22.

42. van Anken E, Romijn EP, Maggioni C, Mexghrani A, Sitia R, et al. Sequential waves of functionally related proteins are expressed when B cells prepare for antibody secretion, *Immunity*, **2003**, *18*, 243-53.

43. Suh K, Bergmann JE, Gabel CA. Selective retention of monoglucosylated high mannose oligosaccharides by a class of mutant vesicular stomatitis virus G proteins. *J. Cell Biol.*, 1989, *108*, 811-19.

44. Sousa MC, Ferreri-Garcia MA, Parodi AJ. Recognition of the oligosaccharide and protein moieties of glycoproteins by the UDP-Glc: glycoprotein glucosyltransferase. *Biochemistry*, **1992,** *31*, 97-105

45. Ou WJ, Cameron PH, Thomas DY, Bergeron JJ. Association of folding intermediates of glycoproteins with calnexin during protein maturation. *Nature*, **1993,** *364*, 771-76.

46. Hammond C, Helenius A. Folding of VSV G protein: sequential interaction with BiP and calnexin, *Science*, **1994,** *266*, 456-58.

47. Lizal C, Gerber S, Numao S, Aebi M, Locher K. X-ray Structure of a Bacterial Oligosaccharyltransferase, *Nature*, **2011**, *474*, 350-55

48. Karaveg K, Siriwardena A, Tempel W, Liu ZJ, Glushka J, Wang BC, Moremen K. Mechanism of Class 1 (Glycosylhydrolase Family 47) a-Mannosidases Involved in *N*-glycan Processing and Endoplasmic Reticulum Quality Control, *J. Bio. Chem.*, **2005**, *280*, 16197-16207.

49. van den Elsen J.M.H., Kuntz D.A., Rose D.R. Structure of Golgi a-mannosidase II: a target for inhibition of growth and metastasis of cancer cells, *The EMBO Journal*, **2001**, *20*, 3008-3017.

CHAPTER 2

THE DEVELOPMENT OF SELECTIVE INHIBITORS FOR ER α-MANNOSIDASE I BY COMBINATORIAL MODIFICATION OF KIFUNENSINE

Jessica Cardot, Yong Xiang, Kelley Moremen, Geert-Jan Boons

To be submitted to J. Am. Chem. Soc.

Abstract

Selective inhibitors of endoplasmic reticulum α-mannosidase I (ER Man I) have the potential to be used for treatment of a number of genetic diseases. Although potent inhibitors for this enzyme have been described, in general these compounds display poor selectivity and often inhibit Golgi α-mannosidase I. To address this difficulty, we have synthesized and combinatorial modified kifunensine, which is a potent GH47 α-mannosidase I inhibitor. Thus, kifunensine was modified by a hydrazone moiety, which could easily be extended by reaction with a range of aldehydes. The library of hydrazone-linked analogues was screened for inhibition of human ER Man I and mouse Golgi Man I. It was found that a pyridine functionalized kifunensine analog selectively inhibited ER Man I. Based on this finding, a second generation of analogues was prepared in which a functionalized pyridine scaffold was coupled to kifunensine through a hydrazone moiety.

Introduction and Literature Review

N-glycans are widely expressed on the cell surface of eukaryotic cells and are responsible for many biological processes. Several diseases are specifically associated with disruption or breakdown of *N*-glycan biosynthesis, such as lysosomal storage disease and neurological disorders. [1, 2] The *N*-glycan biosynthetic pathway consists of a cascade of trimming and elongation steps performed by various glycosyl hydrolase and transferase enzymes. During this cascade, if a nascent protein is detected the endoplasmic reticulum contains a quality control mechanism known as endoplasmic reticulum associated degradation (ERAD) to ensure that only native glycoproteins are translocated to the Golgi apparatus for further elongation and expression. The nascent glycoproteins

are sequestered in the ER and translocated to the cytosol for disposal. [1, 2] ER-α-mannosidase I (ER Man I) is a predominant enzyme in ERAD and is responsible for the trimming of a specific mannose residue from the core $Man_9GlcNAc_2$ structure during the maturation of the glycoproteins. Several studies have shown that ER Man I inhibition results in a decrease in nascent glycoprotein disposal, whereas overexpression of ER Man I lead to an increase in glycoprotein disposal. These results lead to the proposed model that trimming of the $Man_9GlcNAc_2$ core to the $Man_8GlcNAc_2$ structure of nascent or incompletely folded glycoproteins was the rate-determining step in initiating glycoprotein disposal, thus making ER Man I a promising target for drug therapies for diseases associated with misfolded glycoproteins. [3, 4]

Although there are many glycosidases involved in *N*-glycan biosynthesis they can be categorized by two main catalytic subtypes; inverting and retaining mechanisms. Catalytic mechanism and classification is dependent mainly on sequence similarities, and preferred substrates. However, inverting and retaining enzymes can be further classified into CAZy glycosyl hydrolase (GH) families based on product stereochemistry, bond specificity, and inhibitor structure. Therefore, α-mannosidases within the same CAZy GH family will have remarkably similar catalytic binding domains and substrate specificity.

ER Man I is a GH47 enzyme that is believed to play a vital role in *N*-glycan biosynthesis and degradation. The GH47 family contains three subfamilies: ER Man I and Golgi Man IA-IC (α-1,2-mannosidases), and EDEM1-3 (ER stress induced proteins). GH47 enzymes are one of three GH families that are calcium dependent. Although the GH47 enzymes have been implicated in nascent glycoprotein disposal, their roles and

actual involvement is under investigation. Therefore, the development of a selective inhibitor that could distinguish between the various GH47 enzymes would not only be a target for drug development but would also aid in the understanding of the degradation pathway.

Polyhydroxylated iminosugars are widely known as strong glycosidase inhibitors and have demonstrated promising results as therapeutic agents. Although iminosugars are potent glycosidase inhibitors there have been limited successful therapeutics developed. The lack of safe and efficacious glycosidase inhibitors is largely due to promiscuity and lack of selectivity towards glycosidase families inherent of these substrates. Kifunensine, a naturally occurring alkaloid, is a potent GH47 α-mannosidase inhibitor, however, kifunensine cannot differentiate between different GH47 enzymes such as ER Man I and Golgi Man I.[7] Golgi Man I is a critical enzyme in *N*-glycan maturation and elongation, therefore inhibition of this enzyme is problematic for proper cellular function. [5] Due to the fact that there are many potent inhibitors in the literature, modification of these known compounds with motifs to increase selectivity is a promising avenue for drug development.

The two most common methods for iminosugar modifications are alkylation of the amine group and functionalization of the hydroxyls. Previous studies have shown that amine alkylations of kifunensine were unable to increase selectivity while maintaining potency.[10] A co-crystal structure of kifunensine bound in the catalytic site of ER Man I has since been published and gives insight to why *N*-alkylation was not favorable. Upon examination of the co-crystal structure it is evident that the amine group is positioned along the wall of the catalytic domain, thus leaving very little room for

modifications; however, the carbonyl groups are oriented in a plan that appears to be directed outside the catalytic site. We envisaged that modification of the kifunensine carbonyls with various functionalities could potentially increase selectivity while maintaining high potency. Here we report the first selective modification of the C2 carbonyl of kifunensine resulting in a selective potent inhibitor. Our strategy employed a chemoselective coupling between a kifunensine derivative functionalized with a hydrazone moiety at the C2 position. The hydrazone analogue was utilized as a lead substrate in the combinatorial synthesis of a small library of kifunensine analogues using a small selection of commercially available aldehydes. The resulting dihydrazone-based library was tested against GH47 inverting enzymes Human ER Man I, and Mouse Golgi Man I for selective inhibition. A pyridine functionalized KIF analogue demonstrated high selectivity and potency. The pyridine functionalized analogue underwent further biological testing to determine if the potency and selectivity would transfer from a mocrotiter plate assay to a cell study.

Results and Discussion

The initial challenge was to devise a synthetic strategy that could distinguish between the C2 and C3 carbonyls and allow selective installation of a chemical handle for diversification. This motif had to be highly selective and efficient to be a viable linker. A hydrazone group was determined to be an appealing option for library synthesis due to the highly selective and robust reaction with aldehydes, even in the presence of complex substrates.

Synthesis of Azidolactone

Commercially available L-gulonic-γ-lactone is an inexpensive starting material that allows for the synthesis of compound **6** in five synthetic manipulations. The first step was isopropylidene protection of the two diols with copper sulfate, acetone with a catalytic amount of sulfuric acid to achieve the desired bisacetonide **2** in a quantitative reaction.[8] Selective removal of the 5,6-*O*-isopropylidene of **2** by treatment with acetic acid/water (7/1), at room temperature, afforded compound **3** in 93 % yield. Silyl protection of the primary alcohol using *tert*-butyldimethylsilyl chloride (TBS-Cl) and imidazole in DMF furnished silyl ether **4** in 89 % yield.[9] The secondary alcohol underwent intermediate triflation by treatment with triflic anhydride and pyridine in DCM. The crude triflate was charged with sodium azide in DMF to afford the desired azidolactone **6** in 72 % yield over two steps.[9, 10] (Scheme 1)

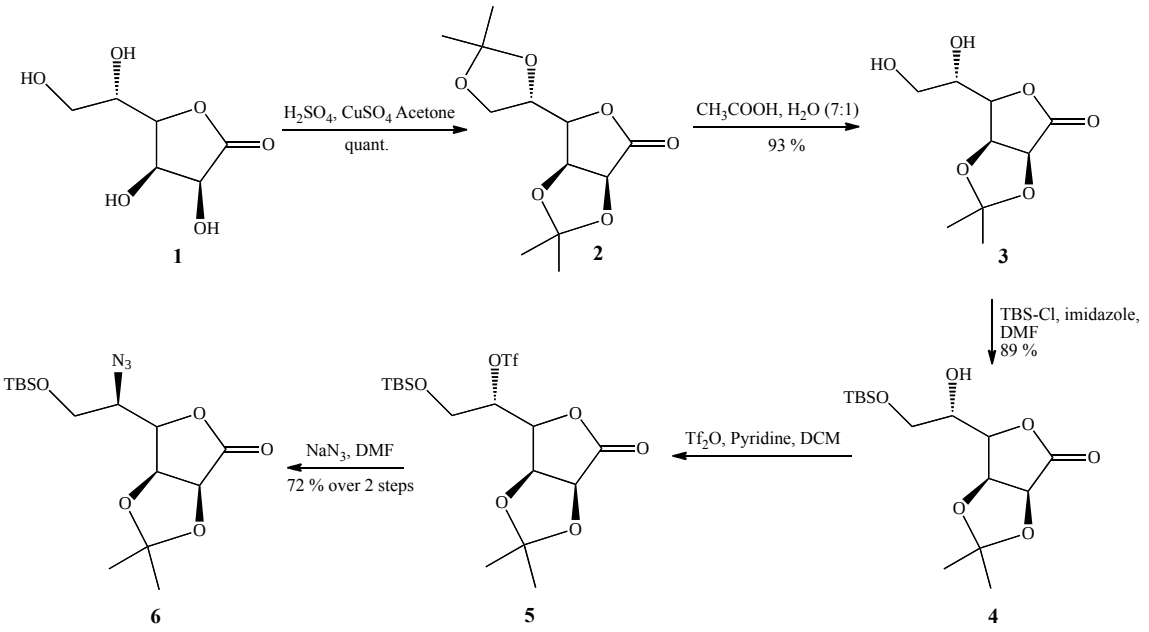

Scheme 1: Synthetic scheme for azido lactone **6.**

Synthesis of Bisacetonide KIF

Reduction of lactone **6** using sodium borohydride afforded diol **7** in 85 % yield**,**[11] which underwent selective protection of the primary alcohol as a pivaloyl ester using Piv-Cl and pyridine to give **8** in an 80 % yield. The silyl ether of **8** was selectively removed by treatment with TBAF in THF to afford a second diol, which was transformed into acetonide **9** using 2-methoxypropene and catalytic PTSA in 92 % yield.[12] Treatment of **9** with lithium aluminum hydride effectively reduced both the azide and ester moieties to achieve the essential amine **10** in a 90 % yield. Under standard peptide coupling conditions, using HOBt and EDC, oxamic acid was coupled to amine **10** affording the precursor to bisacetonide KIF, diamide **11**.[13] The yield of the coupling reaction ranged from 70-90 % yield depending on the quality of EDC and MP-carbonate used. DMP oxidation of the primary alcohol to an aldehyde allowed for the subsequent cyclization of the diamide in the presence of ammonia in methanol to afford bisacetonide KIF **12** in a yield of 33-55 % over two steps.[10] This reaction relies on the quality of DMP as well as ensuring removal of excess DMP and the DMP by-product formed during the oxidation prior the introduction of ammonia, which is difficult do to since the intermediate aldehyde decomposes on silica gel (Scheme 2).

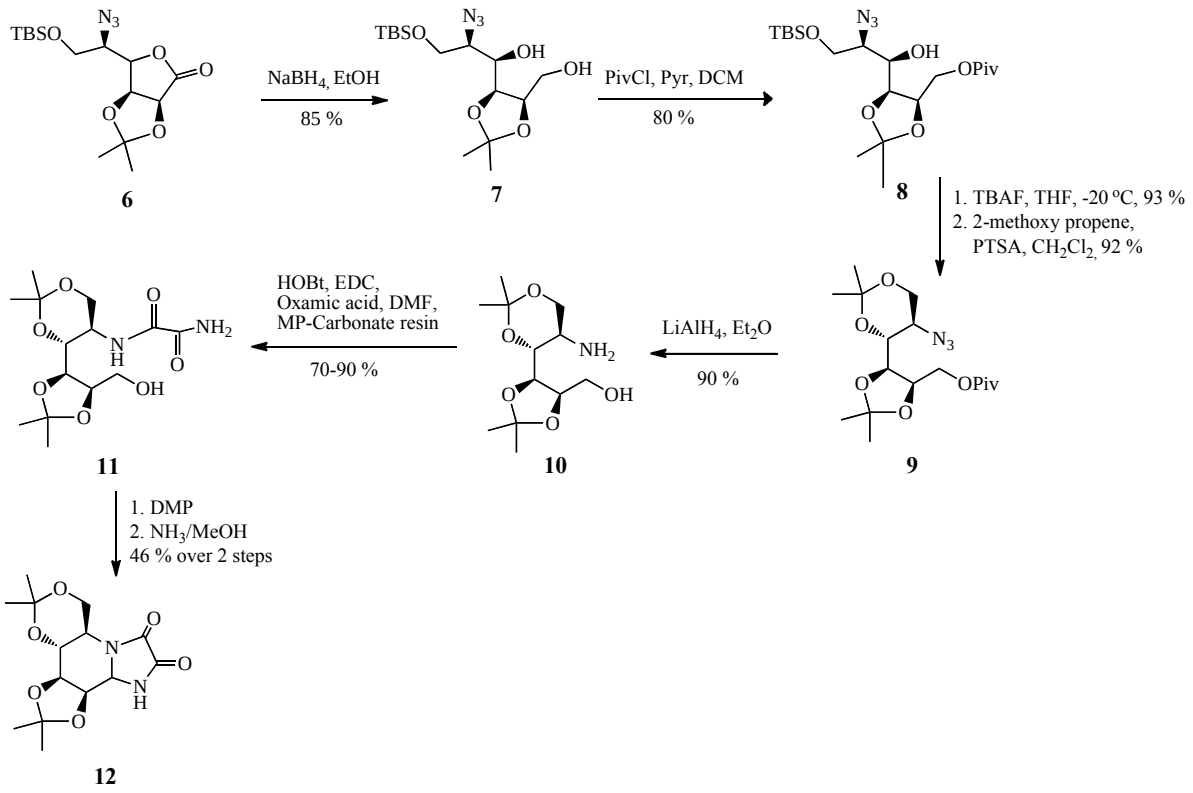

Scheme 2: Synthesis of bisacetonide Kifunensine

Synthesis of Novel Hydrazone Modified KIF

The synthesis of a novel hydrazone KIF began with the selective thionation of the C2 carbonyl of KIF utilizing Lawesson's reagent. During the reaction, the secondary amide of the C2 position coordinates with the Lawesson's reagent fascilitating the transformation preferentially occurring at the C2 position and not the C3 carbonyl. Once **12** was synthesized, the bicyclic diamide was subjected to Lawesson's thionation reagent, which converted the secondary amide into thioamide **13** in yields ranging from 65-90 %. The success of this reaction relies on two features, i: that any remaining DMP/by-products from the previous reaction are removed, and ii: that the Lawessons reagent is of high quality.[14] Deprotection of **13** with 75 % TFA/water to deblock the acetonide protecting groups resulted in the formation thioKIF in quantitative yields. Treatment of

14 with hydrazine hydrate resulted in the hydrazone analogue **15** in 83 % yield.[15] Hydrazone KIF is a suitable candidate for combinatorial modification (Scheme 3).

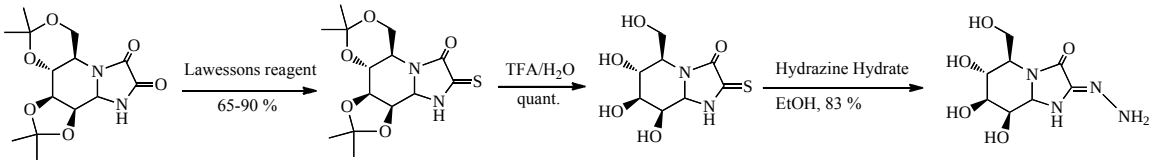

Scheme 3: Synthesis of novel Hydrazone KIF

Synthesis of Novel Kifunensine Analogues

With the successful synthesis of hydrazone functionalized KIF and the purchase of fourteen different aldehydes including aromatic, heterocyclic, and aliphatic aldehydes, a small library of dihydrazone functionalized KIF analogues was synthesized. Hydrazone **15** was dissolved in 1 % AcOH in DMSO followed by the addition of the selected aldehyde (Figure 10).

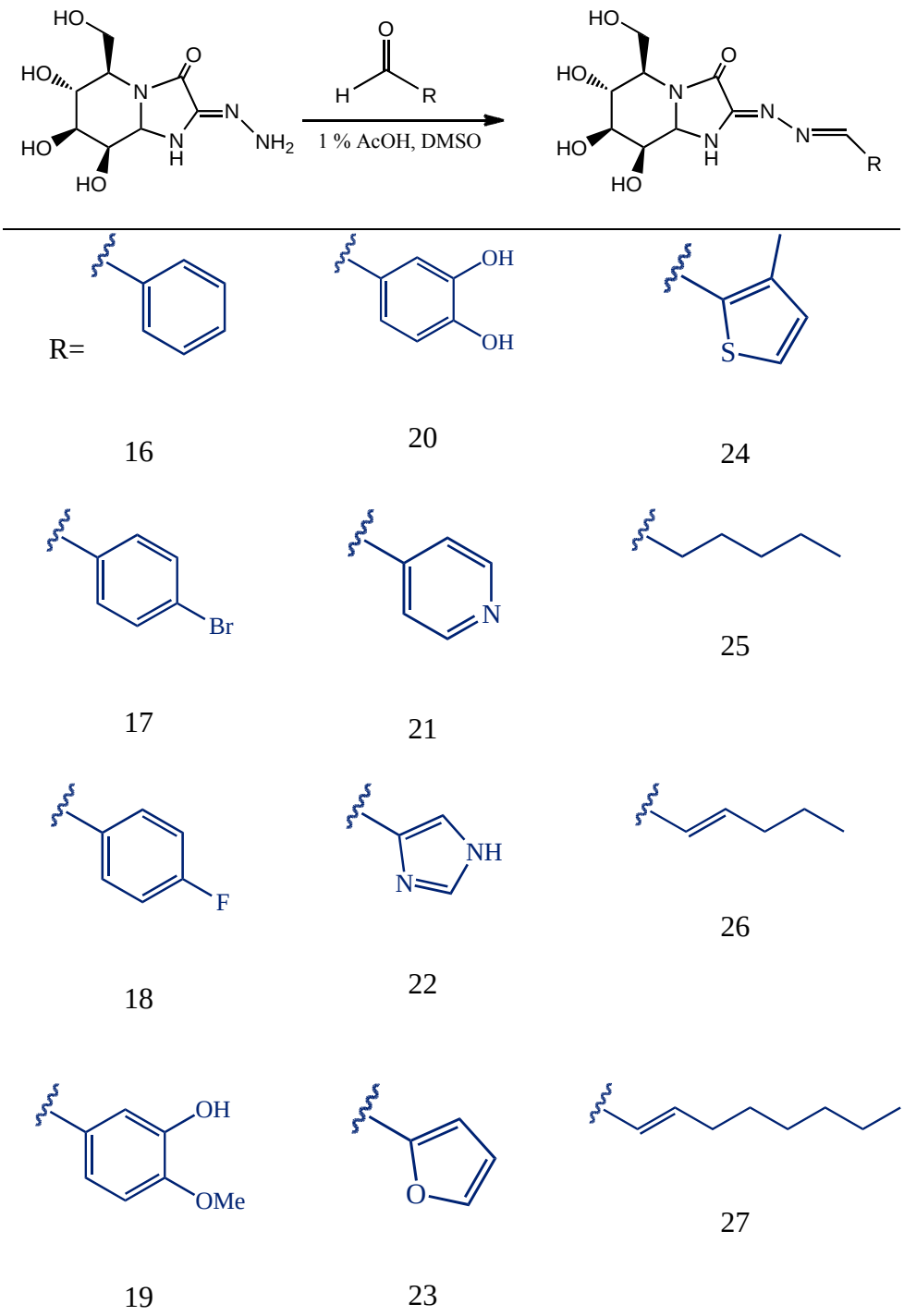

Figure 10: Structures of compounds in initial library screening, **15-27**

The reaction was monitored by HRMS-MALDI-TOF. Once complete, the compounds were purified by HPLC and screened for inhibition and selectivity towards ER Man I, and Golgi Man I. (Table 2).

Table 2: K_i Inhibition data for kifunensine analogues **15-27.**

Inhibitor	ER Man I (μM)	Golgi Man I (μM)	Golgi/ER
Kifunensine	0.06	0.08	1.0
Hydrazone (**15**)	0.83	0.68	1.0
16	1.94	3.10	1.5
17	2.31	1.30	0.5
18	0.93	2.32	2.5
19	1.70	0.86	0.5
20	0.27	0.98	3.5
21	0.07	0.66	9.5
22	0.69	2.10	3.0
23	1.60	2.00	1.5
24	1.05	2.40	2.5
25	1.62	1.90	1.0
26	1.00	1.92	2.0
27	1.50	2.00	1.5

The initial modification to kifunensine with a hydrazone moiety resulted in approximately a 10-fold decrease in activity along with no selectivity. It is known that many proteins contain phenylalanine, tryptophan, and tyrosine residues each of which contain an aromatic side chain. The aromatic substituents are generally buried within the more hydrophobic core and help stabilize the structure of the protein through pi-pi stacking interactions. With this in mind, a range of aromatic substituents was coupled to Kif through the hydrazone linker in order to promote possible pi-pi stacking interactions

within the catalytic site. A baseline reaction with benzaldehyde, **16**, resulted in a decrease in activity. Moderately deactivated aromatic substituents, compounds **17** and **18**, had comparable inhibition to **16**, but were still less effective than both kifunensine and the hydrazone. A moderately activated aromatic substituent, containing an electron donating hydroxy functionality, **19,** resulted in a minor increase in activity. Although **19** had comparable activity to the hydrazone, no selectivity was achieved. The more strongly activated diol substituted aromatic compound **20** resulted in a 4-fold increase in activity compared to the hydrazone along with 3-fold selectivity towards the ER-Man I enzyme. These results indicate that a more electron rich aromatic ring has more favorable interactions with the ER-Man I catalytic site in respect to the more electron deficient aromatics.

Heterocyclic aromatic rings were then investigated. The pyridine functionalized analogue **21** demonstrated a significant increase in activity compared the hydrazone analogue with a K_i of 0.07 μM for ER Man I, which is the same as kifunensine. Interestingly, analogue **21** had a K_i of 0.66 mM for the Golgi Man I enzyme, resulting in a 9.5-fold preference to the ER enzyme over the Golgi enzyme. To date, this is the first selective inhibitor for ER-Man I that maintained potency. The introduction of the ring nitrogen in analogue **21** led to a 28-fold increase in activity for the ER enzyme and only a 4.5-fold increase in activity for the Golgi enzyme, as seen in the comparison of analogues **16** and **21**. These two analogues have comparable configurations but differ in electronics. In contrast to benzene, the electron density of pyridine is not evenly distributed resulting in a dipole, as well as the nitrogen is slightly basic, one or both of these properties may influence the increased binding affinity.

A series of analogues containing heterocyclic aromatic substituents was synthesized including imidazole (**22**), furan (**23**), and thiophene (**24**) functionalized kifunensine. Of these heterocycles, the imidazole functionalized derivative demonstrated the best results with an ER Man I K_i comparable to the parent hydrazone, as well as 3-fold selectivity towards the ER. These results indicate that the nitrogen atom plays a key role in the interactions between enzyme and substrate

Long aliphatic chain substituents, analogues **25**, **26**, and **27**, were synthesized and yielded no selectivity, and low potency.

A small library of functionalized pyridine analogues was synthesized from commercially available aldehydes to investigate substituent effects on potency and selectivity (Figure 11).

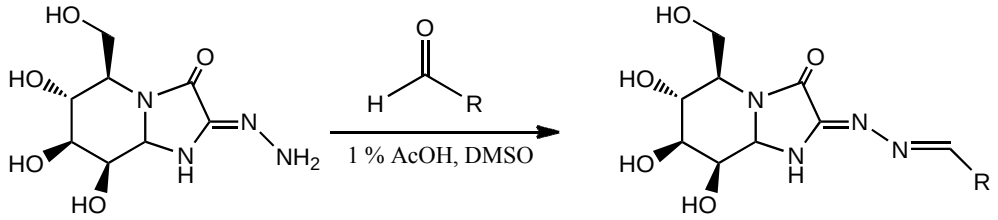

R =

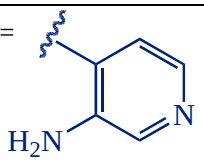

28

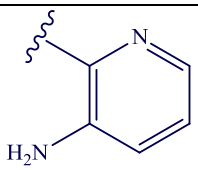

29

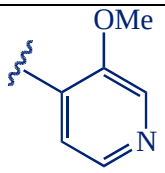

30

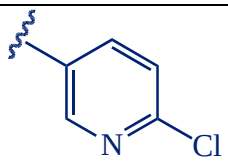

31

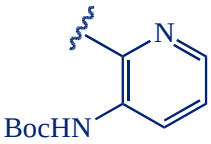

32

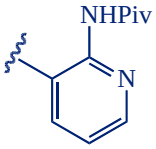

33

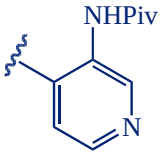

34

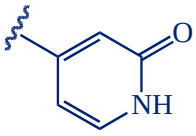

35

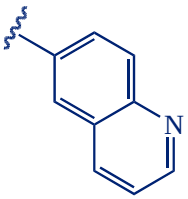

36

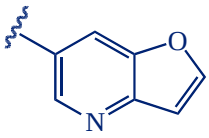

37

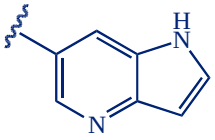

38

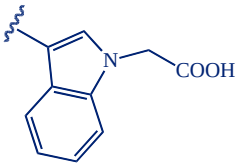

39

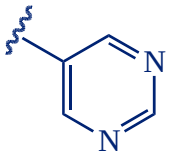

40

Figure 11: Functionalized Pyridine dihydrazone kifunensine analogues, **28-40**

Table 3: K_i Inhibition data for pyridine kifunensine analogues **28-40**

Inhibitor	ER Man I (μM)	Golgi Man I (μM)	Golgi/ER
Kifunensine	0.06	0.08	1.3
Pyridine-Kif, **21**	0.07	0.66	9.5
28	1.29	2.67	2.0
29	0.37	0.91	2.5
30	1.48	3.55	2.5
31	0.18	0.80	4.5
32	1.08	5.00	4.5
33	2.25	11.23	5.0
34	0.86	3.06	3.5
35	1.26	4.73	4.0
36	0.62	3.23	5.5
37	0.81	2.79	3.5
38	1.41	5.20	4.0
39	1.29	8.55	6.5
40	0.39	1.70	4.5

From the functionalized pyridine series, there were eight analogues that demonstrated greater than 4-fold selectivity towards the ER; however the inhibition was mediocre. It appears that the selectivity is caused more by the Golgi enzyme having unfavorable interactions with the bulkier substituents rather than positive interactions with the ER enzyme, evident by the high K_i values. However, the 4-chloropyridine and pyrimidine functionalized Kifunensine analogues, **16** and **25** respectively**,** demonstrated

4.5 fold selectivity and high nanomolar inhibition. This set of analogues indicates that the Golgi enzyme does not have the ability to accept larger substrates into the binding pocket in comparison to the ER enzyme.

Cellular Study of Pyridine Kifunensine

Analogue **21** was subjected to an endoglycosidase F (Endo F) sensitivity assay to determine influences on *N*-glycan processing in the Golgi apparatus. Endo F resistant glycans are mature glycans that have been extended and elaborated in the core structure, where as Endo F sensitive glycans are glycans that are in earlier stages of the biosynthesis. In other words, if the inhibitor inhibits Golgi Man I then the *N*-glycans will contain the core high mannose structure needed for recognition by Endo F thereby being Endo F sensitive. As seen in figure 12, compound **21** takes approximately 10-25 mM concentration to transition from Endo F resistant to Endo F sensitive glycans indicating that **21** is approximate 5-20 fold worse at inhibiting Golgi Man I than Kif. Kifunensine was used as a standard and was found to take approximately 5 mM concentration to convert from Endo F resistant to Endo F sensitive glycans.

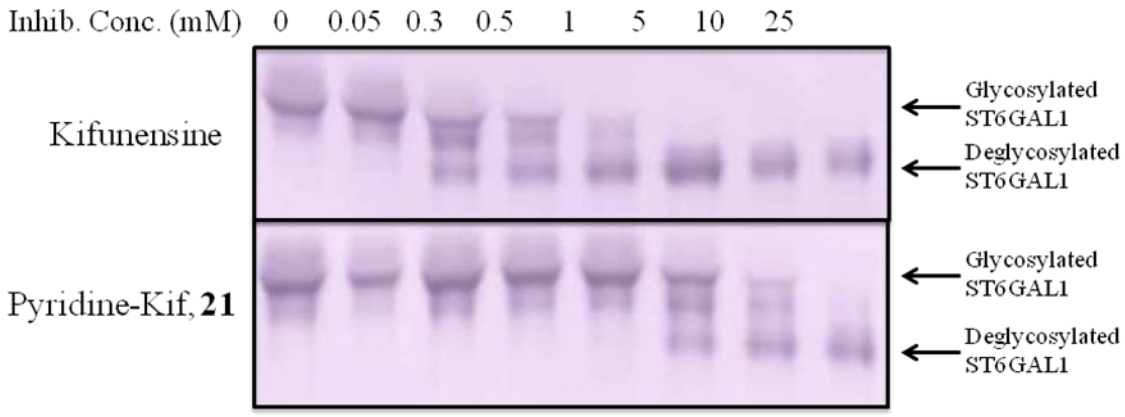

Figure 12: Effect of inhibitor treatment on the endoglycosidase sensitivity of a reporter glycoprotein expressed in mammalian cells. HEK293 cells were transfected with an expression construct encoding a soluble secreted form the rat sialyltransferase, ST6GAL1, a protein containing 2 complex type type *N*-glycan structures. Following transfection the cells were treated for 4 days with the indicated inhibitor concentration and the conditioned medium containing the recombinant ST6GAL1 was harvested, incubated with recombinant endoglycosidase F1 (endoF1) at room temperature overnight, resovled by SDS-PAGE, and immunoblotted using an antibody specific for rat ST6AGL1. ST6AGL1 secreted into the medium from untreated cell cultures was resistant to endoF1 cleavage since the glycans wereall complex type. Inhibition of mannose processing *in vivo* resulted in conversion of the glycans from endoF1-resistant structures to structures that were sensitive to cleavage by endoF1. Glycan cleavage resulted in a faster mobility of ST6AGL1 by SDS-PAGE. The data indicate that treatment of cells with >5 mM Kif resulted in conversion to endoF1 sensitive glycan structures, while concentrations >25 mM of the Kif-derivative were required to produce endoF1 sensitive glycans on ST6GAL1.

These results correspond to the initial K_i studies in which **21** demonstrated 10-fold worse inhibition of Golgi Man I in respect to Kif, however, **21** and Kif had nearly identical ER Man I inhibition.

Conclusions

In summary, the design and synthesis of a novel C2 hydrazone functionalized Kifunensine analogue was achieved. Through this synthetic route a library of dihydrazone functionalized Kifunensine analogues was prepared and tested for inhibitory activity against Human ER Man I and Mouse Golgi Man I. A pyridine functionalized derivative, **21**, was found to be a potent and selective inhibitor of ER Man I. Analogue **21** had a K_i of 0.07 μM for ER Man I and 0.66 μM for Golgi Man I indicating a 10-fold preference for the ER enzyme. The selectivity was further demonstrated through an Endo F sensitivity assay in which compound **21** was around 5-10 fold worse than Kif at inhibiting downstream *N*-glycan processing.

Acknowledgments- I would like to thank the Moremen laboratory for performing all of the K_i assays and cellular studies for our inhibitor molecules.

Experimental Section

General Methods and Materials

All chemicals were commercially available and used without further purification. Reactions were carried out using anhydrous solvents under an Argon atmosphere unless otherwise stated. Anhydrous DCM was distilled from calcium hydride under a nitrogen atmosphere. All column chromatography was carried out on Silica gel 60 (EM Science 70-230 mesh), and reactions were monitored using TLC (EM science, kiesel gel 60 F254 on aluminum) stained with cerium sulfate/ ammonium molybdate solution.

2,3:5,6-Di-isopropylidene-L-gulunolactone (2) L-gulonic-γ-lactone (**1**) (25 g, 0.14 mol) was dissolved in acetone (820 mL) and charged with anhydrous $CuSO_4$ (89.6 g, 0.56 mol) and catalytic H_2SO_4 (2.55 mL). The reaction mixture was stirred under argon for 48 hrs until all starting material and intermediate mono protected intermediate were consumed. Once complete, the reaction was filtered through a buchner funnel and the filtrate was quenched with $NaHCO_3$. The solids were again filtered and the filtrate was concentrated on a rotovap to an oily solid residue. Recrystallization from EtOAc yields pure product as an off white solid in quantitative yields (36 g). ^{1}H NMR (300 MHz, $CDCl_3$) δ 4.83 (d, *J* = 5.6 Hz, H-3, 1H), 4.74 (dd, *J* = 5.6, 3.5 Hz, H-2, 1H), 4.56 – 4.35 (m, 2H), 4.22 (dd, *J* = 8.9, 6.3 Hz, H-5, 1H), 3.82 (dd, *J* = 8.8, 6.0 Hz, 1H), 1.56 (s, 2H), 1.47 (s, 6H), 1.40 (s, 3H), 1.38 (s, 3H). Calculated MW was 258.27 MALDI-TOF found [M+H] 259.27.

2,3-isopropylidene-L-gulunolactone (3) 2,3:5,6-Diisopropylidene-L-gulunolactone **2** (36 g, 0.14 mol) was dissolved in AcOH/Water (7/1, 240 mL) and was stirred at r.t. for 24-48 hrs until no starting material remained. Once complete, the solvents were removed under reduced pressure and the oily solids were recrystallized from EtOAc in 93 % yield as light yellow solids (28.3 g). Calculated MW was 218.20, MALDI-TOF found [M+H] 219.20.

6-O-*tert*-butyldimethylsilyl-2,3-O-isopropylidene-L-gulunolactone (4) 2,3-isopropylidene-L-gulunolactone (28.3 g 0.13 mol) was dissolved in anhydrous DMF and cooled to -40 ^{o}C. To the cooled solution, *tert*-butyldimethylsilyl chloride (21.5 g 0.14

mol) and imidazole (13.26 g .20 mol) were added and the reaction was stirred at -40 ^{o}C for 2 hrs and checked by TLC. Once no starting material remained the reaction was warmed to r.t. and DMF was removed under reduced pressure. The crude material was dissolved in DCM (300 mL) and Brine (300 mL). The organic layer was set aside and the Brine was extracted by DCM (2 x 200 mL). The combined organic layers were dried over $MgSO_4$, filtered and evaporated to dryness. The colorless oil was purified by flash silica gel chromatography with hexanes/EtOAc (3/1) mobile phase resulting in clear oil in 89 % yield (38.4 g). ^{1}H NMR (300 MHz, $CDCl_3$) δ 5.06 – 4.65 (m, 1H), 4.50 (dd, *J* = 6.5, 3.4 Hz, 1H), 3.96 (dd, *J* = 5.5, 3.0 Hz, 1H), 3.73 (dd, *J* = 4.5, 1.9 Hz, 1H), 2.75 (d, *J* = 3.6 Hz, 1H), 1.34 (d, *J* = 23.8 Hz, 6H), 0.81 (s, 9H), -0.00 (s, 6H). Calculated MW was 332.46, MALDI-TOF found [M+Na] 355.45.

(3S,4S,5R)-5-[(1'R)-1'-Azido-2'-*tert*-butyldimethylsilanyloxyethyl]-3,4-isopropylidenedioxytetrahydrofura*N*-2-one (6) 6-O-*tert*-butyldimethylsilyl-2,3-O-isopropylidene-L-gulunolactone **4** (30.5 g 0.09 mol) was dissolved in dry DCM (250 mL) and cooled to – 30 ^{o}C. Anhydrous pyridine (22.2 mL 0.28 mol) was charged to the vessel and Tf_2O (31 mL 0.18 mol) was added slowly over 5 minutes. The reaction was stirred at -30 ^{o}C for 1 hr. The reaction progress was monitored by TLC (Hexanes/EtOAc 1/1) and when no starting material remained the reaction was warmed to r.t. diluted with DCM and washed with 1 N HCl (200 mL) followed by water (200 mL), and a final wash with saturated aqueous Na_2CO_3 (200 mL). The DCM layer was dried with $MgSO_4$, filtered and concentrated under reduce pressure. The crude triflate (**5)** was dissolved in dry DMF (200 mL) and sodium azide (17.6 g, 0.27 mol) was added. The reaction was stirred

overnight under argon. The reaction mixture was diluted with EtOAc (200 mL) and Brine (200 mL). The EtOAc layer was set aside and the brine layer was extracted with EtOAc (2 x 200 mL). The combined EtOAc layers were dried with $MgSO_4$, filtered and concentrated. The crude material was purified by flash silica gel chromatography with Hexanes/EtOAc (3/1) to give an off white solid (23.2 g). 5-Azido-6-O-*tert*-butyldimethylsilyl-5-deoxy-2,3-O-isopropylidene-D-mannonolactone was obtained in 72 % over two steps. ^{1}H NMR (300 MHz, $CDCl_3$) δ 4.96 – 4.56 (m, 2H), 4.29 (dd, *J* = 10.0, 3.1 Hz, 1H), 3.95 (d, *J* = 10.8 Hz, 1H), 3.71 (dd, *J* = 12.0, 6.1 Hz, 1H), 1.34 (d, *J* = 23.8 Hz, 6H), 0.91 (s, 9H), -0.11 (s, 6H). Calculated MW was 357.48, MALDI-TOF found [M+H] 358.45.

(2R, 3R, 4R, 5R)-5-Azido-6-*tert*-butyldimethylsilyl-5-deoxy-2,3-isopropylidene-dioxy-1,4-hexanediol (7) (3S,4S,5R)-5-[(1'R)-1'-Azido-2'-*tert*-butyldimethylsilanyloxyethyl]-3,4-isopropylidenedioxytetrahydrofura*N*-2-one (23.2 g, 0.06 mol) was dissolved in EtOH (600 mL) and charged with sodium borohydride (4.9 g 37.8 mol) at r.t.. The reaction was stirred for 4 hrs under argon, TLC showed no more starting material. The reaction was quenched with the addition of ammonium chloride until no more effervescence. The solution was filtered and concentrated to afford an oily white solid. The crude was purified by flash silica gel chromatography with Hexanes/EtOAc (3/1) eluent to afford (2R, 3R, 4R, 5R)-5-Azido-6-O-*tert*-butyldimethylsilyl-5-deoxy-2,3-O-isopropylidene-dioxy-1,4-hexanediol as a clear oil (19.9 g) in 85 % yield. ^{1}H NMR (300 MHz, $CDCl_3$) δ 4.41 (dd, *J* =1.4, 7.3 Hz, 1H), 4.29 (m, 1H), 4.09 (dd, *J* = 3.1, 10.6 Hz, 1H), 3.8-3.9 (m, 2H), 3.79 (dd, *J* = 4.4, 12.4 Hz, 1H),

3.60 (dd, *J* = 1.4, 9.1 Hz, 1H), 3.46 (m, 1H), 1.34 (d, *J* = 23.8 Hz, 6H), 0.91 (s, 9H), -0.11 (s, 6H). Calculated MW was 361.51, MALDI-TOF found [M+H] 362.50.

(2R, 3R, 4R, 5R)-2-Azido-1-*tert*-butyldimethylsilyl-4,5-isopropylidene-dioxy-6-pivaloyl-3-hexanol (8) (2R, 3R, 4R, 5R)-5-Azido-6-*tert*-butyldimethylsilyl-5-deoxy-2,3-isopropylidene-dioxy-1,4-hexanediol (19.9 g, 0.06 mol) was dissolved in dry DCM (200 mL) and charged with anhydrous pyridine (11.1 mL 0.14 mol) and trimethylacetyl chloride (8.1 mL 0.07 mol). The reaction was stirred at r.t. overnight. Once complete, the reaction was diluted with DCM and washed with water (2 x 200 mL). The organic layer was dried with $MgSO_4$, filtered and concentrated in vacuo. The crude material was purified by flash silica gel chromatography with Hexanes/EtOAc (20/1) mobile phase giving (2R, 3R, 4R, 5R)-2-Azido-1-O-*tert*-butyldimethylsilyl-4,5-O-isopropylidene-dioxy-6-pivaloyl-3-hexanol (19.6 g) in 80 % yield. ^{1}H NMR (300 MHz, $CDCl_3$) δ 4.53 – 4.19 (m, 2H), 3.98 (dd, *J* = 10.6, 3.1 Hz, 2H), 3.77 (dd, *J* = 10.6, 6.3 Hz, 1H), 3.51 (t, *J* = 9.1 Hz, 1H), 3.29 (ddd, *J* = 9.2, 6.3, 3.1 Hz, 1H), 2.33 (d, *J* = 9.1 Hz, 1H), 1.40 (s, 3H), 1.29 (s, 3H), 1.11 (s, 9H), 0.82 (s, 9H), 0.00 (d, *J* = 1.8 Hz, 6H). Calculated MW was 445.63, MALDI-TOF found [M+H] 446.60.

(2R, 3R, 4R, 5R)-2-Azido-1,3:4,5-O-di-isopropylidene-dioxy-6-pivaloyl-3-hexanol (9) (2R, 3R, 4R, 5R)-2-Azido-1-O-*tert*-butyldimethylsilyl-4,5-O-isopropylidene-dioxy-6-pivaloyl-3-hexanol (19.6 g, 0.04 mol) was dissolved in THF (500 mL) and cooled to -20 ^{o}C. Tetra-*N*-butylammonium fluoride (5.3 mL, 1 M solution in THF, 0.05 mol) was added to the cooled solution and stirred for 1 hr and monitored by TLC. Once no starting

material remained, the solution was warmed to r.t. and poured into brine, extracted with EtOAc, dried with $MgSO_4$,filtered and evaporated. The yellow oil ((2R, 3R, 4R, 5R)-2-Azido-1,3:4,5-O-diisopropylidene-dioxy-6-pivaloyl-3-hexanol, 13.4 g 0.04 mol) was dissolved in dry DCM (200 mL) at r.t.. PTSA (0.14 g, 0.81 mmol) and 2-methoxypropene (7.7 mL, 0.08 mol) were added to the solution and the reaction was stirred for 30 min. The reaction was quenched with water and extracted with DCM (3 x 200 mL). The combined organic layers were dried with $MgSO_4$, filtered and concentrated. The crude material was purified by flash silica gel chromatography using Hexanes/EtOAc (6/1) as an eluent. (2R, 3R, 4R, 5R)-2-Azido-1,3:4,5-O-diisopropylidene-dioxy-6-pivaloyl-3-hexanol (13.8 g) was obtained in 93 % yield. ^{1}H NMR (300 MHz, $CDCl_3$) δ 4.53 – 4.36 (m, 1H), 4.36 – 4.28 (m, 1H), 3.86 (dd, *J* = 10.1, 3.0 Hz, 1H), 3.72 – 3.60 (m, 1H), 3.49 (ddd, *J* = 9.3, 6.3, 3.0 Hz, 1H), 3.25 (s, 1H), 2.37 (d, *J* = 9.2 Hz, 1H), 1.50 (s, 3H), 1.40 (s, 3H), 1.37 (s, 9H), 1.21 (s, 3H). Calculated MW was 371.43, MALDI-TOF found [M+H] 372.40.

(2R, 3R, 4R, 5R)-5-Amino-2,3:4,6-diisopropylidene-dioxy-hexanol (10) (2R, 3R, 4R, 5R)-2-Azido-1,3:4,5-di-isopropylidene-dioxy-6-pivaloyl-3-hexanol (13.8 g, 0.04 mol) was dissolved in diethyl ether (600 mL) and charged with lithium aluminum hydride (4.6 g 0.12 mol) under an argon atmosphere. The reaction was stirred for 2 hrs and checked by TLC. Once no starting material remained the reaction was quenched with the slow successive addition of water (5.0 mL), 10 % NaOH (5.0 mL) and water (15.0 mL). The ether was decanted off and the water was extracted with EtOAc (2 x 50 mL) The organic layers were combined, dried with $MgSO_4$, filtered and evaporated to a white fluff (10.0

g). The crude amine was pure enough to be used for the next step. Calculated MW was 261.31, MALDI-TOF found [M+H] 262.29.

(2R, 3R, 4R, 5R)- 2,3:4,6-diisopropylidene-5-oxamoylamino alcohol (11) (2R, 3R, 4R, 5R)-5-Amino-2,3:4,6-diisopropylidene-dioxy-hexanol (10 g, 0.04 mol) was dissolved in DMF (300 mL). Oxamic acid (5.3 g 0.06 mol), EDC (11.5 g 0.06 mol) and HOBt (8.1 g mol) were added to the solution and stirred for 3 hrs. After 3 hrs MP-Carbonate resin (Loading capacity 3.01 mmol/g, 59.8 g 0.18 mol) was added to the solution and the reaction was stirred overnight. Once complete, the reaction mixture was filtered through a cotton plug and washed with DCM (30 mL) to remove the resin. The solvents were evaporated and the crude material was purified with flash silica gel chromatography using EtOAc/Hexanes/TEA (10/1/0.1) as a solvent system. (2R, 3R, 4R, 5R)- 2,3:4,6-diisopropylidene-5-oxamoylamino alcohol was obtained as an off white solid in 90 % yield (11.9 g). Calculated MW was 332.35, MALDI-TOF found [M+Na] 355.30.

(3aS,3bS,6bR,10aR,10bS)-2,2,9,9-Tetramethyl-1,3,8,10-tetraoxacyclohexa-[*e*]cyclopenta[*g*]-5,6-dione-4-azai*N*-dolizidine (diisopropylidene Kifunensine) (12) **(**2R, 3R, 4R, 5R)- 2,3:4,6-diisopropylidene-5-oxamoylamino alcohol (1.34 g, 4.0 mmol) was dissolved in dry DCM (60 mL) and fresh Dess Martin Periodinane (2.1 g, 4.8 mmol) was added to the solution. The reaction mixture was stirred for 4 hrs at r.t. under argon. The reaction was diluted in diethyl ether (250 mL) and filtered through a celite pad. The organics were evaporated to dryness. The crude aldehyde intermediate was dissolved in 7.0 N NH_3 in MeOH (5.7 mL, 0.04 mol) and stirred overnight. The reaction was

concentrated and purified by flash silica gel chromatography using Hexanes/EtOAc (1/3) mobile phase. (3aS,3bS,6bR,10aR,10bS)-2,2,9,9-Tetramethyl-1,3,8,10-tetraoxacyclohexa-[*e*]cyclopenta[*g*]-5,6-dione-4-azai*N*-dolizidine (.69 g) was synthesized in 55 % yield over two steps. Calculated MW was 312.32, MALDI-TOF found [M+Na] 335.30.

Thio Analogue of Diisopropylidene Kifunensine 13 (3aS,3bS,6bR,10aR,10bS)-2,2,9,9-Tetramethyl-1,3,8,10-tetraoxacyclohexa-[*e*]cyclopenta[*g*]-5,6-dione-4-azai*N*-dolizidine 200 mg, 0.64 mmol) was dissolved in anhydrous Toluene (10 mL) under an argon atmosphere and heated to reflux (~80 ^{o}C). Lawessons reagent (129. mg 0.32 mmol) was added to the refluxing solution. The resulting reaction mixture was refluxed for 2 hrs. The reactions was monitored by MALDI-TOF, and once no more starting material was present the toluene was removed under reduced pressure and crude product was purified by flash silica gel chromatography using Hexanes/EtOAc (1/2) as an eluent gave 189 mg in 90 % yield. ^{1}H NMR (500 MHz, $CDCl_3$) δ 4.82 (d, *J* = 8.6 Hz, 1H), 4.66 (dd, *J* = 11.0, 4.9 Hz, 1H), 4.32 (t, *J* = 8.0 Hz, 1H), 4.13 (dd, *J* = 11.3, 8.0 Hz, 1H), 4.02 (t, *J* = 8.3 Hz, 1H), 3.73 (t, *J* = 10.7 Hz, 1H), 3.56 (td, *J* = 10.6, 4.7 Hz, 1H), 1.50 (s, 6H), 1.42 (s, 3H), 1.31 (s, 3H).Calculated MW was 328.38 . MALDI-TOF found [M+H] 329.36.

Thio analogue of Kifunensine 14 Thio analogue of diisopropylidene Kifunensine **13** (189 mg, 0.58 mmol) was dissolved in 3/1 TFA/Water (4 mL) and stirred for 1 hr. Reaction progress was monitored by MALDI-TOF and once global deprotection was complete the reaction mixture was diluted in water and lyophilized. Crude product (143

mg, quantitative yield) was pure enough to be used in the next reaction. ^{1}H NMR (500 MHz, CD_3OD) δ 4.92 (d, *J* = 8.9 Hz, 1H), 4.33 – 4.22 (m, 1H), 4.01 – 3.80 (m, 3H), 3.67 (dd, *J* = 11.8, 5.2 Hz, 1H), 3.46 (d, *J* = 9.0 Hz, 1H), 3.21 (s, 2H). Calculated MW was 248.26, MALDI-TOF found [M+H] 249.25.

Hydrazone analogue of Kifunensine 15 Thio analogue of Kifunensine (143 mg, 0.58 mmol) was dissolved in EtOH (40 mL) under argon and Hydrazine hydrate was added (0.28 mL, 0.58 mmol) to the reaction at 45 ^{o}C. The reaction was stirred for 2 hrs and checked by MALDI-TOF. Once complete, the solvents were evaporated and the crude material was purified by a HPLC equipped with a semi-preparative agilent zorbax C18 column with a flow rate of 1 mL/min, mobile phase A was 0.1 % TFA in water, and mobile phase B was 0.1 % TFA in acetonitrile. Isolated product was 118 g 83 % yield. ^{1}H NMR (500 MHz, d_2o) 5.18 (d, *J* = 9.3 Hz, 1H), 4.28 (dd, *J* = 9.5, 4.4 Hz, 1H), 4.06 (d, *J* = 3.1 Hz, 1H), 3.99 (t, *J* = 3.1 Hz, 1H), 3.87 (dd, *J* = 12.0, 9.7 Hz, 1H), 3.71 (dd, *J* = 12.1, 4.6 Hz, 1H), 3.62 (dd, *J* = 9.3, 3.0 Hz, 1H). Calculated MW was 246. 22, MALDI-TOF found [M+H] 247.19.

General Procedure for Hydrazone Coupling Reaction

Compound **15** (5 mg, 0.02 mmol) was dissolved in 1 % AcOH in DMSO (1 mL) in a small glass vial. The aldehyde was added (0.04 mmol) and the vials were stirred for 48 hrs. The reaction progress was monitored by MALDI-TOF and once no starting material was observed in the MALDI-TOF spectrum the reaction was stopped. The solvents were frozen using liquid nitrogen and then the samples were lyophilized. Once the DMSO was

removed the samples were dissolved in Water/Acetonitrile (1/1) and purified by HPLC equipped with a semi-preparative agilent zorbax C18 column with a flow rate of 1 mL/min, mobile phase A was 0.1 % TFA in water, and mobile phase B was 0.1 % TFA in acetonitrile. The samples were lyophilized and submitted for inhibition studies.

General Procedure for Inhibition Study

Each kifunensine analogue was tested for inhibitory activity at three concentrations (0.05, 0.5, and 5 mM) using recombinant human ER mannosidase I or Golgi Man IA. ER Man I assays were performed using 20 μg of enzyme and Man_9-$GlcNAc_2$-PA (20 μM) as substrate in a final volume of 20 μL containing 20 mM MES/NaOH, pH 7.0, 150 mM NaCl, and 5 mM $CaCl_2$. The enzyme reactions were allowed to proceed for 15 min at 37 ^oC and were stopped by addition of 20 μL of 1.25 M Tris-HCl pH 7.6. The human ER Man I product, Man_8-$GlcNac_2$-PA, was resolved from $Man_9GlcNac_2$-PA by HPLC on a Hypersil APS-2 NH_2 column. $Man_9GlcNac_2$-PA was prepared by reductive pyridylamination of $Man_9GlcNac_2$ isolated from crude soybean agglutinin. Golgi Man IA assays were performed using 10 μg of enzyme in a reaction containing 20 mM potassium phosphate, pH 6.0, 150 mM NaCl, 5mM Man-α-1,2-Man-α-O-CH_3 in a total volume of 25 μL. Enzyme reactions were allowed to proceed for 30 min at 37 ^oC and terminated by the additionof 25 μL of 1.25 Tris-HCl, pH 7.6. The amount of mannose released was quantified using a glucose oxidase and peroxidase reagent. The recombinant enzymes were expressed and purified. For determination of the compound inhibition, enzyme activity was plotter as a percentage of residual activity (compared to no added compound) versus compound concentration and the IC_{50} values were estimated from the

plots. All inhibitory assays and cellular studies were performed by the Dr Kelley Moremen lab at the CCRC of the University of Georgia.

Benzaldehyde Derivative (16) ^{1}H NMR (500 MHz, d_2o) 8.44 (s, 1H), 7.78 (d, *J* = 7.3 Hz, 2H), 7.47 (dt, *J* = 26.7, 7.2 Hz, 3H), 5.31 (d, *J* = 9.3 Hz, 1H), 4.36 (dd, *J* = 9.5, 4.4 Hz, 1H), 4.12 (d, *J* = 3.4 Hz, 1H), 4.04 (t, *J* = 3.0 Hz, 1H), 3.93 (dd, *J* = 12.0, 9.7 Hz, 1H), 3.74 (m, 10.6, 3.8 Hz, 2H). Calculated MW = 334.33, MALDI-TOF found [M+H]= 335.30.

4-Bromobenzaldehyde Derivative (17) ^{1}H NMR (500 MHz, d_2o) 8.32 (s, 1H), 7.61 (dd, *J* = 21.6, 8.6 Hz, 4H), 5.29 (d, *J* = 9.3 Hz, 1H), 4.35 (dd, *J* = 9.5, 4.6 Hz, 1H), 4.11 (d, *J* = 3.3 Hz, 1H), 4.04 (t, *J* = 3.2 Hz, 1H), 3.92 (dd, *J* = 12.0, 9.6 Hz, 1H), 3.77 (dd, *J* = 12.1, 4.6 Hz, 1H), 3.70 (dd, *J* = 9.2, 2.9 Hz, 1H). Calculated MW = 413.22, MALDI-TOF found [M+H]= 414.22.

4-Fluorobenzaldehyde Derivative (18) ^{1}H NMR (500 MHz,) 8.43 (s, 1H), 7.81 (dd, *J* = 8.5, 5.6 Hz, 2H), 7.17 (t, *J* = 8.8 Hz, 2H), 5.33 (d, *J* = 9.2 Hz, 1H), 4.36 (dd, *J* = 9.5, 4.4 Hz, 1H), 4.12 (d, *J* = 3.2 Hz, 1H), 4.04 (s, 1H), 3.93 (dd, *J* = 11.9, 9.8 Hz, 1H).Calculated MW = 352.32, MALDI-TOF found [M+H]= 353.30.

3-Hydroxy-4-Methoxybenzaldehyde Derivative (19) ^{1}H NMR (500 MHz, d_2o) 8.44 (s, 1H), 7.40 (d, *J* = 8.7 Hz, 1H), 6.57 (dd, *J* = 8.7, 2.2 Hz, 1H), 6.48 (d, *J* = 2.1 Hz, 1H), 5.22 (d, *J* = 9.3 Hz, 1H), 4.35 (dd, *J* = 9.6, 4.4 Hz, 2H), 4.10 (d, *J* = 3.2 Hz, 1H), 4.03 (s,

1H), 3.98 (m, 1H) 3.78 (m, 1H), 3.78 (s, 3H), 3.73 (m, 1H), 3.67 (dd, *J* = 9.2, 2.9 Hz, 1H). Calculated MW = 380.35, MALDI-TOF found [M+H]= 381.32.

3,4-Dihydroxybenzaldehyde Derivative (20) ^{1}H NMR (500 MHz, d_2o) 9.52 (s, 1H), 8.19 (s, 1H), 7.27 (d, *J* = 2.0 Hz, 1H), 7.13 (dd, *J* = 8.3, 1.9 Hz, 1H), 6.85 (d, *J* = 8.2 Hz, 1H), 5.31 (d, *J* = 9.3 Hz, 1H), 4.35 (dd, *J* = 9.5, 4.5 Hz, 1H), 4.11 (d, *J* = 3.6 Hz, 1H), 4.03 (t, *J* = 3.2 Hz, 1H), 3.92 (dd, *J* = 12.1, 9.6 Hz, 1H), 3.85- 3.69 (m, 1H). Calculated MW = 366.33, MALDI-TOF found [M+H]= 367.30.

4-Pyridinecarboxaldehyde Derivative (21) ^{1}H NMR (500 MHz, d_2o) 8.71 (d, *J* = 6.6 Hz, 2H), 8.46 (s, 1H), 8.29 (d, *J* = 6.6 Hz, 2H), 5.25 (d, *J* = 9.4 Hz, 1H), 4.31 (dd, *J* = 9.4, 4.4 Hz, 1H), 4.09 (d, *J* = 3.3 Hz, 1H), 4.02 (t, *J* = 2.8 Hz, 1H), 3.91 (dd, *J* = 11.8, 9.8 Hz, 1H), 3.75 (dd, *J* = 12.1, 4.5 Hz, 1H), 3.58 (dd, *J* = 9.3, 2.9 Hz, 1H). Calculated MW =335.32 , MALDI-TOF found [M+H]= 336.28.

4- Imidazolecarboxaldehyde Derivative (22) ^{1}H NMR (500 MHz, d_2o) 8.75 (d, *J* = 0.7 Hz, 1H), 8.35 (s, 1H), 7.79 (d, *J* = 1.1 Hz, 1H), 5.23 (d, *J* = 9.3 Hz, 1H), 4.32 (dd, *J* = 9.6, 4.5 Hz, 1H), 4.09 (dd, *J* = 3.6, 0.6 Hz, 1H), 4.01 (t, *J* = 3.3 Hz, 1H), 3.90 (dd, *J* = 12.0, 9.6 Hz, 1H), 3.75 (dd, *J* = 12.1, 4.6 Hz, 1H), 3.61 (dd, *J* = 9.3, 3.0 Hz, 1H). Calculated MW = 324.29, MALDI-TOF found [M+H]= 325.27.

Furaldehyde Derivative (23) ^{1}H NMR (500 MHz, d_2o) 8.27 (s, 1H), 7.68 (s, 1H), 7.03 (d, *J* = 3.3 Hz, 1H), 6.63 -6.53 (m, 1H), 5.30 (d, *J* = 9.2 Hz, 2H), 4.35 (dd, *J* = 9.3, 4.3

Hz, 2H), 4.11 (d, *J* = 3.2 Hz, 1H), 4.05 -3.31 (m, 2H). Calculated MW = 324.29, MALDI-TOF found [M+H]= 330.27.

3-Methyl-2-thiophene carboxaldehyde Derivative (24) ^{1}H NMR (500 MHz, D_2O) 8.64 (s, 1H), 7.52 (d, *J* = 5.1 Hz, 1H), 6.95 (d, *J* = 5.1 Hz, 1H), 5.29 (d, *J* = 9.2 Hz, 1H), 4.36 (dd, *J* = 9.7, 4.4 Hz, 1H), 4.11 (d, *J* = 3.3 Hz, 1H), 4.08 -3.77 (m, 1H), 3.77 - 3.65 (m, 2H), 2.31 (s, 3H). Calculated MW =354.38 , MALDI-TOF found [M+H]= 355.35

1-Hexanal Derivative (25) ^{1}H NMR (500 MHz, D_2O) 8.23- 7.69 (m, 1H), 5.20 (d, *J* = 9.3 Hz, 1H), 4.35 (m, 1H), 4.12-3.05 (m, 2H), 3.84 (m, 1H), 3.62 (m, 1H), 2.32 (dd, *J* = 13.4, 7.3 Hz, 2H), 1.76- 1.25 (m, 2H), 1.22 (dd, *J* = 13.2, 9.4 Hz, 4H), 0.77 (dd, *J* = 13.2, 7.0 Hz, 3H). Calculated MW =328.36 , MALDI-TOF found [M+H]=329.34

***trans*-1,2-Hexenal Derivative (26)** ^{1}H NMR (500 MHz, D_2O) 8.03 (d, *J* = 9.5 Hz, 1H), 6.57 (m, 1H), 6.29 (m, 1H), 5.27 (d, *J* = 9.4 Hz, 1H), 4.33 (dd, *J* = 9.4, 4.3 Hz, 1H), 4.0-4.2 (m, 2H), 3.9 (m, 1H), 3.78 (m, 1H), 3.67 (d, *J* = 9.5 Hz, 1H), 2.18 (dd, *J* = 14.3, 7.1 Hz, 2H), 1.40 (td, *J* = 14.6, 7.3 Hz, 2H), 0.81 (t, *J* = 7.4 Hz, 3H). Calculated MW = 326.35, MALDI-TOF found [M+H]= 327.31.

***trans*-1,2-Nonenal Derivative (27)** ^{1}H NMR (500 MHz, d_2o) 8.01 (d, *J* = 9.5 Hz, 1H), 6.54(m, 1H), 6.27 (dd, *J* = 15.5, 9.6 Hz, 1H), 5.23 (d, *J* = 9.1 Hz, 1H), 4.35 (m, 1H), 4.03 (m, 2H), 3.93 (dd, *J* = 40.0, 27.9 Hz, 1H), 3.75 (dd, *J* = 12.0, 4.6 Hz, 1H), 3.64 (dd, *J* = 9.2, 3.0 Hz, 1H), 2.20 (dd, *J* = 14.0, 7.0 Hz, 2H), 1.56-1.15 (m, 2H), 1.12 (d, *J* = 23.3 Hz,

6H), 0.75 (d, *J* = 6.8 Hz, 3H). Calculated MW = 368.43, MALDI-TOF found [M+H]= 369.40.

4-Amino-Pyridine-3-Carboxaldehyde Derivative (28) Calculated MW = 350.33, MALDI-TOF found [M+H]= 351.35

(2-Formyl-pyridine-3-yl) Derivative (29) Calculated MW =350.33, MALDI-TOF found [M+H]= 351.35

2-Methoxy Pyridine Derivative (30) ^{1}H NMR (500 MHz, d_2o) 8.63 (s, 1H), 8.28 (dd, *J* = 7.6, 1.7 Hz, 1H), 8.17 (dd, *J* = 5.1, 1.9 Hz, 1H), 7.07 (dd, *J* = 7.5, 5.2 Hz, 1H), 5.34 (d, *J* = 9.3 Hz, 1H), 4.37 (dd, *J* = 9.6, 4.5 Hz, 1H), 4.13 (d, *J* = 3.2 Hz, 1H), 4.05 (t, *J* = 3.2 Hz, 1H), 3.99- 3.88 (m, 3H), 3.76 (ddd, *J* = 12.2, 10.7, 3.8 Hz, 2H). Calculated MW = 365.34, MALDI-TOF found [M+H]= 366.39.

4-Chloro Pyridine Derivative (31) Calculated MW = 369.76, MALDI-TOF found [M+H]= 370.80

(2-Formyl-pyridi*N*-3-yl)-carbamic acid *tert*-butyl ester Derivative (32) Calculated MW = 450.45, MALDI-TOF found [M+H]= 451.50

***N*-(3-Formyl-pyridi*N*-2-yl)-2,2-dimethyl-propionamide Derivative (33)** Calculated MW = 434.45, MALDI-TOF found [M+H]= 435.50

***N*-(4-Formyl-pyridi*N*-3-yl)-2,2-dimethyl-propionamide Derivative (34)** Calculated MW = 434.45, MALDI-TOF found [M+H]= 435.50

2-Hydroxy-4-Pyridine Carboxaldehyde Derivative (35) Calculated MW = 351.31, MALDI-TOF found [M+H]= 352.32.

6-Quinoline Derivative (36) Calculated MW = 385.37, MALDI-TOF found [M+H]= 386.39

Furo(3,2-bypyridine) Carboxaldehyde Derivative (37) Calculated MW = 375.34 , MALDI-TOF found [M+H]= 376.39

1H-Pyrrole[3,2-b]-pyridine-6-carboxaldehyde Derivative (38) Calculated MW = 374.35, MALDI-TOF found [M+H]= 375.40

3-Formylindol-1-yl-acetic Acid Derivative (39) Calculated MW = 431.40, MALDI-TOF found [M+H]= 432.45

REFERENCE

1. Elbein, A. D., Inhibitors of the Biosynthesis and Processing of *N*-Linked Oligosaccharide Chains. *Annual Review of Biochemistry* **1987**, *56*, 497-534.

2. Vallee, F.; Karaveg, K.; Herscovics, A.; Moremen, K. W.; Howell, P. L., Structural basis for catalysis and inhibition of *N*-glycan processing class I alpha 1,2-mannosidases. *Journal of Biological Chemistry* **2000**, *275* (52), 41287-41298.
3. Molinari, M.; Calanca, V.; Galli, C.; Lucca, P.; Paganetti, P., Role of EDEM in the release of misfolded glycoproteins from the calnexin cycle. *Science* **2003**, *299* (5611), 1397-1400.

4. Oda, Y.; Hosokawa, N.; Wada, I.; Nagata, K., EDEM as an acceptor of terminally misfolded glycoproteins released from calnexin. *Science* **2003**, *299* (5611), 1394-1397.

5. Moremen, K. W.; Molinari, M., *N*-linked glycan recognition and processing: the molecular basis of endoplasmic reticulum quality control. *Current Opinion in Structural Biology* **2006**, *16* (5), 592-599.

6. Fuhrmann, U.; Bause, E.; Legler, G.; Ploegh, H., Novel Mannosidase Inhibitor Blocking Conversion of High Mannose to Complex Oligosaccharides. *Nature* **1984**, *307* (5953), 755-758.

7. Kayakiri, H.; Takase, S.; Shibata, T.; Okamoto, M.; Terano, H.; Hashimoto, M.; Tada, T.; Koda, S., Structure of Kifunensine, a New Immunomodulator Isolated from an Actinomycete. *Journal of Organic Chemistry* **1989**, *54* (17), 4015-4016.

8. Sano, H.; Sugai, S., Synthesis of an Optically-Active Carbocyclic Derivative of (+)-Hydantocidin. *TetrahedroN-Asymmetry* **1995**, *6* (5), 1143-1150.

9. Fleet, G. W. J.; Ramsden, N. G.; Witty, D. R., Practical Synthesis of Deoxymannojirimycin and Mannonolactam from L-Gulonolactone - Synthesis of L-Deoxymannojirimycin and L-Mannonolactam from D-Gulonolactone. *Tetrahedron* **1989**, *45* (1), 319-326.

10. Hering, K. W.; Karaveg, K.; Moremen, K. W.; Pearson, W. H., A practical synthesis of kifunensine analogues as inhibitors of endoplasmic reticulum alpha-mannosidase I. *Journal of Organic Chemistry* **2005**, *70* (24), 9892-9904.

11. Fairbanks, A. J.; Fleet, G. W. J.; Jones, A. H.; Bruce, I.; Aldaher, S.; Dibello, I. C.; Winchester, B., Synthesis from a Heptonolactone and Effect on Glycosidases of (1s,2r,6r,7s)-1,2,6,7-Tetrahydroxypyrrolizidine. *Tetrahedron* **1991**, *47* (1), 131-138.

12. Wolfrom, M. L.; Diwadkar, A. B.; Gelas, J.; Horton, D., New Method of Acetonation Synthesis of 4,6-Ortho-Isopropylidene-D-Glucopyranose. *Carbohydrate Research* **1974**, *35* (1-2), 87-96.

13. Kayakiri, H.; Kasahara, C.; Nakamura, K.; Oku, T.; Hashimoto, M., Synthesis of Kifunensine, an Immunomodulating Substance Isolated from a Microbial Source. *Chemical & Pharmaceutical Bulletin* **1991**, *39* (6), 1392-1396.

14. Scheibye, S.; Pedersen, B. S.; Lawesson, S. O., Studies on Organophosphorus Compounds .21. Dimer of Para-Methoxyphenylthionophosphine Sulfide as Thiation Reagent - New Route to Thiocarboxamides. *Bulletin Des Societes Chimiques Belges* **1978**, *87* (3), 229-238.

15. El-Sharief, A. M. S.; Ammar, Y. A.; Mohamed, Y. A.; Aly, M. M.; El-Gaby, M. S. A.; Aly, A. S., A comparative study between imidazolidineiminothiones and 4-thioxoimidazolidine-2,5-diones towards some nucleophilic and binucleophilic reagents: Synthesis of some new imidazo(diimines, dihydrazones, quinoxalines & azine) and diimidazolidinone. *Phosphorus Sulfur and Silicon and the Related Elements* **2001**, *173*, 39-58.

CHAPTER 3

THE DEVELOPMENT OF SELECTIVE INHIBITORS FOR ER α-MANNOSIDASE I BY COMBINATORAL MODIFICATION OF DEOXYMANNOJIRIMYCIN

Jessica Cardot, Yong Xiang, Kelley Moremen, Geert-Jan Boons

To be submitted to J. Org. Chem

Abstract

Selective inhibitors of endoplasmic reticulum α-mannosidase I (ER Man I) have the potential to be used for treatment of a number of genetic diseases. Although potent inhibitors for this enzyme have been described, in general these compounds display poor selectivity and often inhibit Golgi α-mannosidase I. To address this difficulty, we have synthesized and combinatorial modified deoxymannojirimycin (DMJ), which is a weak GH47 α-mannosidase I inhibitor. DMJ was modified by a hydrazine moiety, which was readily extended by reaction with a range of aldehydes. The library of hydrazine-linked analogues was screened for inhibition of human ER Man I and mouse Golgi Man I. It was found that a 3-methyl-thiophene functionalized DMJ analog (**49**) selectively inhibited ER Man I over Golgi Man with 32.5 fold selectivity. Analogue **49** also had over a 100 fold increase in potency in respect to DMJ (K_i = 21.1 μM) with K_i of 0.30 μM.

Introduction and literature Review

Carbohydrates are expressed on the cell surface and have diverse a set of biological functions. With the advanced understanding of carbohydrate functions there is interest in carbohydrate-processing enzymes, including glycosyl transferases and glycosidases, as therapeutic agents. Through the inhibition of glycosidases there is the potential for better understanding of the hydrolytic mechanism of these enzymes, as well as the potential for therapeutics for the treatment of metabolic disorders, tumor metastasis, and viral infections. Aza-sugars are known as potent glycosidase inhibitors, and since the introduction of Glyset in 1996 the field of iminosugars has grown

significantly. An iminosugar is a sugar molecule in which the endocyclic oxygen is replaced by a nitrogen atom.

Glycosidases can be categorized into two main catalytic subtypes, inverting and retaining mechanisms. Catalytic mechanism and classification is dependent mainly on sequence similarities, and preferred substrates. For retaining glycosidases, the mechanism of hydrolysis goes through a two step process in which an oxocarbenium ion intermediate is formed. At physiological pH, the basic ring nitrogen of an azasugar is protonated, thus the positively charged iminosugars are believed to inhibit the glycosidase enzymes by mimicking the positively charged oxocarbenium ion.

Inverting and retaining enzymes can be further classified into CAZy glycosyl hydrolase (GH) families based on product stereochemistry, bond specificity, and inhibitor structure. Therefore, α-mannosidases within the same CAZy GH family will have remarkably similar catalytic binding domains and substrate specificity. ER Man I is a GH47 enzyme that is believed to play a vital role in *N*-glycan biosynthesis and degradation. The GH47 family contains three subfamilies: ER Man I and Golgi Man IA-IC (α-1,2-mannosidases), and EDEM1-3 (ER stress induced proteins). GH47 enzymes are one of three GH families that are calcium dependent. Although the GH47 enzymes have been implicated in nascent glycoprotein disposal, their roles and actual involvement is under investigation. Therefore, the development of a selective inhibitor that could distinguish between the various GH47 enzymes would not only be a target for drug development but would also aid in the understanding of the degradation pathway.

Although iminosugars are strong glycosidase inhibitors there have been limited successful therapeutics developed. The lack of safe and efficacious glycosidase

inhibitors is largely dictated by the promiscuity and lack of selectivity towards glycosidase families inherent of these substrates. The design and synthesis of potential glycosidase inhibitors should take into account the configuration of the hydroxyls, conformation of the sugar and charge of the molecules. With this in mind we set out to synthesize a small library of mannosidase inhibitors through the combinatorial modification of deoxymannojirimycin (DMJ), a known weakly active mannosidase inhibitor. DMJ was modified with a hydrazine motif, which was then diversified with a small array of aldehydes.

Results and Discussion

Synthesis of Hydrazine DMJ

The synthesis of DMJ analogues started with the hydrogenation of azidolactone **6** by H_2 10% Pd/C, resulting in the reduction of the azide to form the intermediate amine. The amine underwent *in situ* cyclization to form the more stable lactam **40** in 88 % yield. Reduction of the lactam by borane methyl disulfide rendered the protected form of DMJ **41** in 65 % yield. Treatment of **41** with 1N TBAF in THF afforded the silyl ether deprotected **42** in 72 % yield. *N*-nitrosation of the secondary amine with *t*-butyl nitrite in THF resulted in nitrosamine **43**, which upon treatment with lithium aluminum hydride produced hydrazine analogue **44** in 50 % yield over two steps. Final deprotection of the acetonide by treatment with TFA/water afforded the deprotected hydrazine DMJ lead **45** in 65 % yield (Scheme 4).

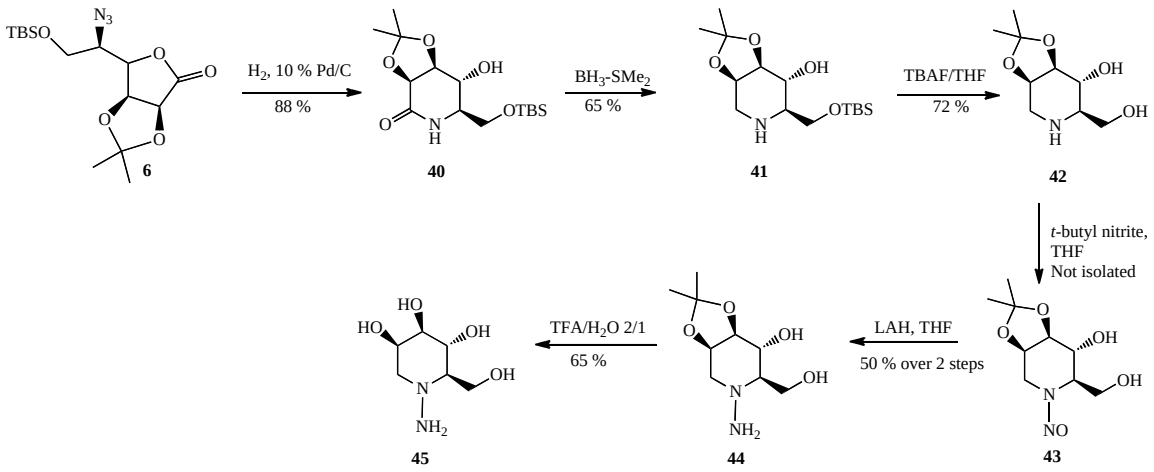

Scheme 4: Synthesis of hydrazine DMJ analogue

Synthesis of Hydrazone DMJ Analogues

Once the synthesis of **45** was complete, a small library of hydrazone functionalized DMJ analogues was synthesized from five aldehydes containing aromatic and heterocyclic moieties. Hydrazine **45** was dissolved in 1 % AcOH in DMSO followed by the addition of the selected aldehyde (Figure 13).

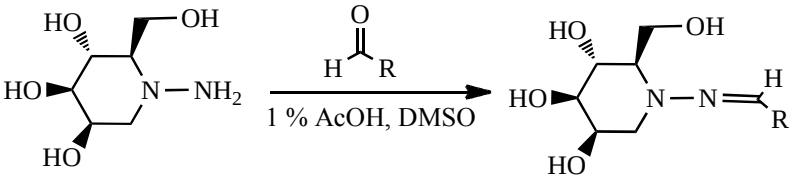

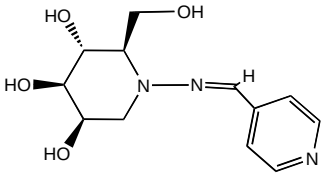

46

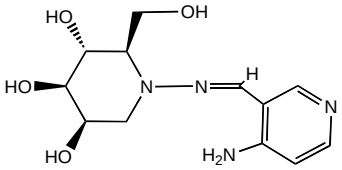

47

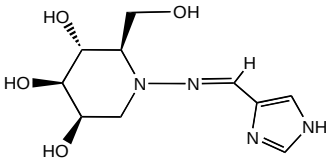

48

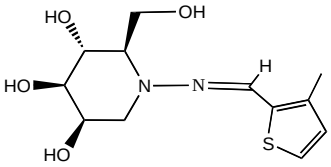

49

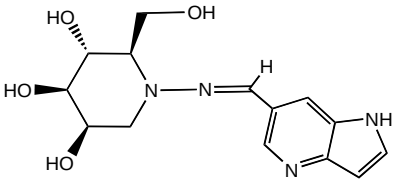

50

Figure 13: Structures of DMJ analogues or initial library screening, **46-50**

The reaction was monitored by HRMS-MALDI-TOF. Once complete, the compounds were purified by HPLC and screened for inhibition and selectivity towards ER Man I, and Golgi Man I. (Table 4).

Table 4: K_i data for DMJ analogues **46-50**

Inhibitor	ER Man I (μM)	Golgi Man I (μM)	Golgi/ER
DMJ	21.1	15.4	0.75
46	39.3	286.2	7.5
47	24.1	496.9	21
48	9.0	65.5	7.5
49	0.30	9.7	32.5
50	2.1	8.1	4

The parent substrate, DMJ, has a K_i of 21.1 μM which is very poor along with relatively no selectivity between the ER and Golgi enzymes. All five hydrazone DMJ analogues demonstrated increased selectivity towards ER Man I over Golgi Man I. Analogues **47** and **49** had the highest degree of selectivity with 21 and 32.5 fold selectivity respectively. 3-methyl-thiophene analogue **49** not only had a very high degree of selectivity but also had a remarkable increase in potency. The K_i for **49** is in the high nanomolar range which results in over 100-fold higher potency than DMJ.

Conclusions

In summary, a novel hydrazine functionalized DMJ analogue was synthesized and utilized as a lead compound in the synthesis of five hydrazone modified DMJ analogues. A 3-methyl-thiophene functionalized DMJ analogue was prepared and found to have over a 100 fold improvement in inhibition in respect to DMJ. Analogue **49** had a K_i of 0.30

μM and 32.5 fold selectivity towards the ER α-mannosidase, making it the first selective and potent ER Man I inhibitor derived from DMJ.

Acknowledgments- I would like to thank the Moremen laboratory for performing all of the K_i assays and cellular studies for our inhibitor molecules.

Experimental Section:

General Methods and Materials

All chemicals were commercially available and used without further purification. Reactions were carried out using anhydrous solvents under an Argon atmosphere unless otherwise stated. Anhydrous DCM was distilled from calcium hydride under a nitrogen atmosphere. All column chromatography was carried out on Silica gel 60 (EM Science 70-230 mesh), and reactions were monitored using TLC (EM science, kiesel gel 60 F254 on aluminum) stained with cerium sulfate/ ammonium molybdate solution.

6-O-*tert*-butyldimethylsilyl-2,3-O-isopropylidene-D-mannono-δ-lactam (40)

Azidolactone **6** (1.0 g, .0028 mol) was dissolved in MeOH (50 mL) and the reaction vessel was flushed with argon. Pd/C (catalytic) was added to the reaction and the solution was stirred overnight under a H_2 atmosphere. Once complete, the reaction was diluted in MeOH and filtered through a celite pad to remove the catalyst. The solution was concentrated and purified by Normal silica gel chromatography (70 % Hexanes/#0 % EtOAc to 100 % EtOAc), affording 6-O-*tert*-butyldimethylsilyl-2,3-O-isopropylidene-D-mannono-δ-lactam in 88 % yield as a white fluffy solid (0.8156 g, 0.0025 mol). ^{1}H NMR

(300 MHz, $CDCl_3$) δ 6.16 (s, 1H), 4.54 (d, *J* = 7.8 Hz, 1H), 4.21 (t, *J* = 7.9 Hz, 1H), 3.91 (dd, *J* = 10.2, 4.0 Hz, 1H), 3.52 (dt, *J* = 17.1, 8.5 Hz, 2H), 3.29 (td, *J* = 8.7, 4.0 Hz, 1H), 1.43 (s, 3H), 1.32 (s, 3H), 0.92 – 0.67 (m, 8H), -0.00 (s, 5H). Calculated MW = 375.34 , MALDI-TOF found [M+H]= 376.39.

6-O-*tert*-butyldimethylsilyl-2,3-O-isopropylidene-1-deoxy-D-mannono-δ-lactam (41) 6-O-*tert*-Butyldimethylsilyl-2,3-O-isopropylidene-D-mannono-δ-lactam (5.0 g, 0.0150 mol) was dissolved in anhydrous THF (60 mL). The solution was charged with borane dimethyl sulfide complex (4.2 mL, 0.0450 mol) and stirred for 4 hrs. Once TLC showed no starting material, the reaction was slowly quenched with MeOH until effervescence stopped. The solvents were evaporated under vacuum anf the product was purified by normal silica gel chromatography with a solvent gradient starting at hexanes/EtOAc (1/1) and finished with EtOAc. 6-O-*tert*-butyldimethylsilyl-2,3-O-isopropylidene-1-deoxy-D-mannono-δ-lactam was obtained as a white fluff in 65 % yield (3.1 g, 0.0098 mol). Calculated MW = 317.50, MALDI-TOF found [M+H] 318.48 .

2,3-O-isopropylidene-1-deoxy-D-mannono-δ-lactam (42) 6-O-*tert*-Butyldimethylsilyl-2,3-O-isopropylidene-1-deoxy-D-mannono-δ-lactam (1.8 g, 0.0056 mol) was dissolved in THF (25 mL) and cooled to -20 ^{o}C. TBAF (1 M in THF, 6.7 mL, 0.0067 mol) was added to the cooled solution and the reaction was stirred at -20 ^{o}C for 2 hrs. Once no starting material was observed on TLC, the reaction was warmed to rt, diluted in EtOAc and poured into brine. The EtOAc layer was isolated and the brine layer was extracted in EtOAc (2 x 100 mL). The combined organic layers were dried with $MgSO_4$, filtered and

concentrated. The crude residue was purified by flash silica gel chromatography using Hexanes/EtOAc (1/1) as an eluent. 2,3-O-isopropylidene-1-deoxy-D-mannono-δ-lactam (0.082g, 0.0040 mol) was obtained in 72 % yield. Calculated MW = 203.24, MALDI-TOF found [M+H] 204.20.

1-deoxy -2,3-O-isopropylidene-*N*-amino-D-mannono-δ-lactam (44) 2,3-O-Isopropylidene-1-deoxy-D-mannono-δ-lactam (0.30 g, 0.0015 mol) was dissolved in anhydrous THF (5.0 mL) and *t*-butyl nitrite (0.36 mL, 0.0030 mol) was added to the solution. The reaction was stirred at reflux in the dark for 18 hrs. Once complete the solvent and excess *t*-butyl nitrite was removed under reduced pressure. The crude 1-deoxy -2,3-O-isopropylidene-*N*-nitroso-D-mannono-δ-lactam (**43)** was used in the next step without further isolation. Lithium aluminum hydride (0.1139 g, 0.0030 mol) was suspended in THF (10 mL) in a 2-neck flask. The suspension was heated to ~65 ^{o}C and a solution of **43 (**0.34 g, .0015 mol) in THF (5 mL) was added slowly. The reaction was refluxed for 7 hrs. Once complete, the excess LAH was quenched with aqueous ammonia followed by 1M LiOH. The solids were filtered off through a celite pad and the filtrate was concentrated. 1-deoxy -2,3-O-isopropylidene-*N*-amino-D-mannono-δ-lactam (0.1635 g, 0.75 mmol) was obtained in 50 % yield over two steps. The crude hydrazine was pure enough for the subsequent reactions. Calculated MW = 218.25, MALDI-TOF found [M+H] 219.20.

1-deoxy-*N*-amino-D-mannono-δ-lactam (45) 1-Deoxy -2,3-O-isopropylidene-*N*-amino-D-mannono-δ-lactam (0.1635 g, 0.75 mmol) was dissolved in TFA/H_2O (2/1, 3 mL) and

stirred for 1 hr. Once no starting material remained, the solvents were removed by freeze drying. The dried material was ready for use in the hydrazine coupling reactions. Calculated MW = 178.19 MALDI-TOF found [M+H] 179. 17.

General Procedure for Hydrazine Coupling Reaction

45 (20 mg, 0.11 mmol) was dissolved in 2 % AcOH in DMSO (1 mL) in a small glass vial. The aldehyde was added (0.12 mmol) and the vials were stirred for 48 hrs. The reaction progress was monitored by MALDI-TOF and once no starting material remained the reaction was stopped. The solvents were frozen using liquid nitrogen and then the samples were lyophilized. Once the DMSO was removed the samples were dissolved in Water/ACN (1/1) and purified by HPLC. The samples were lyophilized and submitted for inhibition studies.

General Procedure for Inhibition Study

Each kifunensine analogue was tested for inhibitory activity at three concentrations (0.05, 0.5, and 5 mM) using recombinant human ER mannosidase I or Golgi Man IA. ER Man I assays were performed using 20 μg of enzyme and Man_9-$GlcNAc_2$-PA (20 μM) as substrate in a final volume of 20 μL containing 20 mM MES/NaOH, pH 7.0, 150 mM NaCl, and 5 mM $CaCl_2$. The enzyme reactions were allowed to proceed for 15 min at 37 ^oC and were stopped by addition of 20 μL of 1.25 M Tris-HCl pH 7.6. The human ER Man I product, Man_8-$GlcNac_2$-PA, was resolved from $Man_9GlcNac_2$-PA by HPLC on a Hypersil APS-2 NH_2 column. $Man_9GlcNac_2$-PA was prepared by reductive pyridylamination of $Man_9GlcNac_2$ isolated from crude soybean agglutinin. Golgi Man IA

assays were performed using 10 μg of enzyme in a reaction containing 20 mM potassium phosphate, pH 6.0, 150 mM NaCl, 5mM Man-α-1,2-Man-α-O-CH_3 in a total volume of 25 μL. Enzyme reactions were allowed to proceed for 30 min at 37 ^oC and terminated by the additionof 25 μL of 1.25 Tris-HCl, pH 7.6. The amount of mannose released was quantified using a glucose oxidase and peroxidase reagent. The recombinant enzymes were expressed and purified. For determination of the compound inhibition, enzyme activity was plotter as a percentage of residual activity (compared to no added compound) versus compound concentration and the IC_{50} values were estimated from the plots. All inhibitory assays and cellular studies were performed by the Dr Kelley Moremen lab at the CCRC of the University of Georgia.

Pyridine-DMJ (46) ^{1}H NMR (500 MHz, D_2O) δ 8.35 (d, *J* = 6.8 Hz, 2H), 7.86 (d, *J* = 6.8 Hz, 3H), 7.55 (s, 2H), 4.24 (dd, *J* = 12.2, 2.8 Hz, 1H), 4.16 – 4.03 (m, 3H), 3.80 (t, *J* = 8.7 Hz, 1H), 3.66 (dd, *J* = 8.7, 3.2 Hz, 1H), 3.33 (ddd, *J* = 8.5, 5.6, 2.8 Hz, 1H), 3.19 (dd, *J* = 13.9, 1.9 Hz, 1H). Calculated MW = 267.28, MALDI-TOF found [M+H] 268.32

.

4-Amino-pyridine-3-DMJ (47) Calculated MW =282.30, MALDI-TOF found [M+H] = 283.35.

4- Imidazole-DMJ (48) ^{1}H NMR (500 MHz, d_2o) δ 9.72 (s, 1H), 8.83 (s, 1H), 8.54 (d, *J* = 12.3 Hz, 1H), 8.20 (s, 1H), 6.05 (s, 1H), 4.27 – 4.21 (m, 1H), 4.11 – 4.00 (m, 1H), 3.94 (dd, *J* = 12.1, 3.7 Hz, 1H), 3.78 (ddd, *J* = 16.7, 15.3, 6.0 Hz, 1H), 3.61 – 3.44 (m, 1H),

2.94 – 2.82 (m, 1H), 2.59 (s, 2H). Calculated MW = 256.26, MALDI-TOF found [M+H] = 257.30.

3-Methyl-2-thiophene DMJ (49) Calculated MW =286.35, MALDI-TOF found [M+H] = 287.42.

1H-pyrrole[3,2-b]-pyridine-6-DMJ (50) Calculated MW = 306.32, MALDI-TOF found [M+H] = 307.40.

CHAPTER 4

THE EXTRACYCTOPLASMIC DOMAIN OF THE *MYCOBACTERIUM TUBERCULOSIS* SER/THR KINASE PKnB BINDS SPECIFIC MUROPEPTIDES AND IS REQUIRED FOR PKnB LOCALIZATION

Mushtaq Mir[1], Jinkeng Asong[2], Xiuru Li[2], Jessica Cardot[2], Geert-Jan Boons[2], Robert N. Husson[1]*

PLoS Pathogens July 2011

Short title: Muropeptides bind and localize PknB

Mushtaq Mir[1], Jinkeng Asong[2], Xiuru Li[2], Jessica Cardot[2], Geert-Jan Boons[2], Robert N. Husson[1]*

1 Division of Infectious Diseases, Children's Hospital Boston and Harvard Medical School, Boston, MA 02115

2 Department of Chemistry and the Complex Carbohydrate Research Center, University of Georgia, Athens, GA 30602

*Corresponding Author:

Robert N. Husson

Division of Infectious Diseases

Children's Hospital Boston

300 Longwood Ave.

Boston, MA 02115

Tel: 617-919-2883

Fax: 617-730-0254

Email: robert.husson@childrens.harvard.edu

Abstract

Mycobacterium tuberculosis Ser/Thr kinase PknB has been implicated in the regulation of cell growth and morphology in this organism. The extracytoplasmic domain of this membrane protein comprises four penicillin binding protein and Ser/Thr kinase associated (PASTA) domains, which are predicted to bind stem peptides of peptidoglycan. Using a comprehensive library of synthetic muropeptides, we demonstrate that the extracytoplasmic domain of PknB binds muropeptides in a manner dependent on the presence of specific amino acids at the second and third positions of the stem peptide, and on the presence of the sugar moiety *N*-acetylmuramic acid linked to the peptide. We further show that PknB localizes strongly to the mid-cell and also to the cell poles, and that the extracytoplasmic domain is required for PknB localization. In contrast to strong growth stimulation by conditioned medium, we observe no growth stimulation of *M. tuberculosis* by a synthetic muropeptide with high affinity for the PknB PASTAs. We do find a moderate effect of a high affinity peptide on resuscitation of dormant cells. While the PASTA domains of PknB may play a role in stimulating growth by binding exogenous peptidoglycan fragments, our data indicate that a major function of these domains is for proper PknB localization, likely through binding of peptidoglycan fragments produced locally at the mid-cell and the cell poles. These data suggest a model in which PknB is targeted to the sites of peptidoglycan turnover to regulate cell growth and cell division.

Author Summary

Regulation of growth by *Mycobacterium tuberculosis* is important in the pathogenesis of tuberculosis (TB), including asymptomatic latent TB infection and active TB disease. The *M. tuberculosis* kinase PknB regulates cell growth and cell division by phosphorylating proteins involved in these processes to modify their function. The activity of PknB is thought to respond to extracellular stimuli by binding specific molecules with its extracytoplasmic domain. In this work we show that cell wall fragments bind to this domain, and that strong binding requires that these interacting molecules have specific molecular features. We demonstrate that a peptidoglycan fragment that binds strongly can stimulate growth of dormant bacteria, but that it does not affect growth of no*N*-dormant bacteria. We also show that PknB localizes to the site of cell division and to the growing tip of the bacterium, where cell wall synthesis and degradation occur, and that the extracytoplasmic domain is required for this localization. These findings indicate that a major function of the extracytoplasmic domain of PknB is to place it at the sites of cell wall turnover, and suggest a model by which PknB can regulate growth and cell division, and thereby contribute to the pathogenesis of TB.

Introduction and Literature Review

Bacterial cell growth and cell division are highly regulated processes, requiring the coordination of multiple activities within the cell. DNA replication and chromosome segregation for example, must occur at the correct time and in the correct location, and be coordinated with septum formation and cytokinesis. The molecules involved in septum formation and the sequence in which they are recruited to the division site have been the subject of intense investigation in the model organisms *Bacillus subtilis* and *Escherichia coli*, and the identities and functions of many bacterial cell division proteins have been elucidated [1], [2]. In addition to divisome assembly and DNA segregation, bacterial growth and cell division require remodeling of the peptidoglycan (PGN) mesh that forms the cell wall [3]. The enzymes and the sequence of reactions involved in cell wall synthesis are relatively well understood as are the enzymatic activities of many of the PGN hydrolases that can degrade this polymer [4], [5]. In the model organism *B. subtilis*, the mechanisms by which cell wall hydrolases are regulated to achieve morphogenesis are at least partially understood [6]. In other bacteria, including the slow growing actinomycete *Mycobacterium tuberculosis*, less is known about the regulation of PGN synthesis and hydrolysis, how these opposing processes are balanced, and how they are coordinated with other cell processes in growing and dividing vs. no*N*-growing dormant cells.

Because of the apparent ability of *M. tuberculosis* to become dormant in the human host, leading to asymptomatic latent infection, there has been great interest in understanding how cell growth and cell division are regulated in this organism [7]. A longstanding observation that “spent” or “conditioned” medium, i.e. filter-sterilized

supernatant from bacterial cultures grown in liquid medium, is able to stimulate growth of dormant cells, led to the identification of a resuscitation promoting factor (Rpf) by purifying from spent medium a component that was able to stimulate growth of the actinomycete *Micrococus luteus* [8]. Rpf is small protein that has homologues in other actinobacteria, including *M. tuberculosis*, which has five *rpf* genes [9]. Functional studies of these genes in *M. tuberculosis* have shown that individually they are not required for resuscitation of dormant *M. tuberculosis* cells and single *rpf* mutant strains do not have other growth or morphologic phenotypes. When two or more *rpf* genes are inactivated, however, growth or resuscitation defects are observed [10], [11], [12]. The recent demonstration that the Rpf's are PGN hydrolases suggests that growth stimulation of dormant cells may result from the enzymatic activity of these secreted proteins, possibly through alterations in PGN structure or through the interaction of PGN degradation products with the bacterial cell surface [13].

A domain found to occur in the extracytoplasmic regions of penicillin binding proteins and serine/threonine kinases (PASTA domain) was identified by bioinformatic analysis and predicted to bind to the stem peptide of u*N*-crosslinked PGN precursors, based on the structure of the PASTA-containing penicillin binding protein PBP2X of *Streptococcus pneumoniae* bound to a cephalosporin antibiotic [14]. Recently the PASTA domain of a Ser/Thr kinase of *B. subtilis* was shown to bind both intact and hydrolyzed PGN [15]. Incubation of *B. subtilis* spores with PGN stimulated spore germination and increased Ser/Thr phosphorylation. Some specificity with respect to the source of PGN and these functional effects was observed, suggesting a preference for meso-

diaminopimelic acid (m-DAP)-containing PGN in stimulating spore germination in this organism.

The *M. tuberculosis* genome encodes two proteins that contain PASTA domains, the Ser/Thr protein kinase PknB (Rv0014c) whose extracytoplasmic region comprises four PASTA domains, and the bifunctional penicillin binding protein PBP2 (PonA2, Rv3682), which has a single PASTA domain at the extreme carboxy-terminus of the protein distal to the extracytoplasmic transpeptidase and transglycosylase-containing regions [16]. In this work we investigated the quantitative binding of a series of synthetic muropeptides to the extracytoplasmic region of PknB. We identified specific features of these molecules that are required for high affinity binding, and investigated the functional effects of these compounds *in vivo* on mycobacterial growth, morphology and the localization of PknB. We determined that PknB is strongly localized to septum and less strongly to the cell poles, the sites of active PGN synthesis in mycobacteria, and that the PASTA domains of PknB are required for its localization.

RESULTS

Binding of PGN fragments to the extracytoplasmic domain of PknB

The region of *pknB* that encodes the extracytoplasmic domain of PknB (ED-PknB) was amplified by PCR, cloned and ED-PknB was expressed in *Escherichia coli* as an *N*-terminal Glutathione-S-transferase (GST) fusion protein. The ED-PknB comprises 4 PASTA motifs that share limited sequence similarity aside from the key residues that define the motif (Figure S1). Soluble recombinant GST-ED-PknB was affinity purified to

>95% purity and after removal of the GST tag was used in subsequent binding experiments (Figure S2).

A series of PGN fragments (muropeptides) were synthesized as tri-, tetra- and penta-peptides linked to *N*-acetylmuramic acid (MurNAc) or as unlinked peptides. Amino acids characteristic of PGN stem peptides from Gram-positive bacteria, Gram-negative bacteria or actinobacteria were incorporated into different compounds. Modifications of amino acid side chains that correspond to PGN modifications that are found *in vivo* were also included in the compound series (Figure 14).

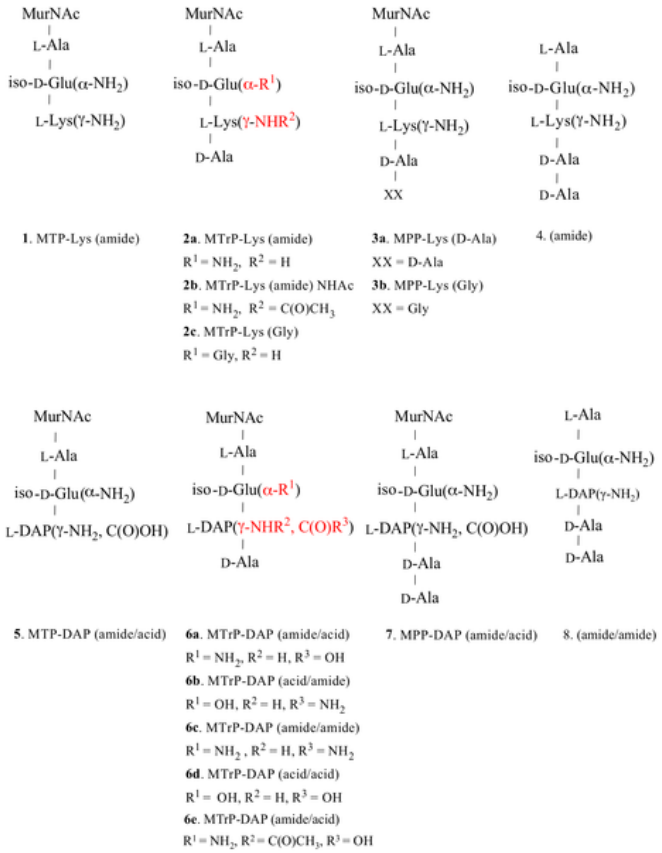

Figure 14. Structures of synthetic muropeptides used in the binding and phenotypic assays. Lys-containing compounds are typical of Gram-positive bacteria and DAP-containing compounds are typical of Gram-negative bacteria and Actinomycetes, including mycobacteria. Variations in substituents are indicated in red, and the specific variations are listed immediately below the

These compounds were then used in surface plasmon resonance (Biacore) experiments to measure binding affinities of the muropeptides to ED-PknB. To obtain kinetic and thermodynamic parameters, a range of compound concentrations was assayed and kinetic analysis was performed using Biacore Software. An example of a set of sensorgrams for a compound with a relatively low K_D is shown in Figure 15. Sensorgrams for the other compounds tested are shown in Figure S3. Table S1 shows detailed kinetic parameters obtained from these experiments.

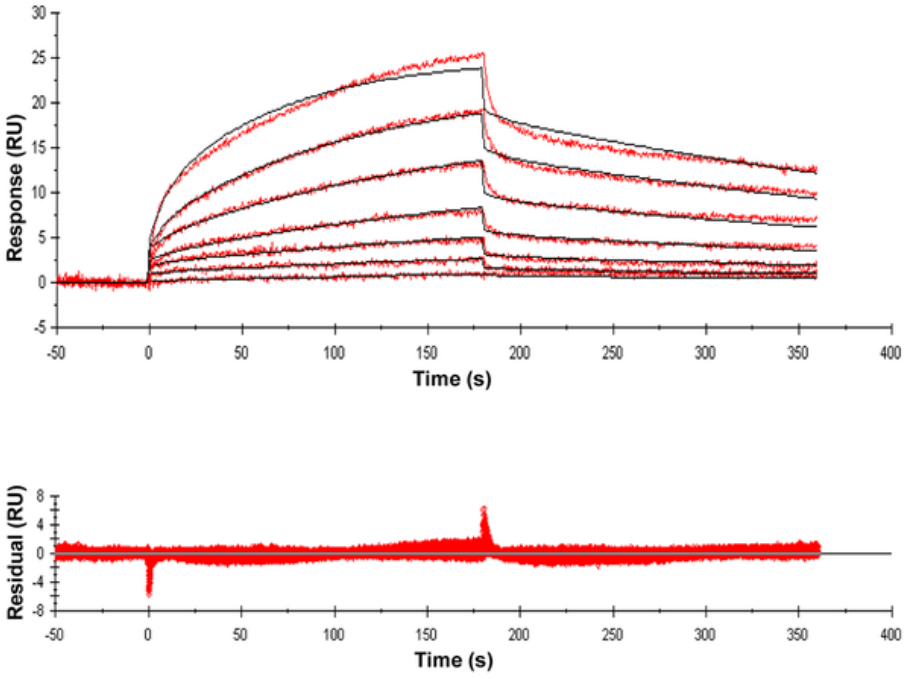

Figure 15. Sensorgram of a compound with relatively high binding affinity for ED-PknB. The sensorgram shows the simultaneous concentratio*N*-dependent kinetic analysis of two-fold serial dilutions of MTrP-DAP (amide/acid) (Compound 6c in Figure 14) at concentrations from 1.56 µM to 100 µM. ED-PknB was bound to the sensor chip and at time 0 the muropeptide ligand was flowed over the chip as described in the methods section. Vertical deflection of the curve indicates binding in RU (resonance units). The primary data are shown in red. The data were fitted with a two-state binding model (black lines). The corresponding residual values, which are the signal remaining after the data are fitted to the kinetic model,

are plotted below the sensorgrams. The kinetic parameters calculated from the model are shown below the graphs.

As shown in Table 5, these experiments demonstrated moderately strong binding of several PGN fragments that have DAP at the third position of the stem peptide.

Table 5. Affinity of synthetic muropeptides for the extracytoplasmic domain of *M. tuberculosis* PknB.

Analyte	K_D (μM)
MTP-Lys (amide) **1**	>500
MTrP-Lys (amide) **2a**	21.5
MTrP-Lys (amide) NHAc **2b**	>500
MTrP-Lys (Gly) **2c**	> 500
MPP-Lys (D-Ala) **3a**	> 500
MPP-Lys (Gly) **3b**	>500
Peptide **4** (amide)	> 500
MTP-DAP (amide/acid) **5**	21.8
MTrP-DAP (amide/acid) **6a**	12.7
MTrP-DAP (acid/amide) **6b**	>100
MTrP-DAP (amide/amide) **6c**	14.9
MTrP-DAP (acid/acid) **6d**	53.6
MTrP-DAP(amide/acid)NHAc **6e**	73.8
MPP-DAP (amide/acid) **7**	25.1
Peptide **8** (amide/amide)	>500

Recombinant ED-PknB was immobilized on NHS-activated groups of a CM-5 sensor chip surface (5,000 RU) and titration experiments were performed with the synthetic compounds **1–8** (Figure 1). The binding constants of all compounds were determined by fitting the data using a two-state binding model. Kinetic binding parameters and the sensorgrams for the kinetic analyses are presented in Table S1 and Figure S3. MTP, muramyl-tripeptide; MTrP, muramyl-tetra peptide; MPP, muramyl-pentapeptide.
doi:10.1371/journal.ppat.1002182.t001

N-acetylation of the amino group of DAP as in compound **6e** (MTrP-DAP (amide/acid) NHAc), which is designed to mimic branching of the PGN subunits within the PGN polymeric structure, resulted in a six-fold decrease in binding compared to compound **6a**. The MurNAc-pentapeptide, compound **7**, corresponding to newly synthesized PGN prior to remodeling, bound strongly though about two-fold less than the corresponding MurNAc-tetrapeptide (**6a)**.

In addition to preference for DAP at the third position of the stem peptide, another clear result of these experiments is the requirement for amidation of D-isoglutamate (D-iGlu) to D-isoglutamine (D-iGln) at the second position, in order to achieve high affinity binding. Compound **6a**, which contains both D-iGln and DAP at the second and third positions, respectively, exhibited the highest affinity, while compound **6d**, which is identical except for D-iGlu at the second position, bound four-fold less strongly. Similarly, compound **6c**, which also bound with a relatively high affinity (K_D = 15 μM), contains D-iGln together with amidation of the carboxyl group of DAP. In contrast, a similar compound, (**6b**), that has D-iGlu at the second position instead of D-iGln did not show measurable binding. The importance of this residue is further underscored by the finding that among the Lys-containing compounds, the only one that showed detectable interaction was compound **2a**, the muramyl tetrapeptide incorporating a D-iGln moiety. While the data indicate a preference for DAP at the third position, the ε-carboxylic acid group that is a major feature that distinguishes DAP from Lys is not an essential requirement for binding. To determine whether the MurNAc moiety was important for binding, compounds **4** and **8**, pentapeptides not linked to MurNAc and containing either Lys or DAP at the third position, respectively, were tested. Neither compound showed

significant interaction, indicating an important contribution of MurNAc in binding to the PknB PASTA domains.

Muropeptides stimulate resuscitation of dormant *M. tuberculosis* cells

The Rpf's have been shown to have PGN hydrolytic activity, and are thought to cleave the ß-1–4 glycosidic linkage between *N*-acetylmuramic acid and *N*-acetylglucosamine [13]. This muralytic activity has been shown to be essential for the resuscitation activity of these Rpf proteins, but the mechanism remains uncertain. To determine whether muropeptides that bind to the PASTA domains of ED-PknB can stimulate resuscitation of dormant *M. tuberculosis* cells, we utilized an established *M. tuberculosis* dormancy and resuscitation model [17]. In this assay, *M. tuberculosis* cells are incubated under hypoxic conditions for several months, at which point the number of cells capable of resuming growth in liquid culture is markedly decreased. In this assay, addition of sterile spent medium "resuscitates" dormant cells, leading to an increase in the number of cells that can grow on solid or in liquid medium.

In two independent experiments, we took *M. tuberculosis* stationary phase cultures that had been incubated under hypoxic conditions for 6 or 9 months, and performed this resuscitation assay. In addition to cells incubated in Sauton's medium alone, cells were incubated with a synthetic muropeptide with a high affinity for ED-PknB (**6c** in Figure 14), a muropeptide with low affinity for ED-PknB (**3b** in Figure 14), or with sterile conditioned medium as a positive control. The muropeptides were used at a concentration of 10 times the K_D of the high affinity compound as determined in the SPR experiments. Using most probable number analysis [18], which has been used to

analyze results from this assay, we observed three and nine-fold increases in the viability of cells that were incubated with the high affinity muropeptide in the two independent experiments. No increase in viability was observed for cells incubated with the low affinity peptide. The cells incubated with sterile spent medium showed a much stronger resuscitation phenotype, with 14 and 100-fold increased viability relative to the cells incubated in fresh medium alone (Table 6).

Table 6. Resuscitation of dormant *M. tuberculosis* cultures.

Additive to Culture Medium	Fold increase*
Experiment 1:6 month old dormant culture	
MTrP-DAP (amide/amide) (6c)	9
MPP-Lys (Gly) (3b)	0.9
50% spent medium	100
Experiment 2:9 month old dormant culture	
MTrP-DAP (amide/amide) (6c)	3
MPP-Lys (Gly) (3b)	1
50% spent medium	13.6

*Fold increase in viable cell number relative to cultures grown in Sauton's medium without additive.

doi:10.1371/journal.ppat.1002182.t002

The original identification of Rpf in *M. luteus* was based on the observation that stationary phase cells show decreased viability when plated or diluted to low density in liquid medium, but that addition of sterile conditioned medium stimulates growth [8]. A similar phenomenon is observed when mycobacteria are inoculated at low density. To

determine whether synthetic muropeptides stimulate growth when stationary phase cells are inoculated at low density, cells from cultures of *M. tuberculosis* ($O.D_{600}$ of 2.4–3.6) were washed and diluted 10,000-fold in minimal medium with or without the addition of the high or low affinity muropeptide. As shown in Figure 16, no growth stimulation by either muropeptide was observed in this assay. In contrast, strong growth stimulation by conditioned medium was observed.

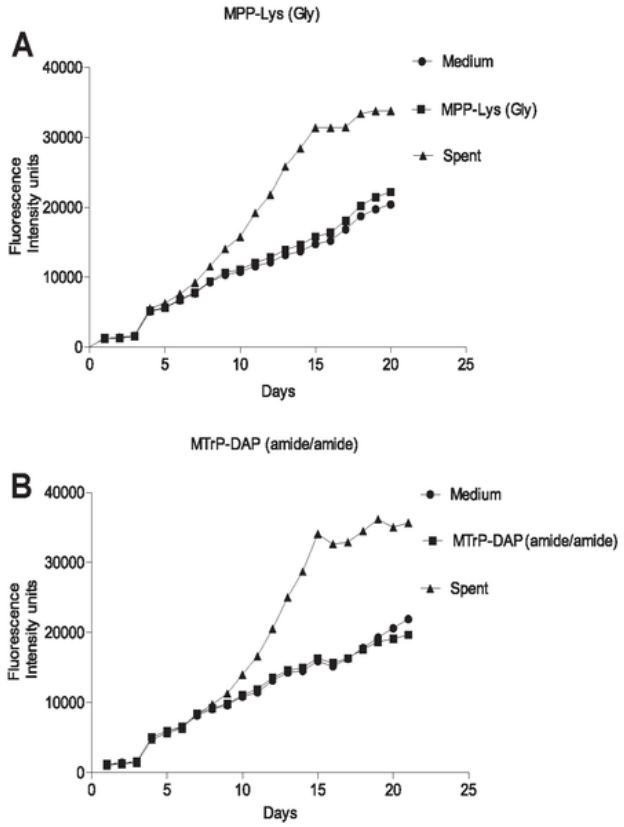

Figure 16. Growth stimulation assay of low inoculum cultures of *M. tuberculosis*. *M. tuberculosis* cells were grown in Sauton's medium alone or in medium supplemented with a synthetic muropeptide at a concentration 10 times the K_D, or with 50% (v/v) sterile conditioned (spent) medium. Cells were grown to stationary phase, diluted and inoculated into medium containing alamar blue and grown at 37° C, with measurement of fluorescence at 595 nm at serial time points. **A**. Growth curves for MTrp-DAP (Compound 6c in Figure 14). **B**. Growth curves for MPP-Lys (Compound 3b in Figure 14). ■, Sauton's medium. ▲, Sauton's medium plus synthetic muropeptide. ▼, Sauton's medium plus spent medium.

PknB is present in the cell envelope of *M. tuberculosis*

Based on its sequence, PknB is predicted to have a single transmembrane segment, with an intracellular kinase domain and an extracytoplasmic region that incorporates the four PASTA domains [16]. To determine whether PknB is a membrane protein and in which subcellular fraction(s) PknB is located, we performed immunoblotting with a PknB-specific monoclonal antibody. As a control, we probed these subcellular fractions with an antibody to the membrane protein PknA, which like PknB has a single transmembrane segment, but which has a small extracytoplasmic region that is not known to interact with cell wall components. We found that PknB does, as predicted, localize to the membrane fraction of the cell (Figure 17). An even stronger signal was seen in the cell wall fraction, further confirming the association of PknB with the cell envelope. The PknA antibody gave equally strong signals from the membrane and cell wall fractions. These results demonstrate that PknB is a membrane protein and that membrane is present in the cell wall fractions used in these experiments

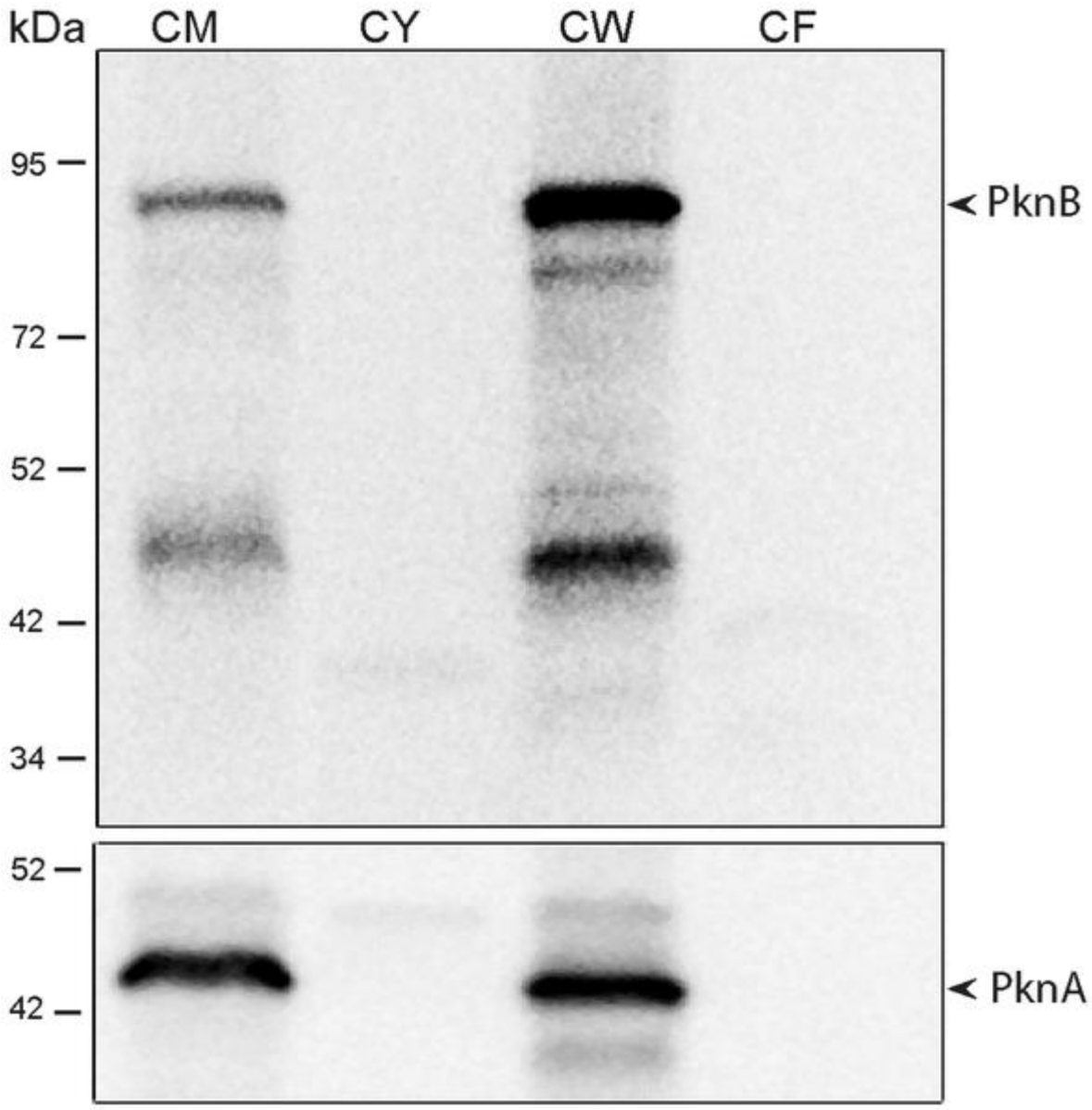

Figure 17. Subcellular localization of *M. tuberculosis* PknB. Top panel: Immunoblot of subcellular fractions of *M. tuberculosis*, probed with a mouse monoclonal antibody that recognizes *M. tuberculosis* ED-PknB. Bottom panel: immunoblot in which the same fractions were probed with rabbit polyclonal sera raised against *M. tuberculosis* membrane protein PknA. CM, membrane fraction; CY, cytoplasmic fraction; CW, cell wall fraction; CF, culture filtrate fraction.

PknB localizes to the septum and poles, and the extracytoplasmic domain is required for proper PknB localization

A construct designed to express a PknB-RFP fusion protein, in which RFP is fused to the amino terminus of PknB, was introduced into wild type *M. smegmatis*. Additional constructs, in which RFP is fused a) to the PknB kinase domain, intracellular juxtamembrane sequence and transmembrane segment, but which lacks the extracytoplasmic domain, and b) to the membrane and ED-PknB regions but which lacks the intracellular linker and kinase domains, were also introduced into wild type *M. smegmatis*. Cells were grown to early log phase, expression of the fusion protein was induced, and the cells were examined using fluorescence microscopy (Figure 18). Cells expressing the full-length PknB-RFP fusion showed strong localization of this protein to the mid-cell and symmetrical, less intense localization to both cell poles. In contrast, in cells expressing the fusion that lacks the extracytoplasmic domain containing the PASTA domains, foci of fluorescence were visible at discrete sites along the length of the cell. While in some cells there appears to be increased signal at the poles, we did not observe clear mid-cell localization in cells expressing this construct. To confirm that these foci are not cytoplasmic aggregates, we prepared subcellular fractions of these cells and confirmed that the large majority of this protein is present in the cell membrane and cell wall fractions (Figure S4). Cells expressing the ED-PknB-RFP fusion lacking the intracellular linker and kinase domains showed clear localization to the mid-cell but minimal signal from the poles. This result indicates that the extracytoplasmic PASTA domains are required for proper localization of PknB to the mid-cell and likely to the cell poles and suggests that the intracellular linker-kinase region makes a contribution to

localization at the cell poles. To verify these findings, we performed additional imaging of live cells (Figure S5 and Protocol S1), which demonstrates the same localization patterns observed with the fixed cell preparations.

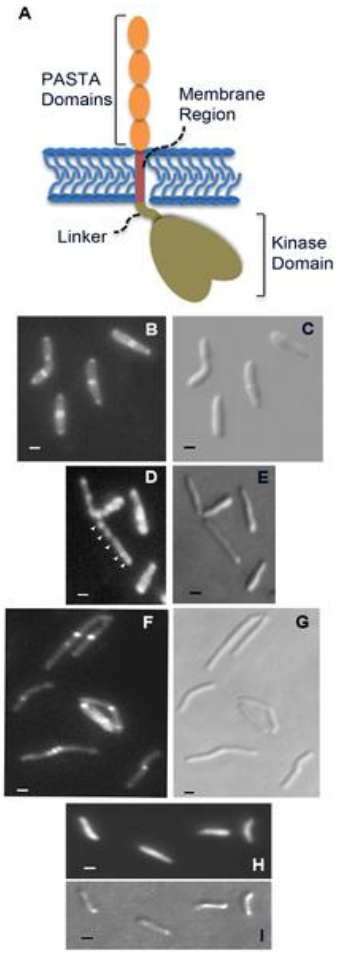

Figure 18. Localization of PknB to sites of peptidoglycan turnover in the mycobacterial cell. A. Schematic representation of domain organization of *M. tuberculosis* PknB, including the kinase domain (residues 11-274; the juxtamembrane linker (residues 275-331), the transmembrane segment (residues 332-354) and the extracytoplasmic PASTA domains (residues 355-626). B-I. Flourescence (B, D, F and H) and DIC (C, E, G and I) images of *M. smegmatis* expressing RFP fused to full-length PknB (B and C), PknB lacking the extracytoplasmic domain (D and E), PknB lacking the intracellular kinase domain and linker (F and G) and unfused RFP (H and I). Arrowheads in panel D point to focal RFP signals along the length of the bacillus.

To determine whether diffusible, no*N*-localized muropeptides might bind ED-PknB and disrupt PknB localization, we incubated *M. smegmatis* with the high affinity muropeptide used in the resuscitation experiments for 8 hours. No change in the morphology of wild type bacteria were observed, and in the strain expressing the PknB-RFP fusion protein the RFP signal remained localized to the septum and poles (not shown).

Discussion

In this work we report three major findings. First, we demonstrated that muropeptides bind to the extracytoplasmic region of PknB, which contains four PASTA domains, and defined molecular requirements for ligand binding. These requirements include both specific residues at the second and third positions in the stem peptide, and the presence of the sugar moiety (MurNAc) linked to the amino-terminal residue of the peptide. Using an extensive series of chemically synthesized compounds, we found moderately high affinity binding by muropeptides that contain DAP at the third position of the stem peptide, in which the D-iGlu at the second position is amidated to D-iGln. The preference for DAP is consistent with the predominant structure of the stem peptide of mycobacteria, where DAP is present at this position, in contrast to most Gram-positive organisms in which Lys occurs at this position. D-iGln at the second position has been reported to be predominant in *M. tuberculosis* PGN, however D-iGlu is present in a minority of stem peptides [19], [20]. Whether synthesis of PGN incorporating D-iGlu vs. D-iGln is site- or growth-stage specific in *M. tuberculosis* is not known. The markedly stronger binding of compounds containing D-iGln suggests that variation in the structure of PGN stem peptides may affect binding by ED-PknB *in vivo*, with potentially important

physiologic effects. A recent paper examining stimulation of *B. subtilis* spore germination using synthetic muropeptides confirmed prior results using purified native PGN in showing the importance of DAP at the third position of the stem peptide for this phenotype in this species [21]. In this assay the presence of *N*-acetylglucosamine linked to MurNAc was also required for potent activity.

A second finding of this work is that PknB localizes strongly to the mid-cell and less strongly to the cell poles of mycobacteria, the sites of active PGN synthesis and hydrolysis in these organisms [22]. Our results with RFP fusions to full-length PknB and to separate domains of this protein in *M. smegmatis* demonstrate that the PASTA motif-containing extracytoplasmic domain of PknB is required for its localization to the mid-cell. We attempted to perform a similar experiment with full-length PknB-RFP in *M. tuberculosis*, however we were unable to obtain consistent expression of the fusion protein. We observed fluorescence in a minority of cells, which was highly variable from cell to cell, and we observed markedly abnormal morphology of many cells, suggesting severe toxicity of *pknB* overexpression, as previously described [23]. Despite these limitations, we were able to see similar localization of full-length PknB in a minority of rod-shaped cells expressing the *pknB-rfp* fusion (data not shown).

In the context of our *in vitro* binding results, these data suggest that binding of PGN fragments by its extracytoplasmic domain is critical for PknB localization to the mid-cell and possibly to the poles. This result, together with the finding that PknB is found in the cell wall and membrane fractions of *M. tuberculosis* lysates, suggests that the PASTA motifs of PknB bind endogenous cell wall or membrane-anchored PGN

precursors and/or PGN hydrolysis fragments produced at the septum and poles of the cell. The finding that incubation of growing cells with a high affinity muropeptide had no effect on PknB localization is consistent with this model, and suggests that exogenous muropeptides may not be able to penetrate the complex, lipid-rich mycobacterial cell envelope to reach the PknB PASTA domains at the surface of the cytoplasmic membrane. Because both *de novo* synthesized PGN precursors and PGN hydrolysis products are likely to be localized at the septum and the poles, our data do not indicate which of these are the major PknB PASTA ligands *in vivo*.

The third important finding of this work is that, in contrast to spent medium, which strongly stimulated both growth of no*N*-dormant *M. tuberculosis* cells and resuscitation of dormant cells, a muropeptide with relatively high affinity for the PASTA domains of ED-PknB did not stimulate *M. tuberculosis* growth and had only a modest effect on resuscitation. This result suggests that while muropeptide binding may play a role in resuscitation of *M. tuberculosis*, other factors present in spent medium may be more important in stimulating *M. tuberculosis* growth. In this regard, D-amino acids present in conditioned medium have recently been shown to be a potent growth stimulus for *Vibrio cholerae* and to play a key role in biofilm disruption leading to resumption planktonic growth in *B. subtilis* [24], [25]. Alternatively, PknB may require a different muropeptide ligand, e.g. a disaccharide muropeptide or a multivalent muropeptide, or higher concentrations of these ligands, which may be present *in vivo*, for greater stimulation of growth or resuscitation.

The first structure of a PASTA domain was determined as part of the structure of PBP2x from *S. pneumoniae* bound to a cephalosporin antibiotic [26]. In this structure two PASTA domains interacted to form a compact globular domain. In recent work, the structure of the PASTA motifs of *M. tuberculosis* ED-PknB was determined using NMR and small angle X-ray scattering [27]. While the individual folds of each PASTA domain were similar to those of the PBP2x PASTA domains, the four PASTA domains of PknB are organized as a linear molecule, which is maintained with what the authors termed a ß′/ß″ brace that prevents interactions between the individual PASTA domains of a single molecule of PknB. A previous structure of the PknB intracellular domain demonstrated the presence of a highly flexible intracellular juxtamembrane segment linking the transmembrane segment to the intracellular kinase domain, indicating that ligand binding resulting in transmembrane propagation of conformational changes leading to PknB activation is unlikely [28].

Based on the PknB PASTAs structure, a model was proposed in which binding of a single ligand to two molecules of PknB would result in dimerization of the extracytoplasmic domains, which would then cause dimerization of the intracellular kinase domains, resulting in kinase activation [27]. Our data showing relatively high affinity binding of muropeptide monomers, however, suggest an alternative model by which muropeptide binding to ED-PknB could lead to localization and activation of this kinase. In this model, at sites of active PGN hydrolysis and synthesis, i.e. the septum and the cell poles, local concentrations of PGN precursors and PGN hydrolysis products will be high, and binding of these ligands by ED-PknB would result in the septal and polar localization of PknB that we observed. The recruitment of PknB to these sites will

consequently result in high concentrations of the intracellular kinase domain, leading to the dimerization that results in kinase activation [28], [29], [30]. PknB activation will then lead to phosphorylation of protein substrates, resulting in regulation of cell division and cell wall synthesis (Figure 19). In this model, there is no requirement for binding of a single muropeptide by PASTA domains from two PknB molecules, or for muropeptides that diffuse from a distance, to achieve PknB localization and activation.

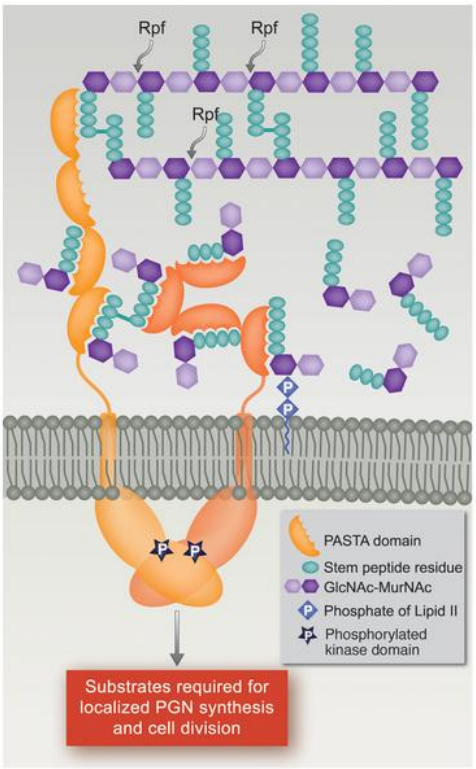

Figure 19. Model of PknB localization and activation by interaction of its extracytoplasmic domain with peptidoglycan fragments. In this model, the extracytoplasmic domains of PknB bind PGN precursors and/or hydrolysis products produced at the mid-cell and poles, the two sites where active PGN synthesis and degradation occur in mycobacteria. This interaction leads to localization of PknB at the theses sites, and to PknB activation by dimerization of the intracellular kinase domains. Both linear and no*N*-linear forms of the extracytoplasmic domain are shown to allow for possible changes following ligand binding. RPF, resuscitation promoting factor.

In summary, we have demonstrated sequence-specific binding of muropeptides to the PASTA domai*N*-containing extracytoplasmic region of *M. tuberculosis* PknB, and that the presence of the PASTA domains is required for localization of PknB to sites of PGN turnover. In the context of our phenotypic data and the finding that peptides that bind with high affinity have peptide sequences characteristic of *M. tuberculosis* PGN, our results suggest that in *M. tuberculosis*, the PknB PASTAs bind to PGN precursors or fragments resulting from local PGN synthesis and/or hydrolysis at the mid-cell and poles. This PASTA domai*N*-mediated localization provides a mechanism by which PknB and the co-regulated kinase PknA can regulate cell division and PGN turnover by reversible phosphorylation of proteins involved in these processes, several of which have been shown to be PknA or PknB substrates and to localize to these sites [22], [23], [31], [32], [33].

Materials and Methods

Strains, media, and recombinant plasmid construction and protein production

Escherichia coli TOP10 (Invitrogen) was used for cloning and was grown in LB broth. *E. coli* BL21 (DE3) (Stratagene) was used for expression of recombinant ED-PknB. *M. tuberculosis* H37Rv or *M. smegmatis* mc^2-155 were grown at 37°C in Middlebrook 7H9 liquid medium (Difco) supplemented with albumi*N*-dextrose complex (ADC), 0.2% Glycerol and 0.05% Tween 80, except for resuscitation experiments where *M. tuberculosis* was grown in Sauton's medium (Difco). Kanamycin (50 μg ml^{-1}) or ampicillin (100 μg ml^{-1}) was added to culture media or agar when appropriate.

For expression and purification of ED-PknB, the nucleotide sequence encoding PknB from Gly_{354} to Gln_{626} was PCR-amplified from genomic DNA of *M. tuberculosis* H37Rv and cloned in pGEX-4T-3 (GE Healthcare) for expression as a glutathione-S-transferase (GS) fusion protein. Recombinant GST-ED- PknB was affinity purified to >95% homogeneity using immobilized glutathione agarose (Pierce) (Figure S2). To cleave the GST from the fusion protein, the thrombin CleanCleave kit (Sigma) was used. In brief 900 µg of purified recombinant ED-PknB-GST was incubated with 100 µL of 50% (v/v) suspension of thrombin agarose for 1 hr at room temperature. After centrifugation the supernatant containing ED-PknB and free GST was incubated with 500 µL of 50% (v/v) suspension of Glutathione-agarose for 15 min. After centrifugation the supernatant containing ED-PknB was collected. For SPR analysis the supernatant was dialyzed against phosphate buffered saline (PBS) pH 7.4 prior to use.

For localization of PknB or PknB lacking the extracytoplasmic domain (PknBΔED) in wild *type M. smegmatis*, the full length *pknB* gene or the nucleotide sequence encoding the region from Met_1 to Gly_{354} of PknB (*pknBΔED*) respectively, were PCR-amplified from genomic DNA of *M. tuberculosis H37Rv*. Overlap PCR amplification of the above PCR products was performed with the PCR product of the red fluorescent protein (*rfp)* gene using a forward primer annealing to the 5′ region of *rfp* and a reverse primer annealing to the 3′ region of *pknB* or *PknBΔED* to obtain the PCR products *rfp-pknB* or *rfp-pknBΔED.* A PacI site was introduced between *rfp* and *pknB.* The fusion PCR products were cloned into the integrating vector pMV306-p_{acet} downstream of the inducible acetamide promoter at NdeI and XbaI sites to obtain pMV306-p_{acet}-*rfp-pknB* or pMV306-p_{acet}-*rfp- pknBΔED*. To obtain recombinant clone

pMV306-p_{acet}-*rfp-pknBΔKD* expressing RFP linked to transmembrane and extracellular domains of PknB (ED-PknB-RFP) the *pknB* gene of the clone pMV306-p_{acet}-*rfp-pknB* was replaced with the nucleotide sequence encoding Ile_{326} - Gln_{626} using PacI and XbaI sites. Cloned DNA was sequenced to verify the absence of mutations. A mycobacterial replicating vector that constitutively expresses RFP was a gift from Eric Rubin.

Chemical synthesis of PGN fragments

Compounds were synthesized using classical fluorenylmethoxycarbonyl (Fmoc) chemistry and standard manual solid-phase peptide synthesis techniques as previously described [34], [35], [36], [37], [38], [39]. In the preparation of the peptide portion of the compounds, Sieber Amide resin was swelled in dimethylformamide (DMF) for 45 min and then treated with piperidine in DMF. After a reaction time of 30 min, the solvents were removed by filtration and the resin washed with DMF, and then treated with Fmoc-linked amino acid building blocks. This generated PGN partial structures with *N*-termini.

Compound 8 was newly synthesized for this work as follows. Rink amide AM LL resin (0.1 mmol) was swelled in dichloromethane for 30 min and then rinsed with DMF (3×5 mL). The resin was treated with piperidine in DMF (20%, 3×5 mL). After a reaction time of 30 min, the solvents were removed by filtration and the resin was washed with DMF (3×5 mL), followed by treatment with Fmoc-D-Ala-OH (155.7 mg, 0.5 mmol) in DMF in the presence of HATU (mg, 0.5 mmol) and DIPEA (mL). The reaction progress was monitored by a Kaiser test. After completion of the coupling, the resin was washed with DMF (3×5 mL). The Fmoc protecting group was removed by treatment with piperidine in DMF (20%, 3×5 mL, 3×10 min). The reaction cycle was repeated using

Fmoc-D-Ala-OH (155.7 mg, 0.5 mmol), Fmoc-DAP(BOC,tBu)-OH (113.7 mg, 0.2 mmol), Fmoc-D-iso-Gl*N*-OH (73.7 mg, 0.2 mmol), Fmoc-L-Ala-OH (155.7 mg, 0.5 mmol). The final Fmoc protecting group was removed by treatment with piperidine in DMF (20%, 3×5 mL, 3×10 min). The resin was washed with DMF (3×5 mL) and the resin bound peptide was capped by treatment with acetic anhydride and (10%) and DIPEA (5%) in DMF (3×5 mL, 3×10 min). The resin was washed with DMF (3×5 mL), dichloromethane (7×5 mL), and methanol (3×5 mL) and dried *in vacuo* overnight. The peptide was released from the resin by treatment with TFA/TIPS/Water (95%/2.5%/2.5%) in DMF for 2 h. The resin was filtered and washed with TFA (1×10 mL). The filtrate was concentrated under reduced pressure and co-evaporated with toluene. The crude peptide was dissolved in water/acetonitrile and purified by semi-preparative HPLC (Eclipse XDB-C18 column, 5 mm, 9.4×250 mm, eluent: water/acetonitrile/0.1%TFA) to afford, after lyophilization of the appropriate fraction, the target compound **8**. HRMS-MALDI-TOF calculated for $C_{23}H_{40}N_8O_9Na$ [M + Na]: 595.29, experimental: 595.41.

Surface plasmon resonance binding assays and kinetic analysis

Binding interactions between ED-PknB and PGN analytes were examined using a Biacore T100 biosensor system (Biacore Life Sciences - GE Healthcare). Soluble ED-PknB was immobilized by standard amine coupling using an amine coupling kit (Biacore). The surface was activated using freshly mixed *N*-hydroxysuccimide (NHS; 100 mM) and 1-(3-dimethylaminopropyl)-ethylcarbodiimide(EDC; 391 mM) (1/1, v/v) in water. Next, ED-PknB (50 µg/ml) in aqueous NaOAc (10 mM, pH 4.5) was passed over

the chip surface until a ligand density of approximately 5,000 RU was achieved. The remaining active esters were quenched by aqueous ethanolamine (1.0 M; pH 8.5). The control flow cell was activated with NHS and EDC followed by immediate quenching with ethanolamine. HBS-EP (0.01 M HEPES, 150 mM NaCl, 3 mM EDTA, 0.005% polysorbate 20; pH 7.4) was used as the running buffer for the immobilization and kinetic studies. Analytes were dissolved in running buffer and a flow rate of 20 µL/min was employed for association and dissociation at a constant temperature of 25°C. A double sequential 60 s injection of aqueous NaOH (50 mM; pH 11.0) at a flow rate of 50 µl/min followed by 5 min stabilization with running buffer was used for regeneration and achieved prior baseline status. The same experimental surface was used for approximately 4 weeks and maintained under running buffer conditions. MTP-DAP (amide/acid) (**5**) was used as a positive control in each experiment to check the stability of the ED-PknB surface activity during the course of the experiments.

To minimize bulk refractive index changes, nonspecific binding and instrument drift on the generated binding sensorgrams, a double referencing of the data was performed. First, bulk refractive index change effects were minimized by preparing all analytes in the HBS-EP buffer. Then, the binding responses over the reference surface were subtracted from the active surface to correct for nonspecific binding. A blank analyte run of running buffer alone was also subtracted from the specific binding sensorgrams to minimize instrument noise. Using Biacore T100 evaluation software, the response curves of various analyte concentrations were globally fitted to the two-state binding model [40].

Conditioned medium preparation

Conditioned medium was prepared as previously described [41]. Briefly, supernatant was obtained from *M. tuberculosis* H37Rv culture grown in ADC-supplemented Sauton's medium containing 0.05% Tween 80 at 37°C with shaking to an optical density at 600 nm (OD_{600}) of 1.2. After centrifugation (4000 rpm, 10 min), the supernatant was sterilized by passage through 0.22 µm filter, tested for sterility, and used for the resuscitation experiments.

Dormancy and resuscitation assay

To obtain no*N*-culturable dormant bacilli, *Mycobacterium tuberculosis* H37Rv was grown under long-term oxygen starvation in broth growth medium (Sauton's medium containing 0.05% tween 80 and supplemented with ADC) as previously described [10]. In brief, *M. tuberculosis* was initially grown to late stationary phase at 37°C with shaking. From this initial culture, 100 µL was subcultured into 20 ml of growth medium and grown to an optical density at 600 nm ($OD_{600)}$ of 1.8 to 2. Finally 100 µL was inoculated into 75 ml of growth medium containing 1.5 µg/ml methylene blue in a sealed 250-ml flask and grown with shaking at 37°C for 6 or 9 months. Methylene blue became colorless by 10 days of incubation, indicating oxygen depletion.

For resuscitation experiments muropeptides were dissolved in sterile Sauton's medium to a concentration of 20 times the binding constant (K_D) of the high affinity compound (**6c**) The dormant culture was serially diluted (10^{-1} to 10^{-6}) in growth medium. From each dilution 4 sets of triplicate 100 µL culture were aliquoted in wells of

96 well plates (one set each for muropeptides (2 muropeptides tested), growth medium and spent medium). 100 µL of growth medium, muropeptide, or spent medium was added to each well of the corresponding set. The final concentration of muropeptide was 10 times the K_D of the high affinity compound, and of the spent medium was 50%. Plates were incubated at 37°C. Drying was prevented by maintaining sterile water in outer wells of the plate. After 2 months the wells with visibly turbid growth were recorded and MPN values were calculated as previously described [42].

Growth stimulation assay

To investigate the effect of muropeptides on growth initiation of low inoculum cultures of *M. tuberculosis*, stationary phase ($O.D_{600}$ of 2.4–3.6) cultures grown in Sauton's medium supplemented with ADC and 0.05% Tween 80 were passed through five micron pore filter (Millipore) to remove clumps. To obtain a single cell suspension, the culture was passed five times through a 27½ gauge needle followed by washing three times with Sauton's medium. 100 µl of a 10^{-4} dilution was inoculated into wells of a 96 well plate for a final volume of 200 µl. 1x alamar Blue was included in each well. As above, the final concentration of the muropeptides was 10 times the K_D of the high affinity compound, and of the spent medium was 50%. Each condition was tested in duplicate. Growth was monitored in each well by measuring fluorescence using excitation of 550 nm and emission of 595 nm and plotted as fluorescence intensity units versus time in days.

Microscopy

For cellular localization of RFP fusions to intact PknB or its domains, the corresponding plasmid expressing the fusion under control of the acetamidase promoter was electroporated into *M. smegmatis* cells. The resulting strains were grown in Middlebrook 7H9 liquid medium supplemented with ADC, 0.2% Glycerol and 0.05% Tween 80 to mid-log phase, followed by induction with 0.2% acetamide for 6 hrs. Cells were fixed in 4% paraformaldehyde at 37°C for 30 min followed by incubation with 50 mM ammonium chloride for 5 min at room temperature. Cells were transferred onto a glass slide, air-dried and one drop of Prolong Gold antifade reagent (Invitrogen) was applied before covering with a coverslip. After 24 hrs of curing in the dark, cells were observed using a Zeiss Axiophot microscope with a 63x differential interference contrast (DIC) oil immersion objective and red fluorescence filter. Images were captured by a Spot cooled CCD camera (Diagnostic Instruments), acquired with Spot software and processed by Adobe Photoshop CS2.

Western blotting

For cellular localization of native PknB in wild type *M. tuberculosis* cells, 60 µg total protein of cytosol, cell wall, cell membrane and culture filtrate fractions, prepared at Colorado Statue University and obtained from the Biodefense and Emerging Infections Research Resources Repository, was fractionated on 10% SDS-PAGE and transferred to a PVDF membrane. The blot was blocked in Tris-buffered saline containing 0.1% Tween 20 (TBST) and 5% milk for 1 hr at room temperature. The blot was incubated overnight at 4°C with 1:10,000 dilutions of either a mouse monoclonal antibody raised against

extracytoplasmic domain of PknB or with a rabbit polyclonal antibody against PknA. After thorough washing with TBST, the blot was incubated with a 1:10,000 dilution of HRP-conjugated secondary antibodies (Cell Signaling) for 3 hrs at room temperature. Finally after 3 washes with TBST the blot was developed with Lumiglo (Cell Signaling) and the blot image was obtained on a Kodak Image Station 4000.

Acknowledgments.

We thank and Michael Chao and Eric Rubin for the RFP expression vector, Jessica Wagner for assistance with microscopy and Margreet Wolfert for help with the figures. This work was supported by National Institutes of Health Grants R21AI062275 and R01AI059702 to RNH, and 2R01GM061761 to G-JB. *M. tuberculosis* subcellular fractions were obtained through NIAID Contract No. HHSN266200400091C, entitled "Tuberculosis Vaccine Testing and Research Materials," awarded to Colorado State University. Antibodies to PknA were obtained from Vertex Pharmaceuticals Incorporated.

REFERENCES

1. Goehring NW, Beckwith J (2005) Diverse paths to midcell: assembly of the bacterial cell division machinery. Curr Biol 15: R514-526.

2. Errington J, Daniel RA, Scheffers DJ (2003) Cytokinesis in bacteria. Microbiol Mol Biol Rev 67: 52-65.

3. Blackman SA, Smith TJ, Foster SJ (1998) The role of autolysins during vegetative growth of *Bacillus subtilis* 168. Microbiology 144 (Pt 1): 73-82.

4. Vollmer W, Blanot D, de Pedro MA (2008) Peptidoglycan structure and architecture. FEMS Microbiol Rev 32: 149-167.

5. Vollmer W, Joris B, Charlier P, Foster S (2008) Bacterial peptidoglycan (murein) hydrolases. FEMS Microbiol Rev 32: 259-286.

6. Morlot C, Uehara T, Marquis KA, Bernhardt TG, Rudner DZ (2010) A highly coordinated cell wall degradation machine governs spore morphogenesis in *Bacillus subtilis*. Genes Dev 24: 411-422.

7. Chao MC, Rubin EJ Letting sleeping dos lie: does dormancy play a role in tuberculosis? Annu Rev Microbiol 64: 293-311.

8. Mukamolova GV, Kaprelyants AS, Young DI, Young M, Kell DB (1998) A bacterial cytokine. Proc Natl Acad Sci U S A 95: 8916-8921.

9. Camus JC, Pryor MJ, Medigue C, Cole ST (2002) Re-annotation of the genome sequence of *Mycobacterium tuberculosis* H37Rv. Microbiology 148: 2967-2973.

10. Downing KJ, Mischenko VV, Shleeva MO, Young DI, Young M, et al. (2005) Mutants of *Mycobacterium tuberculosis* lacking three of the five *rpf*-like genes are defective for growth *in vivo* and for resuscitation *in vitro*. Infect Immun 73: 3038-3043.

11. Kana BD, Gordhan BG, Downing KJ, Sung N, Vostroktunova G, et al. (2008) The resuscitatio*N*-promoting factors of *Mycobacterium tuberculosis* are required for virulence and resuscitation from dormancy but are collectively dispensable for growth *in vitro*. Mol Microbiol 67: 672-684.

12. Russell-Goldman E, Xu J, Wang X, Chan J, Tufariello JM (2008) A *Mycobacterium tuberculosis* Rpf double-knockout strain exhibits profound defects in reactivation from chronic tuberculosis and innate immunity phenotypes. Infect Immun 76: 4269-4281.

13. Mukamolova GV, Murzin AG, Salina EG, Demina GR, Kell DB, et al. (2006) Muralytic activity of *Micrococcus luteus* Rpf and its relationship to physiological activity in promoting bacterial growth and resuscitation. Mol Microbiol 59: 84-98.

14. Yeats C, Finn RD, Bateman A (2002) The PASTA domain: a beta-lactam-binding domain. Trends Biochem Sci 27: 438-440.

15. Shah IM, Laaberki MH, Popham DL, Dworkin J (2008) A eukaryotic-like Ser/Thr kinase signals bacteria to exit dormancy in response to peptidoglycan fragments. Cell 135: 486-496.

16. Cole ST, Brosch R, Parkhill J, Garnier T, Churcher C, et al. (1998) Deciphering the biology of *Mycobacterium tuberculosis* from the complete genome sequence. Nature 393: 537-544.

17. Mukamolova GV, Turapov OA, Young DI, Kaprelyants AS, Kell DB, et al. (2002) A family of autocrine growth factors in *Mycobacterium tuberculosis*. Mol Microbiol 46: 623-635.

18. Mukamolova GV, Yanopolskaya ND, Kell DB, Kaprelyants AS (1998) On resuscitation from the dormant state of *Micrococcus luteus*. Antonie Van Leeuwenhoek 73: 237-243.

19. Mahapatra S, Crick DC, McNeil MR, Brennan PJ (2008) Unique structural features of the peptidoglycan of *Mycobacterium leprae*. J Bacteriol 190: 655-661.

20. Lavollay M, Arthur M, Fourgeaud M, Dubost L, Marie A, et al. (2008) The peptidoglycan of stationary-phase *Mycobacterium tuberculosis* predominantly contains cross-links generated by L,D-transpeptidation. J Bacteriol 190: 4360-4366.

21. Lee M, Hesek D, Shah IM, Oliver AG, Dworkin J, et al. (2010) Synthetic peptidoglycan motifs for germination of bacterial spores. Chembiochem : a European journal of chemical biology 11: 2525-2529.

22. Kang CM, Nyayapathy S, Lee JY, Suh JW, Husson RN (2008) Wag31, a homologue of the cell division protein DivIVA, regulates growth, morphology and polar cell wall synthesis in mycobacteria. Microbiology 154: 725-735.

23. Kang CM, Abbott DW, Park ST, Dascher CC, Cantley LC, et al. (2005) The *Mycobacterium tuberculosis* serine/threonine kinases PknA and PknB: substrate identification and regulation of cell shape. Genes Dev 19: 1692-1704.

24. Lam H, Oh DC, Cava F, Takacs CN, Clardy J, et al. (2009) D-amino acids govern stationary phase cell wall remodeling in bacteria. Science 325: 1552-1555.

25. Kolodki*N*-Gal I, Romero D, Cao S, Clardy J, Kolter R, et al. (2010) D-amino acids trigger biofilm disassembly. Science 328: 627-629.

26. Dessen A, Mouz N, Gordon E, Hopkins J, Dideberg O (2001) Crystal structure of PBP2x from a highly penicilli*N*-resistant *Streptococcus pneumoniae* clinical isolate: a mosaic framework containing 83 mutations. J Biol Chem 276: 45106-45112.

27. Barthe P, Mukamolova GV, Roumestand C, Cohe*N*-Gonsaud M (2010) The structure of PknB extracellular PASTA domain from *Mycobacterium tuberculosis* suggests a ligand-dependent kinase activation. Structure 18: 606-615.

28. Young TA, Delagoutte B, Endrizzi JA, Falick AM, Alber T (2003) Structure of *Mycobacterium tuberculosis* PknB supports a universal activation mechanism for Ser/Thr protein kinases. Nat Struct Biol 10: 168-174.

29. Mieczkowski C, Iavarone AT, Alber T (2008) Auto-activation mechanism of the *Mycobacterium tuberculosis* PknB receptor Ser/Thr kinase. Embo J 27: 3186-3197.

30. Ortiz-Lombardia M, Pompeo F, Boitel B, Alzari PM (2003) Crystal structure of the catalytic domain of the PknB serine/threonine kinase from *Mycobacterium tuberculosis*. J Biol Chem 278: 13094-13100.

31. Prisic S, Dankwa S, Schwartz D, Chou MF, Locasale JW, et al. (2010) Extensive phosphorylation with overlapping specificity by *Mycobacterium tuberculosis* serine/threonine protein kinases. Proc Natl Acad Sci U S A 107: 7521-7526.

32. Dasgupta A, Datta P, Kundu M, Basu J (2006) The serine/threonine kinase PknB of *Mycobacterium tuberculosis* phosphorylates PBPA, a penicilli*N*-binding protein required for cell division. Microbiology 152: 493-504.

33. Sureka K, Hossain T, Mukherjee P, Chatterjee P, Datta P, et al. (2010) Novel role of phosphorylatio*N*-dependent interaction between FtsZ and FipA in mycobacterial cell division. PLoS ONE 5: e8590.

34. Chowdhury A, Boons GJ (2005) The synthesis of diaminopimelic acid containing peptidoglycan fragments using metathesis cross coupling. Tetrahedron Lett 46: 1675-1678.

35. Chowdhury A, Siriwardena A, Boons GJ (2002) A highly convergent approach for the synthesis of disaccharide repeating units of peptidoglycan. Tetrahedron Lett 43: 7805-7807.

36. Guan R, Roychowdhury A, Ember B, Kumar S, Boons GJ, et al. (2004) Structural basis for peptidoglycan binding by peptidoglycan recognition proteins. Proc Natl Acad Sci U S A 101: 17168-17173.

37. Kumar S, Roychowdhury A, Ember B, Wang Q, Guan R, et al. (2005) Selective recognition of synthetic lysine and meso-diaminopimelic acid-type peptidoglycan fragments by human peptidoglycan recognition proteins I and S. J Biol Chem 280: 37005-37012.

38. Roychowdhury A, Wolfert MA, Boons GJ (2005) Synthesis and proinflammatory properties of muramyl tripeptides containing lysine and diaminopimelic acid moieties. Chembiochem 6: 2088-2097.

39. Swaminathan CP, Brown PH, Roychowdhury A, Wang Q, Guan R, et al. (2006) Dual strategies for peptidoglycan discrimination by peptidoglycan recognition proteins (PGRPs). Proc Natl Acad Sci U S A 103: 684-689.

40. Asong J, Wolfert MA, Maiti KK, Miller D, Boons GJ (2009) Binding and cellular activation studies reveal that Toll-like receptor 2 can differentially recognize peptidoglycan from Gram-positive and Gram-negative bacteria. J Biol Chem 284: 8643-8653.

41. Sun Z, Zhang Y (1999) Spent culture supernatant of *Mycobacterium tuberculosis* H37Ra improves viability of aged cultures of this strain and allows small inocula to initiate growth. J Bacteriol 181: 7626-7628.

42. de Man J (1975) The probability of most probable numbers. Eur J Appl Microbiol 1: 67-78.

Supporting Figures and Tables

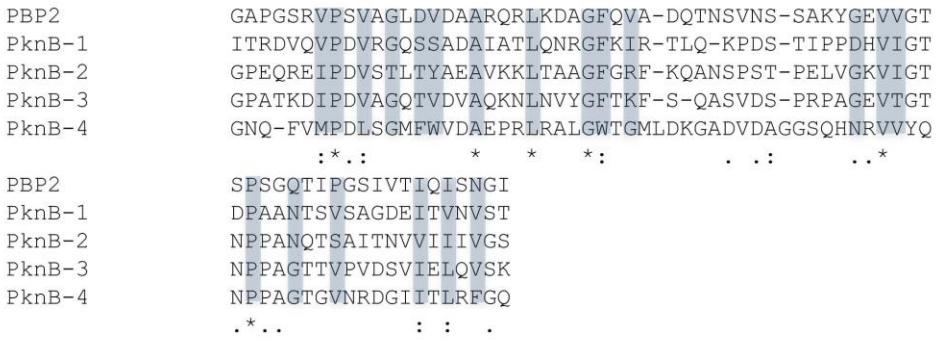

Supporting Figure 1. T-Coffee alignment of the four PASTA domains of *M. tuberculosis* PknB and the single PASTA domain of PBP2. Residues/positions corresponding to those that are conserved in PASTA domains from multiple bacterial species, according to reference 14, are highlighted in blue.

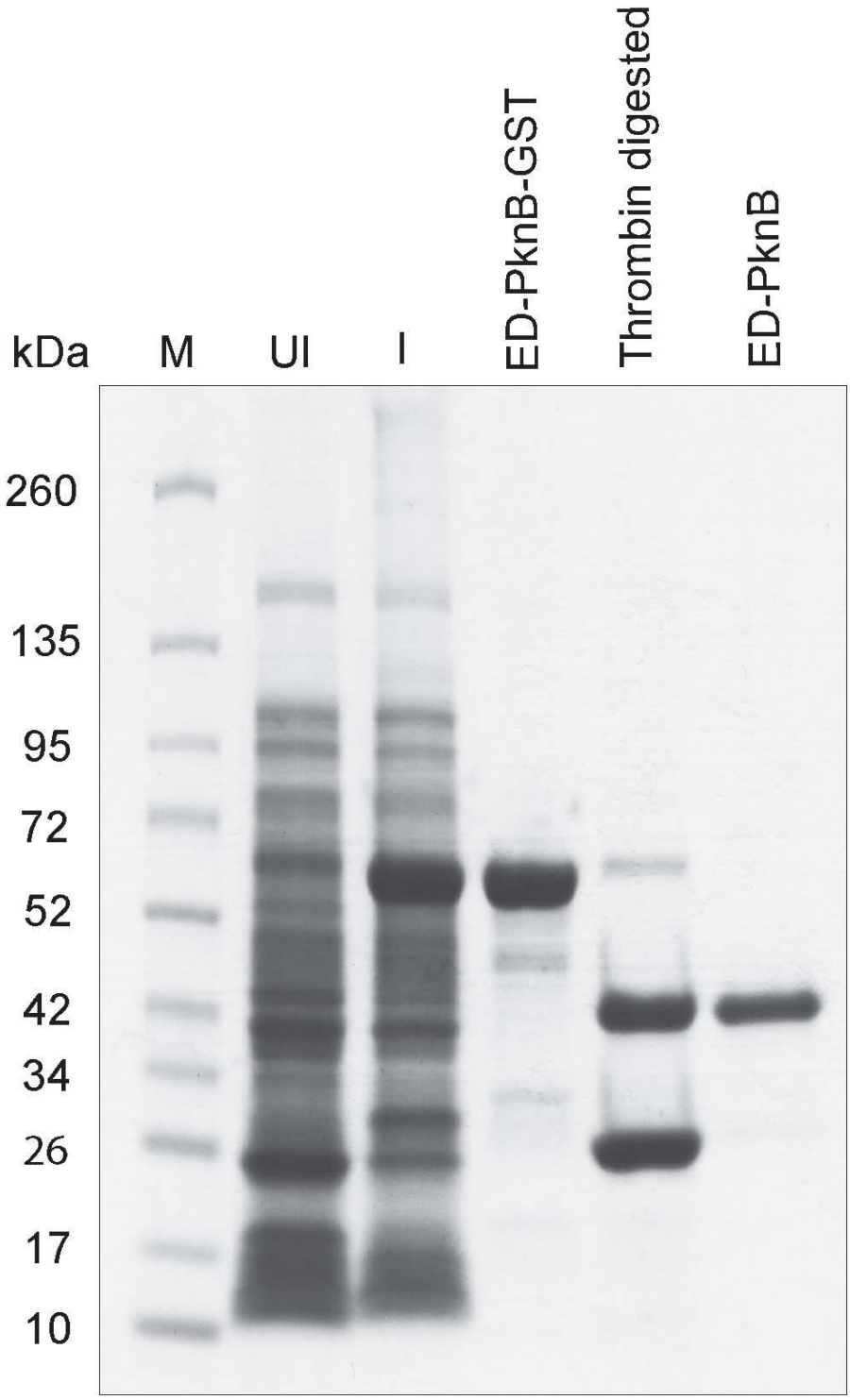

Supporting Figure 2. **SDS-PAGE gel showing expression and purification of ED-PknB**. M, molecular weight markers: UI, lysate from uninduced cultures; I, lysate from induced cultures, The purified protein following removal of the GST tag, shown in the last lane on the right, was used in the binding experiments

Sensorgrams of Lysine containing muropeptides

A) MTP-Lys (amide) (**1**)

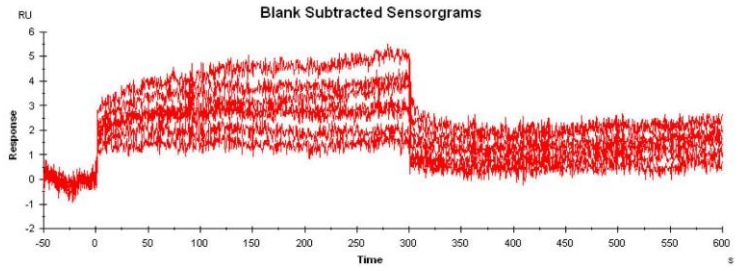

B) MTrP-Lys (amide) (**2a**)

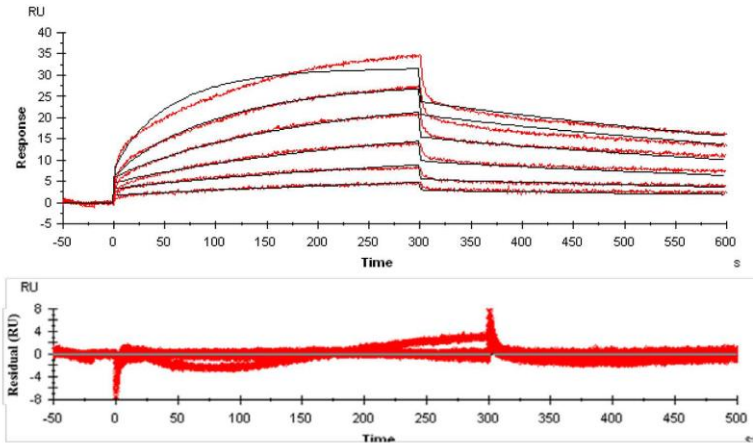

Supporting Figure 3. Sensorgrams of compounds tested in the Biacore binding experiments. The sensorgrams show the simultaneous concentratio*N*-dependent kinetic analysis of two-fold serial dilutions of each compound. ED-PknB was bound to the sensor chip and at time 0 the muropeptide was flowed over the chip as described in the Materials and Methods section. Positive deflection of the curve indicates binding in RU (resonance units). The primary data are shown in red. For compounds that showed significant binding the data were fitted with a two-state binding model (black lines) and the corresponding residual values, which are the signal remaining after the data are fitted to the kinetic model, are plotted below the sensorgrams. Sensorgrams for individual muropeptides are shown in A) MTP-Lys (amide) (1); B) MTrP-Lys (amide) (2a); C) MTrP-Lys (amide) NHAc (2b); D) MTrP-Lys (Gly) (2c); E) MPP-Lys (D-Ala) (3a); F) MPP-Lys (Gly) (3b); G) Peptide (amide) (4); H) MTP-DAP (amide/acid) (5); I) MTrP-DAP (amide/acid) (6a); J) MTrP-DAP (acid/amide) (6b); K) MTrP-DAP (acid/acid) (6d); L) MTrP-DAP(amide/acid)NHAc (6e); M) MPP-DAP (amide/acid) (7); N) Peptide (amide/amide) (8).

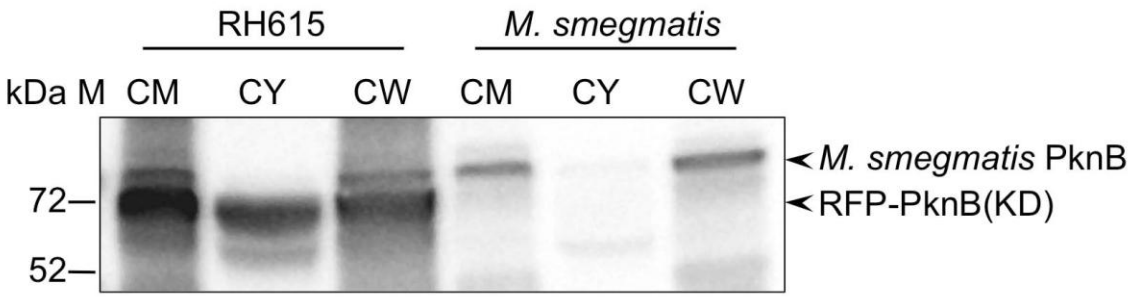

Supporting Figure 4. Immunoblot of subcellular fractions of *M. smegmatis* showing localization of the RFP-PknB kinase domain fusion. *M. smegmatis* was grown to mid log phase, acetamide was added at a concentration of 0.2% for 8 hours. Cells were harvested, lysed with a French Press and sub-cellular fractions were isolated using the protocol developed by the TB Research Materials Contract at Colorado State University (http://www.cvmbs.colostate.edu/mip/tb/pdf/scf.pdf). RH615, *M. smegmatis* expressing the RFP-PknB kinase domain fusion under control of the inducible acetamidase promoter; CM, cytoplasmic membrane fraction; CY, cytoplasm; CW, Cell wall fraction. Though some fusion protein is present in the cytoplasm, the majority is in the cell wall and cell membrane fractions, as is native *M. smegmatis* PknB.

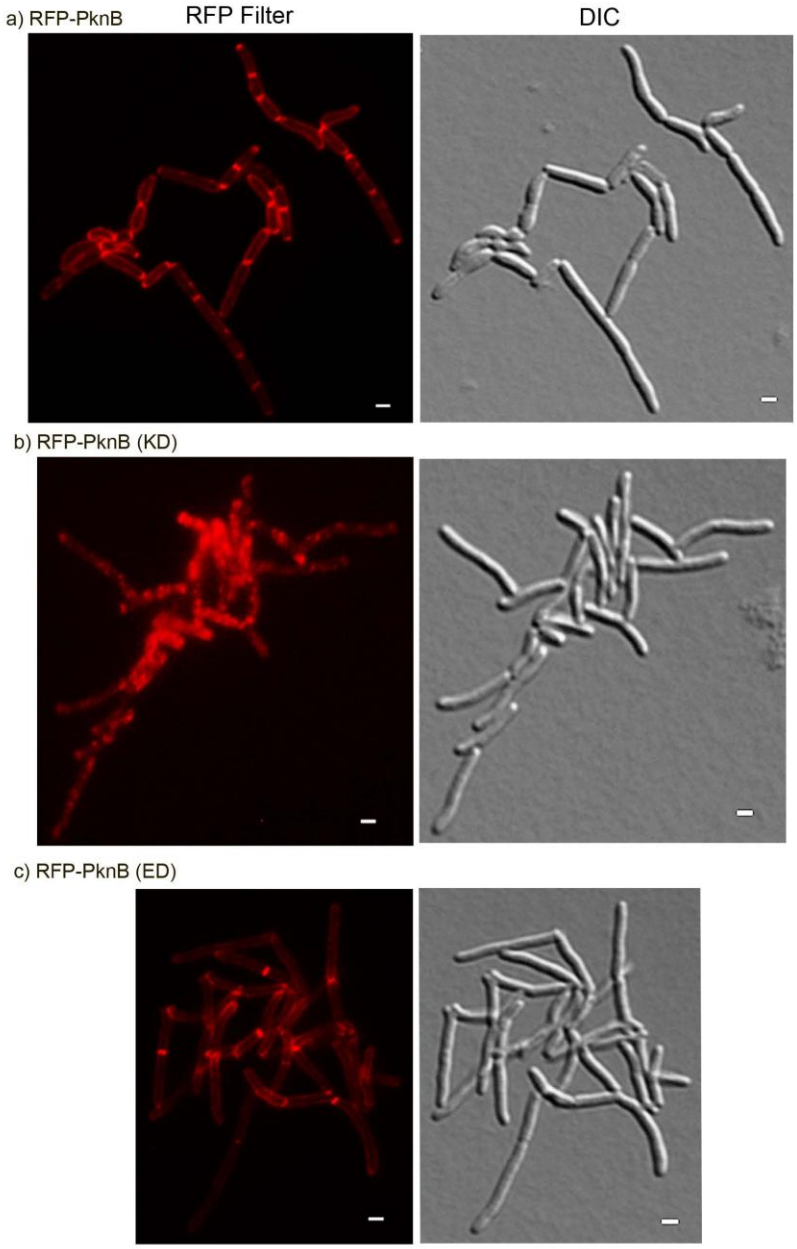

Suppoting Figure 5. Live cell imaging of *M. smegmatis*. Cells expressing RFP fused to a) full-length PknB, b) to the kinase domain, linker and transmembrane segment, or c) to ED-PknB and the transmembrane segment. Fluorescence images are shown on the left and DIC images on the right. Bar = 1 μm.

Table S1. Kinetic binding parameters for the interaction of synthetic muropeptides with the PASTA domains of *M. tuberculosis* PknB

Analyte	k_{a1} (10^{-3} s^{-1})	k_{d1} (10^{-3} s^{-1})	k_{a2} (10^{-3} s^{-1})	k_{d2} (10^{-3} s^{-1})	K_D μM)	χ^2 (RU^2)
MTP-Lys (amide) **1**	-	-	-	-	>500	-
MTrP-Lys (amide) **2a**	82.93	16	44.5	5.5	21.5	0.6
MTrP-Lys (amide) NHAc **2b**	-	-	-	-	>500	-
MTrP-Lys (Gly) **2c**	-	-	-	-	> 500	-
MPP-Lys (D-Ala) **3a**	-	-	-	-	> 500	-
MPP-Lys (Gly) **3b**	-	-	-	-	>500	-
Peptide **4** (amide)	-	-	-	-	> 500	-
MTP-DAP (amide/acid) **5**	5577	172.9	1.64	3.86	21.8	0.3
MTrP-DAP (amide/acid) **6a**	3451	100.7	1.83	1.4	12.7	0.28
MTrP-DAP (acid/amide) **6b**	-	-	-	-	>100	-
MTrP-DAP (amide/amide) **6c**	342.8	57.8	41.5	4.02	14.9	0.2
MTrP-DAP (acid/acid) **6d**	1931	168.7	2.0	3.2	53.6	0.08
MTrP-DAP(amide/acid)NHAc **6e**	354.2	106	6.6	2.2	73.8	0.09
MPP-DAP (amide/acid) **7**	4316	161.5	1.4	2.8	25.1	0.23
Peptide **8** (amide/amide)	-	-	-	-	>500	-

The recombinant extracellular domain of PknB was immobilized on NHS-activated groups of a CM-5 sensor chip surface (5,000 RU) and titration experiments were performed with the synthetic compounds 1-8 (Figure 1). The binding constants of all compounds were determined by fitting the data using a two-state binding model. Sensorgrams for the kinetic analyses are presented in Figure S3. RU, resonance units; MTP, muramyl-tripeptide; MTrP, muramyl-tetra peptide; MPP, muramyl-pentapeptide.

Protocol S1

To determine the localization of PknB in live *M. smegmatis* cells, strains of *M. smegmatis* harboring fusions of *rfp* with full length or different domains of *pknB*, expressed under the acetamidase promoter, were grown in 7H9 to an $O.D_{600}$ of 0.6-0.8. A 1% agarose pad containing 7H9 medium and 0.5% acetamide was prepared in a rectangular chamber made with Frame-Seal (Biorad) rectangular strips on a glass microscope slide. The *M. smegmatis* cells were passed through a 5μm pore filter and 3-4 μl of the culture was spotted onto the agarose pad. After spotting the cells, the chamber was sealed with a coverslip. The slide was incubated at 37^{o} C for 12 hrs and observed

with a Nikon TE2000 microscope equipped with a 100x differential interference contrast (DIC) oil immersion objective and a red fluorescence filter. Images were captured by an OrcaER camera (Hamamatsu Photonics Inc.), acquired with SlideBook (Intelligent Imaging Innovations Inc.) and processed with Adobe Photoshop CS5.

CHAPTER 5

CONCLUSIONS

In summary, the design and synthesis of a novel C2 hydrazone functionalized Kifunensine analogue was achieved. A library of dihydrazone functionalized Kifunensine analogues was prepared and tested for inhibitory activity against Human ER Man I and Mouse Golgi Man I. A pyridine functionalized derivative, **21**, was found to be a potent and selective inhibitor of ER Man I. Analogue **21** had a K_i of 0.07 μM for ER Man I and 0.66 μM for Golgi Man I indicating a 10-fold preference for the ER enzyme. The selectivity was further demonstrated through an Endo F sensitivity assay in which compound **21** was around 5-10 fold worse than Kif at inhibiting downstream *N*-glycan processing. A novel hydrazine functionalized DMJ analogue was synthesized and utilized as a lead compound in the synthesis of five hydrazone modified DMJ analogues. A 3-methyl-thiophene functionalized DMJ analogue was prepared and found to have over a 100 fold improvement in inhibition in respect to DMJ. Analogue **49** had a K_i of 0.30 μM and 32.5 fold selectivity towards the ER α-mannosidase, making it the first selective and potent ER Man I inhibitor derived from DMJ.